Nonzero depolarization volumes in electromagnetic homogenization studies

Jiajia Cui

Doctor of Philosophy
University of Edinburgh
August, 2007

Declaration

I declare that this thesis was composed by myself and that the work contained therein is my own, except where explicitly stated otherwise in the text.

(*Jiajia Cui*)

For my family and my supervisor Tom

Abstract

The work of this thesis concerns depolarization regions in the homogenization of random, particulate composites. In conventional approaches to homogenization, the depolarization dyadics which represent the component phase particles are provided by the singularity of the corresponding dyadic Green function. Thereby, the component particles are effectively treated as vanishingly small, point-like entities. However, through neglecting the spatial extent of the depolarization region, important information may be lost, particularly relating to coherent scattering losses. In this thesis, depolarization regions of nonzero volume are considered. In order to estimate the constitutive parameters of homogenized composite materials (HCMs), the strong-property-fluctuation theory (SPFT) is implemented. This is done through a standard procedure involving the calculation of successive corrections to a preliminary ansatz, in terms of statistical cumulants of the spatial distribution of the component phase particles. The influence of depolarization regions of nonzero volume on the zeroth (and first), second and third order SPFT estimates of HCM constitutive parameters is investigated. Both linear and weakly nonlinear HCMs are considered.

Publications and Presentations

The work described herein has to date yielded the following refereed journal papers:

P1. J. Cui and T.G. Mackay, "Depolarization regions of nonzero volume in bianisotropic homogenized composites", *Waves in Random and Complex Media* **17**, 269-281, 2007;

P2. J. Cui and T.G. Mackay, "Depolarization regions of nonzero volume for anisotropic, cubically nonlinear, homogenized nanocomposites", *Journal of Nanophotonics* **1**, article no. 013506 (13 pages), 2007;

P3. J. Cui and T.G. Mackay, "On convergence of the extended strong–property–fluctuation theory for bianisotropic homogenized composites", *Electromagnetics* **27:8**, 495-506, 2007;

and the following conference paper:

C1. J. Cui and T.G. Mackay, "Depolarization volume and correlation length in the homogenization of bianisotropic composites", *Photon06 — Quantum Electronics and Photonics 17*, The Institute of Physics, Manchester, 2006.

Also, the work has been presented by the author at an Applied Mathematics seminar in the School of Mathematics, University of Edinburgh (May 2007).

Contents

Notation

Symbol	Description	Type
$\underline{\mathrm{E}}$	electric field	3 vector
$\underline{\mathrm{H}}$	magnetic field	3 vector
$\underline{\mathrm{B}}$	magnetic induction	3 vector
$\underline{\mathrm{D}}$	dielectric displacement	3 vector
$\underline{\mathbf{F}}$	electromagnetic field vector	6 vector
$\underline{\mathbf{Q}}$	electromagnetic source vector	6 vector
$\underline{\underline{\mathbf{K}}}$	constitutive dyadic	6×6 dyadic
$\underline{J}_e$	electric current density	3 vector
$\underline{J}_m$	magnetic current density	3 vector
$\underline{\underline{\epsilon}}$	permittivity dyadic	3×3 dyadic
$\underline{\underline{\mu}}$	permeability dyadic	3×3 dyadic
$\underline{\underline{\zeta}}$	magnetoelectric constitutive dyadic	3×3 dyadic
$\underline{\underline{\xi}}$	magnetoelectric constitutive dyadic	3×3 dyadic
$\underline{\underline{U}}$	shape dyadic	3×3 dyadic
L	correlation length	scalar
η	particle size	scalar
$\underline{\underline{\mathbf{G}}}$	dyadic Green function	6×6 dyadic
$\underline{\underline{\mathbf{D}}}$	depolarization dyadic	dyadic
f_ℓ	volume fraction of phase ℓ	scalar
$\underline{\underline{\mathrm{I}}}$	identity dyadic	3×3 dyadic
$\underline{\underline{\mathbf{I}}}$	identity dyadic	6×6 dyadic
ϵ_0	permittivity of free space	scalar
μ_0	permeability of free space	scalar
k_0	free-space wavenumber	scalar
ω	angular frequency	scalar

Vector quantities are underlined. Double underlining and normal (bold) face signifies a 3×3 (6×6) dyadic. The inverse, adjoint, transpose and determinant of a dyadic $\underline{\underline{M}}$ are denoted by $\underline{\underline{M}}^{-1}$, adj $\left[\underline{\underline{M}}\right]$, $\underline{\underline{M}}^T$ and det $\left[\underline{\underline{M}}\right]$.

Abbreviations and Acronyms

Symbol	Description
Br	Bruggeman
MG	Maxwell Garnett
HCM	homogenized composite material
FCM	Farady chiral material
DGF	dyadic Green function
SPFT	strong-property-fluctuation theory

Chapter 1

Introduction

1.1 Overview

The work of this thesis concerns depolarization regions in the homogenization of random, particulate composites. The composite may be regarded as an effectively homogeneous material provided that wavelengths are sufficiently long compared with the dimensions of the component phase particles. In electromagnetics, the estimation of the constitutive parameters of homogenized composite materials (HCMs) is a matter of long-standing, and ongoing, scientific and technological importance [1]. In conventional approaches to homogenization, the depolarization dyadics which represent the electromagnetic responses of component phase particles are provided by the singularity of the corresponding dyadic Green function [2, 3]. Thereby, the component particles are effectively treated as vanishingly small, point-like entities. However, through neglecting the spatial extent of the depolarization region, important information may be lost, particularly relating to coherent scattering losses. In this thesis, depolarization regions of nonzero volume are considered. In order to estimate the constitutive parameters of homogenized composite materials, the strong-property-fluctuation theory (SPFT) is implemented [4, 5, 6, 7, 8]. This is done through a standard procedure involving the calculation of successive corrections to a preliminary ansatz, in terms of statistical cumulants of the spatial distribution of the component phase particles. The influence of depolarization regions of nonzero volume on the zeroth (and

first), second and third order SPFT estimates of HCM constitutive parameters is investigated. Both linear and weakly nonlinear HCMs are considered.

In Chapter 2, the analysis is developed within the most general linear setting of bianisotropic homogenized composite materials. Numerical studies are presented for two representative bianisotropic HCMs, namely a reciprocal bianisotropic material and a Faraday chiral material. These studies reveal that estimates of the HCM constitutive parameters in relation to volume fraction, particle eccentricity, particle orientation and correlation length are all significantly influenced by the size of the component phase particles.

In Chapter 3, we consider weakly nonlinear HCMs. By taking the nonzero particle size into consideration, attenuation is predicted and nonlinear enhancement is somewhat diminished. In these respects, the effect of particle size is similar to that of correlation length within the bilocally-approximated SPFT.

In Chapter 4, we present an extended version of the third–order SPFT in which the component particles are represented as depolarization regions of nonzero volume. Numerical results are provided for a bianisotropic homogenization scenario wherein the HCM is a Faraday chiral material. Thereby, convergence of the extended SPFT at the second–order level of approximation is demonstrated within the long–wavelength regime.

1.2 Maxwell equations and constitutive relations

1.2.1 Time domain

The macroscopic description of the electromagnetic properties of materials is provided in the time domain by the Maxwell equations [9]

$$\nabla \times \underline{\tilde{H}}(\underline{r},t) - \frac{\partial}{\partial t}\underline{\tilde{D}}(\underline{r},t) = \underline{\tilde{J}}_e(\underline{r},t), \tag{1.1}$$

$$\nabla \times \underline{\tilde{E}}(\underline{r},t) + \frac{\partial}{\partial t}\underline{\tilde{B}}(\underline{r},t) = -\underline{\tilde{J}}_m(\underline{r},t), \tag{1.2}$$

$$\nabla \cdot \underline{\tilde{D}}(\underline{r},t) = \tilde{\rho}_e(\underline{r},t), \tag{1.3}$$

$$\nabla \cdot \underline{\tilde{B}}(\underline{r},t) = 0. \tag{1.4}$$

In these four equations, $\underline{\tilde{D}}(\underline{r},t), \underline{\tilde{E}}(\underline{r},t), \underline{\tilde{B}}(\underline{r},t)$ and $\underline{\tilde{H}}(\underline{r},t)$ represent the dielectric displacement, electric field, magnetic induction and magnetic field, respectively, while the electric current and charge densities are represented by $\underline{\tilde{J}}_e(\underline{r},t)$ and $\tilde{\rho}_e(\underline{r},t)$, respectively. The divergence relations (1.3) and (1.4) are just a consequence of the curl relations (1.1) and (1.2), combined with the following continuity equations for the source terms

$$\nabla \cdot \underline{\tilde{J}}_e(\underline{r},t) + \frac{\partial}{\partial t}\tilde{\rho}_e(\underline{r},t) = 0. \tag{1.5}$$

These Maxwell equations represent two vector differential equations in four unknown vector fields, which means that we can not get the solution just from them. In order to specify unique solutions, further equations are required. These are provided by the *constitutive relations*. Here we use the most general linear constitutive relations for spatially-local materials [10, 11],

$$\underline{\tilde{D}}(\underline{r},t) = \int_{-\infty}^{t} [\underline{\underline{\tilde{\epsilon}}}(\underline{r},t-t') \cdot \underline{\tilde{E}}(\underline{r},t') + \underline{\underline{\tilde{\xi}}}(\underline{r},t-t') \cdot \underline{\tilde{H}}(\underline{r},t')]dt', \tag{1.6}$$

$$\underline{\tilde{B}}(\underline{r},t) = \int_{-\infty}^{t} [\underline{\underline{\tilde{\zeta}}}(\underline{r},t-t') \cdot \underline{\tilde{E}}(\underline{r},t') + \underline{\underline{\tilde{\mu}}}(\underline{r},t-t') \cdot \underline{\tilde{H}}(\underline{r},t')]dt', \tag{1.7}$$

where $\underline{\underline{\tilde{\epsilon}}}(\underline{r},t-t'), \underline{\underline{\tilde{\xi}}}(\underline{r},t-t'), \underline{\underline{\tilde{\zeta}}}(\underline{r},t-t')$ and $\underline{\underline{\tilde{\mu}}}(\underline{r},t-t')$ are the time-domain constitutive dyadics. Materials described by the constitutive relations (1.6) and (1.7) are called *bianisotropic*. Field D can be thought of arising in response to an applied field E (and H). In these equations the fields are functions of time. Because no material can respond instantaneously to an applied field, the time dependence of D is different to that of E, so that field D at time t depends on the field E that was acting at all times less than t. This property is called "causality". Weakly nonlinear materials will be considered in Chapter 3.

1.2.2 Frequency domain

In order to make the equations (1.1), (1.2), (1.6) and (1.7) convenient to solve, we use Fourier transformation to transfer them from time-domain to frequency-domain. Let us introduce the frequency-domain constitutive dyadics $\underline{\underline{\epsilon}}(\underline{r},\omega), \underline{\underline{\xi}}(\underline{r},\omega)$, $\underline{\underline{\zeta}}(\underline{r},\omega)$ and $\underline{\underline{\mu}}(\underline{r},\omega)$, defined through the Fourier transformations

$$\underline{\underline{\tilde{\gamma}}}(\underline{r},t) = \frac{1}{2\pi}\int_{-\infty}^{\infty} \underline{\underline{\gamma}}(\underline{r},\omega)\exp(-i\omega t)d\omega, \qquad (\gamma = \epsilon,\xi,\zeta,\mu), \tag{1.8}$$

along with the field phasors $\underline{D}(\underline{r},\omega), \underline{E}(\underline{r},\omega), \underline{B}(\underline{r},\omega)$ and $\underline{H}(\underline{r},\omega)$, defined similarly via

$$\underline{\tilde{T}}(\underline{r},t) = \frac{1}{2\pi}\int_{-\infty}^{\infty} \underline{T}(\underline{r},\omega)\exp(-i\omega t)d\omega, \qquad (T = D,B,E,H). \tag{1.9}$$

Thus, by using the convolution theorem [12], the constitutive relations (1.6) and (1.7) are expressed in the frequency domain as

$$\underline{D}(\underline{r},\omega) = \underline{\underline{\epsilon}}(\underline{r},\omega)\cdot\underline{E}(\underline{r},\omega) + \underline{\underline{\xi}}(\underline{r},\omega)\cdot\underline{H}(\underline{r},\omega), \tag{1.10}$$

$$\underline{B}(\underline{r},\omega) = \underline{\underline{\zeta}}(\underline{r},\omega)\cdot\underline{E}(\underline{r},\omega) + \underline{\underline{\mu}}(\underline{r},\omega)\cdot\underline{H}(\underline{r},\omega). \tag{1.11}$$

Moreover, the Maxwell curl equations (1.1), (1.2) are given in the frequency domain as

$$\nabla\times\underline{H}(\underline{r},\omega) + i\omega\underline{D}(\underline{r},\omega) = \underline{J}_e(\underline{r},\omega), \tag{1.12}$$

$$\nabla\times\underline{E}(\underline{r},\omega) - i\omega\underline{B}(\underline{r},\omega) = 0, \tag{1.13}$$

where the terms $\underline{J}_e(\underline{r},\omega)$ are the Fourier transforms of $\underline{\tilde{J}}_{ef}(\underline{r},t)$, defined as in (1.9).

1.2.3 6×6 dyadic notation

After substituting the constitutive relations (1.10) and (1.11) into the Maxwell curl equations (1.12) and (1.13), we get a self-consistent system of differential equations

$$[\underline{\underline{\mathbf{L}}}(\nabla) + i\omega \underline{\underline{\mathbf{K}}}(\underline{r}, \omega)] \cdot \underline{\mathbf{F}}(\underline{r}, \omega) = \underline{\mathbf{Q}}(\underline{r}, \omega), \tag{1.14}$$

where, in 6-vector/dyadic notation [13], the linear differential operator $\underline{\underline{\mathbf{L}}}(\nabla)$ and constitutive dyadic $\underline{\underline{\mathbf{K}}}(\underline{r}, \omega)$ have the representations

$$\underline{\underline{\mathbf{L}}}(\nabla) = \begin{bmatrix} \underline{\underline{0}} & \nabla \times \underline{\underline{I}} \\ -\nabla \times \underline{\underline{I}} & \underline{\underline{0}} \end{bmatrix}, \tag{1.15}$$

$$\underline{\underline{\mathbf{K}}}(\underline{r}, \omega) = \begin{bmatrix} \underline{\underline{\epsilon}}(\underline{r}, \omega) & \underline{\underline{\xi}}(\underline{r}, \omega) \\ \underline{\underline{\zeta}}(\underline{r}, \omega) & \underline{\underline{\mu}}(\underline{r}, \omega) \end{bmatrix}, \tag{1.16}$$

while the electromagnetic field vector $\underline{\mathbf{F}}(\underline{r}, \omega)$ and source vector $\underline{\mathbf{Q}}(\underline{r}, \omega)$ are defined as

$$\underline{\mathbf{F}}(\underline{r}, \omega) = \begin{bmatrix} \underline{E}(\underline{r}, \omega) \\ \underline{H}(\underline{r}, \omega) \end{bmatrix}, \tag{1.17}$$

$$\underline{\mathbf{Q}}(\underline{r}, \omega) = \begin{bmatrix} \underline{J_e}(\underline{r}, \omega) \\ 0 \end{bmatrix}. \tag{1.18}$$

Since (1.14) is a linear vector equation, we can express its solution in terms of the dyadic Green function $\underline{\underline{G}}(\underline{r} - \underline{r'}, \omega)$ as

$$\underline{\mathbf{F}}(\underline{r}, \omega) = \int_{V'} \underline{\underline{\mathbf{G}}}(\underline{r} - \underline{r'}, \omega) \cdot \underline{\mathbf{Q}}(\underline{r'}, \omega) d^3\underline{r'}, \tag{1.19}$$

where $\underline{r}$ and $\underline{r'}$ are the field and source points respectively, and all source points are contained within the integration volume V'. The dyadic Green function $\underline{\underline{\mathbf{G}}}(\underline{r} - \underline{r'}, \omega)$ itself is the solution of the differential equation [3]

$$[\underline{\underline{\mathbf{L}}}(\nabla) + i\omega \underline{\underline{\mathbf{K}}}(\underline{r}, \omega)] \cdot \underline{\underline{\mathbf{G}}}(\underline{r} - \underline{r'}, \omega) = \delta(\underline{r} - \underline{r'}) \underline{\underline{\mathbf{I}}}, \tag{1.20}$$

in which the Dirac delta function $\delta(\underline{r}-\underline{r}')$ and the 6×6 identity dyadic $\underline{\underline{\mathbf{I}}}$ are the source terms of the equation (1.14).

1.3 Homogenization

1.3.1 Generalities

Here we concentrate on two-phase random composite materials. See (1.1). The component phases are designated as a and b. All space is partitioned into the disjoint regions V_a and V_b which contain the phases a and b, respectively. The volume fraction of phase a is given by f_a, while that of phase b by $f_b = 1-f_a$. The component phases are themselves homogeneous; i.e., their constitutive dyadics are assumed to be independent of the spatial coordinate $\underline{r}$. We consider the most general linear scenario wherein the component phases a and b are taken to be bianisotropic materials with 6×6 constitutive dyadics $\underline{\underline{\mathbf{K}}}_a$ and $\underline{\underline{\mathbf{K}}}_b$, respectively; i.e.,

$$\underline{\mathbf{C}}(\underline{r}) = \underline{\underline{\mathbf{K}}}_\ell \cdot \underline{\mathbf{F}}(\underline{r}), \qquad \underline{r}\in V_\ell, \quad (\ell = a,b), \tag{1.21}$$

wherein the 6-vector electromagnetic fields

$$\underline{\mathbf{C}}(\underline{r}) = \left[\begin{array}{c} \underline{D}(\underline{r}) \\ \underline{B}(\underline{r}) \end{array}\right], \tag{1.22}$$

and

$$\underline{\mathbf{F}}(\underline{r}) = \left[\begin{array}{c} \underline{E}(\underline{r}) \\ \underline{H}(\underline{r}) \end{array}\right], \tag{1.23}$$

are specified in terms of the complex-valued dielectric displacement $\underline{D}$, electric field $\underline{E}$, magnetic field $\underline{H}$ and magnetic induction $\underline{B}$ phasors, while the complex-valued 6×6 constitutive dyadic

$$\underline{\underline{\mathbf{K}}}_\ell = \left[\begin{array}{cc} \underline{\underline{\epsilon}}_\ell & \underline{\underline{\xi}}_\ell \\ \underline{\underline{\zeta}}_\ell & \underline{\underline{\mu}}_\ell \end{array}\right], \tag{1.24}$$

comprises the 3×3 permittivity and permeability dyadics $\underline{\underline{\epsilon}}_\ell$ and $\underline{\underline{\mu}}_\ell$, respectively, as well as the magnetoelectric constitutive dyadics $\underline{\underline{\xi}}_\ell$ and $\underline{\underline{\zeta}}_\ell$. For convenience, henceforth we neglect to write the ω–dependency of the field quantities and constitutive dyadics. Moreover, we assume that the inclusions are randomly distributed, but identically orientated, ellipsoids with surface parameterized as

$$\underline{r}_e(\theta, \phi) = \eta \underline{\underline{U}} \cdot \hat{\underline{r}}(\theta, \phi), \tag{1.25}$$

where $\hat{\underline{r}}(\theta, \phi)$ is the radial unit vector depending on the spherical polar coordinates θ and ϕ, $\underline{\underline{U}}$ is a real-valued symmetric shape dyadic, and η is a linear measure of the inclusion size[3].

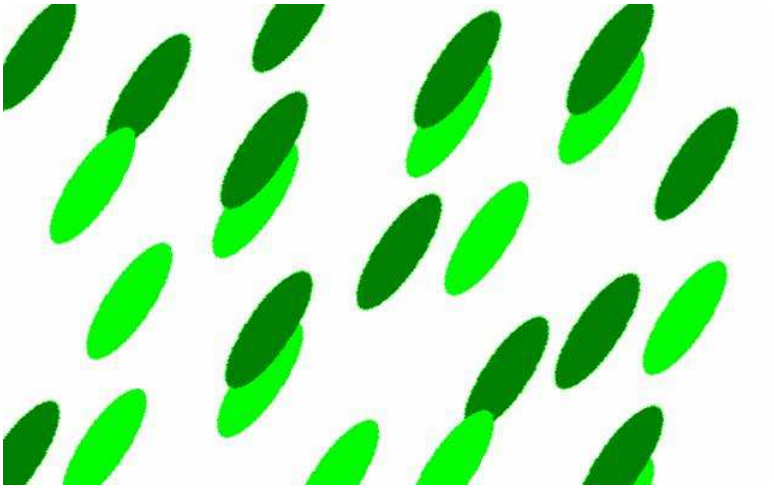

Figure 1.1: A random assembly of two different types of ellipsoidal particles. For the SPFT, the ellipsoids all have the same shape and orientation.

1.3.2 Depolarization dyadic

Suppose now that the component particle is embedded within a bianisotropic comparison material, characterized by the 6×6 constitutive dyadic $\underline{\underline{\mathbf{K}}}_{cm}$. The comparison material is homogeneous. The electromagnetic response of the ellipsoidal particle of size parameter η, occupying the region of volume V_e^η is provided by the depolarization dyadic [3]

$$\underline{\underline{\mathbf{D}}}_{U/cm}(\eta) = \int_{V_e^\eta} \underline{\underline{\mathbf{G}}}_{cm}(\underline{r}) \, d^3\underline{r}. \tag{1.26}$$

In order to consider the depolarization dydic of a particle of nonzero volume, we express $\underline{\underline{D}}_{U/cm}(\eta)$ as the sum

$$\underline{\underline{\mathbf{D}}}_{U/cm}(\eta) = \underline{\underline{\mathbf{D}}}^{0}_{U/cm} + \underline{\underline{\mathbf{D}}}^{>0}_{U/cm}(\eta), \tag{1.27}$$

where $\underline{\underline{\mathbf{D}}}^{0}_{U/cm}$ is the contribution to the depolarization arising in the limit $\eta \to 0$ (i.e., from the singularity of $\underline{\underline{\mathbf{G}}}_{cm}$, while $\underline{\underline{\mathbf{D}}}^{>0}_{U/cm}(\eta)$ is the contribution to the depolarization associated with the the nonzero size of the inclusion particle. In Chapter 2, we describe the details of how to calculate $\underline{\underline{\mathbf{D}}}^{0}_{U/cm}$ and $\underline{\underline{\mathbf{D}}}^{>0}_{U/cm}(\eta)$.

1.3.3 Distributional statistics

We consider the homogenization of two distinct material phases: phase a and phase b, both of which consist of ellipsoidal particles of average size η. All space is taken to be partitioned into the disjoint regions V_a and V_b that contain the phases a and b, respectively. The phases a and b are randomly distributed, as specified by the characteristic functions [8]

$$\Phi_\ell(\underline{r}) = \begin{cases} 1, & \underline{r} \in V_\ell \\ \\ 0, & \underline{r} \notin V_\ell \end{cases}, \qquad (\ell = a, b). \tag{1.28}$$

In particular, within the SPFT statistical moments of Φ_ℓ are utilized to characterize the component phase distributions. The averaging process is taken over all possible assembles of the two component materials. Sometimes this average is called the 'ensemble average'. The volume fraction of phase ℓ is given by the first moment; i.e.,

$$\langle\, \Phi_\ell(\underline{r}) \,\rangle = f_\ell, \qquad (\ell = a, b), \tag{1.29}$$

and we have $f_a + f_b = 1$. The physically–motivated step function [4]

$$\langle\, \Phi_\ell(\underline{r})\, \Phi_\ell(\underline{r}') \,\rangle = \begin{cases} f_\ell, & |\, \underline{\underline{U}}^{-1} \bullet (\underline{r} - \underline{r}') \,| \le L \\ \\ f_\ell^2, & |\, \underline{\underline{U}}^{-1} \bullet (\underline{r} - \underline{r}') \,| > L \end{cases} \qquad (\ell = a, b) \tag{1.30}$$

is often adopted as the second moment for the second–order SPFT. The correlation length L is required to be much smaller than the electromagnetic wavelength(s) but larger than the size of the component phase particles. It is worth noting that the second–order SPFT estimates of the HCM constitutive parameters have been found to be largely insensitive to the particular form of the second moment [26]. In keeping with (1.30), the third–order SPFT has been established for the third moment [14]

$$\langle\, \Phi_\ell(\underline{r})\, \Phi_\ell(\underline{r}')\, \Phi_\ell(\underline{r}'')\, \rangle = \begin{cases} f_\ell^3, & \min\{L_{12}, L_{13}, L_{23}\} > L \\ f_\ell, & \max\{L_{12}, L_{13}, L_{23}\} \leq L \\ \frac{1}{3}\,(f_\ell + 2f_\ell^3), & \text{one of } L_{12}, L_{13}, L_{23} \leq L \\ \frac{1}{3}\,(2f_\ell + f_\ell^3), & \text{two of } L_{12}, L_{13}, L_{23} \leq L \end{cases}, \tag{1.31}$$

where

$$\ell = a, b, \;\; L_{12} = |\underline{\underline{U}}^{-1} \bullet (\underline{r} - \underline{r}')|\,, \;\; L_{13} = |\underline{\underline{U}}^{-1} \bullet (\underline{r} - \underline{r}'')|\,, \;\; L_{23} = |\underline{\underline{U}}^{-1} \bullet (\underline{r}' - \underline{r}'')|\,. \tag{1.32}$$

1.3.4 Homogenization formalisms

Depolarization dyadics are important mathematical constructions in homogenization analyses as they characterize the electromagnetic field inside inclusions (i.e., component phase particles) embedded within a homogenous background. Often the inclusion particles are treated as vanishingly small point–like entities; under this approximation, the corresponding depolarization dyadic is represented by the singularity of the associated dyadic Green function [2, 3]. However, through neglecting the spatial extent of the inclusions, potentially important information may be lost, especially when coherent scattering losses are under consideration [15, 16]. Extended versions of both the Maxwell Garnett homogenization formalism [17, 18] (see §1.3.5) and the Bruggeman homogenization formalism [17, 19]

(see §1.3.6) have been developed in which a nonzero volume is attributed to the component phase particles, but these analyses apply only to isotropic HCMs and adopt a simplistic description of the distributional statistics of the component phases.

1.3.5 Maxwell Garnett formalism

The Maxwell Garnett (MG) formalism is designed for composite materials consisting of well-separated inclusions embedded in a simply connected host material. In the general case of a bianisotropic composite, in which the inclusion and host phases are characterized by the constitutive dyadics $\underline{\underline{\boldsymbol{K}}}_a$ and $\underline{\underline{\boldsymbol{K}}}_b$, respectively, and the ellipsoidal inclusion geometry is specified by the shape dyadic $\underline{\underline{U}}$, we have [20]

$$\underline{\underline{\boldsymbol{K}}}_{MG} = \underline{\underline{\boldsymbol{K}}}_b + f_a \underline{\underline{\boldsymbol{\alpha}}}^{a/b} \cdot (\underline{\underline{I}} - i\omega f_a \underline{\underline{\boldsymbol{D}}}_{I/b}(\eta) \cdot \underline{\underline{\boldsymbol{\alpha}}}^{a/b})^{-1} \tag{1.33}$$

as the MG estimate of the constitutive dyadic of the HCM. The term

$$\underline{\underline{\boldsymbol{\alpha}}}^{a/b} = (\underline{\underline{\boldsymbol{K}}}_a - \underline{\underline{\boldsymbol{K}}}_b) \cdot [\underline{\underline{I}} + i\omega \underline{\underline{\boldsymbol{D}}}_{U/b}(\eta) \cdot (\underline{\underline{\boldsymbol{K}}}_a - \underline{\underline{\boldsymbol{K}}}_b)]^{-1}, \tag{1.34}$$

in (1.33) is a generalized polarisability dyadic, and $\underline{\underline{\boldsymbol{D}}}_{U/b}(\eta)(\underline{\underline{\boldsymbol{D}}}_{I/b}(\eta))$ is the depolarization dyadic associated with an exclusion volume specified by the shape dyadic $\underline{\underline{U}}(\underline{\underline{I}})$, in the phase b host material.

1.3.6 Bruggeman formalism

The Bruggeman formalism (Br) is designed for composite materials in which both component materials consist of particulates and have a similar topology. No assumptions about the volumetric proportions of the component materials are made, which means that when dealing with the Br formalism both the inclusion and host phases maybe assumed to have particulate topologies and the distinction between the "inclusion" and "host" phases is rather artificial. For bianisotropic composites, arising from particulate component phases a and b of ellipsoidal topology characterized by the shape dyadics $\underline{\underline{U}}^a$ and $\underline{\underline{U}}^b$, respectively, the Br estimate of the HCM constitutive dyadic $\underline{\underline{K}}_{Br}$ is obtained by solving the

nonlinear equation

$$f_a \underline{\underline{\boldsymbol{\alpha}}}^{a/Br} + f_b \underline{\underline{\boldsymbol{\alpha}}}^{b/Br} = \underline{\underline{0}}. \tag{1.35}$$

The generalized polarisabilities in (1.35) are

$$\underline{\underline{\boldsymbol{\alpha}}}^{a/Br} = (\underline{\underline{\boldsymbol{K}}}_a - \underline{\underline{\boldsymbol{K}}}_{Br}) \cdot [\underline{\underline{\boldsymbol{I}}} + i\omega \underline{\underline{\boldsymbol{D}}}_{U^a/Br}(\eta) \cdot (\underline{\underline{\boldsymbol{K}}}_a - \underline{\underline{\boldsymbol{K}}}_{Br})]^{-1}, \tag{1.36}$$

$$\underline{\underline{\boldsymbol{\alpha}}}^{b/Br} = (\underline{\underline{\boldsymbol{K}}}_b - \underline{\underline{\boldsymbol{K}}}_{Br}) \cdot [\underline{\underline{\boldsymbol{I}}} + i\omega \underline{\underline{\boldsymbol{D}}}_{U^b/Br}(\eta) \cdot (\underline{\underline{\boldsymbol{K}}}_b - \underline{\underline{\boldsymbol{K}}}_{Br})]^{-1}, \tag{1.37}$$

and $\underline{\underline{\boldsymbol{D}}}_{U^a/Br}(\eta)(\underline{\underline{\boldsymbol{D}}}_{U^b/Br}(\eta))$ is the depolarization dyadic of a $\underline{\underline{U}}_a$-shape ($\underline{\underline{U}}_b$-shape) exclusion volume in the HCM with constitutive dyadic $\underline{\underline{\boldsymbol{K}}}_{Br}$. The usual method of dealing with (1.35) is to apply the simple Jacobi technique [21], by which an iterative solution is developed as

$$\underline{\underline{\boldsymbol{K}}}_{Br}[n] = \tau(\underline{\underline{\boldsymbol{K}}}_{Br}[n-1]), \qquad (n = 1, 2, ...), \tag{1.38}$$

with the initial value $\underline{\underline{\boldsymbol{K}}}_{Br}[0] = \underline{\underline{\boldsymbol{K}}}_{MG}$ and the operator τ defined as

$$\begin{aligned} \tau(\underline{\underline{\boldsymbol{K}}}_{Br}) = &\{f_a \underline{\underline{\boldsymbol{K}}}_a \cdot [\underline{\underline{\boldsymbol{I}}} + i\omega \underline{\underline{\boldsymbol{D}}}_{U^a/Br}(\eta) \cdot (\underline{\underline{\boldsymbol{K}}}_a - \underline{\underline{\boldsymbol{K}}}_{Br})]^{-1} + \\ &f_b \underline{\underline{\boldsymbol{K}}}_b \cdot [\underline{\underline{\boldsymbol{I}}} + i\omega \underline{\underline{\boldsymbol{D}}}_{U^b/Br}(\eta) \cdot (\underline{\underline{\boldsymbol{K}}}_b - \underline{\underline{\boldsymbol{K}}}_{Br})]^{-1}\} \\ &\cdot \{f_a [\underline{\underline{\boldsymbol{I}}} + i\omega \underline{\underline{\boldsymbol{D}}}_{U^a/Br}(\eta) \cdot (\underline{\underline{\boldsymbol{K}}}_a - \underline{\underline{\boldsymbol{K}}}_{Br})]^{-1} + \\ &f_b [\underline{\underline{\boldsymbol{I}}} + i\omega \underline{\underline{\boldsymbol{D}}}_{U^b/Br}(\eta) \cdot (\underline{\underline{\boldsymbol{K}}}_b - \underline{\underline{\boldsymbol{K}}}_{Br})]^{-1}\}^{-1}. \end{aligned} \tag{1.39}$$

1.3.7 Higher order SPFT

An alternative approach to homogenization is provided by the strong–property–fluctuation theory (SPFT), in which a comprehensive description of the distributional statistics of the component phases can be accommodated. While the origins of the SPFT lie in wave propagation studies for continuous random materials [22, 23], the SPFT has lately gained prominence in the homogenization of particulate composites [24, 5, 6, 7, 8]. By means of the SPFT, the HCM constitutive parameters are estimated as successive refinements to the constitutive parameters of a homogeneous comparison material. Iterations are expressed in terms of correlation functions describing the spatial distributions of the compo-

nent phases. In principle, correlation functions of arbitrarily high order may be incorporated; in practice, the SPFT is usually implemented at the second order level of approximation. In fact, convergence of the SPFT scheme at the second order level of approximation has been established for a wide range of linear HCMs [25]. The constitutive dyadic of the HCM, as estimated by the nth–order SPFT, is given by [26],

$$\underline{\underline{\mathbf{K}}}_{HCM}^{[n]} = \underline{\underline{\mathbf{K}}}_{cm} - \frac{1}{i\omega}\left[\underline{\underline{\mathbf{I}}} + \underline{\underline{\boldsymbol{\Sigma}}}^{[n]}(\eta, L) \cdot \underline{\underline{\mathbf{D}}}_{U/cm}(\eta)\right]^{-1} \cdot \underline{\underline{\boldsymbol{\Sigma}}}^{[n]}(\eta, L). \tag{1.40}$$

Herein, the constitutive dyadic $\underline{\underline{\mathbf{K}}}_{cm}$ characterizes a comparison material whose constitutive parameters are provided by the Bruggeman homogenization formalism. The depolarization dyadic $\underline{\underline{\mathbf{D}}}_{U/cm}(\eta)$ corresponds to component particles with shape dyadic $\underline{\underline{U}}$ embedded in the comparison material; the same shape dyadic is assumed for both component phases. Explicit expressions for the nth order mass operator term $\underline{\underline{\boldsymbol{\Sigma}}}^{[n]}(\eta, L)$, which depends on both the size parameter η and the correlation length L, are provided in Chapters 2, 3 and 4. The zeroth and first order SPFT estimates of the HCM constitutive parameters are the same as the Bruggeman estimate of the HCM constitutive parameters. Details of the second order and third order SPFT are presented in Chapter 2, 3 and 4.

Chapter 2

Linear bianisotropic composites

2.1 Overview

In this chapter, we present an extension to the strong–property–fluctuation theory in which depolarization regions of nonzero volume and ellipsoidal geometry are accommodated. Therein, both the size and spatial distribution of the component phase particles are taken into account. The analysis is developed within the most general linear setting of bianisotropic homogenized composite materials (HCMs). Numerical studies of the constitutive parameters are presented for representative examples of HCM; both Lorentz–reciprocal and Lorentz–nonreciprocal HCMs are considered. These studies reveal that estimates of the HCM constitutive parameters in relation to volume fraction, particle eccentricity, particle orientation and correlation length are all significantly influenced by the size of the component phase particles. The theory presented in this Chapter builds on the theory presented in [42]; here we deal with the bianisotropic scenario whereas the anisotropic dielectric scenario was dealt with in [42].

2.2 Homogenization

2.2.1 Depolarization region

Let us consider an ellipsoidal particle of volume V_e^η, oriented arbitrarily in $\mathbb{R}^3$. The ellipsoidal surface of V_e^η is parameterized by

$$\underline{r}_e(\theta,\phi) = \eta\,\underline{\underline{U}}\cdot\hat{\underline{r}}\,(\theta,\phi), \tag{2.1}$$

where $\hat{\underline{r}}\,(\theta,\phi)$ is the radial unit vector specified by the spherical polar coordinates θ and ϕ. The 3×3 shape dyadic $\underline{\underline{U}}$, which is real symmetric with unit determinant, maps the spherical region V^η of radius η onto the ellipsoidal region V_e^η. The linear dimensions of the ellipsoidal particle, as determined by η, are assumed to be sufficiently small that the electromagnetic long–wavelength regime pertains, but not vanishingly small. Suppose now that the ellipsoidal particle is embedded within a bianisotropic comparison material, characterized by the 6×6 constitutive dyadic $\underline{\underline{\mathbf{K}}}_{cm}$. The comparison material is homogeneous. The electromagnetic response of the ellipsoidal particle is provided by the depolarization dyadic [3]

$$\underline{\underline{\mathbf{D}}}(\eta) = \int_{V_e^\eta} \underline{\underline{\mathbf{G}}}_{cm}(\underline{r})\;d^3\underline{r} \;=\; \int_{V^\eta} \underline{\underline{\mathbf{G}}}_{cm}(\underline{\underline{U}}\cdot\underline{r})\;d^3\underline{r}\,. \tag{2.2}$$

Herein, $\underline{\underline{\mathbf{G}}}_{cm}(\underline{r})$ is the 6×6 dyadic Green function of the comparison material which satisfies the nonhomogenous vector Helmholtz equation [3]

$$\left[\underline{\underline{\mathbf{L}}}(\nabla) + i\omega\underline{\underline{\mathbf{K}}}_{cm}\right]\cdot\underline{\underline{\mathbf{G}}}_{cm}(\underline{r}-\underline{r}') = \underline{\underline{\mathbf{I}}}\,\delta(\underline{r}-\underline{r}'), \tag{2.3}$$

with the linear differential operator

$$\underline{\underline{\mathbf{L}}}(\nabla) = \left[\begin{array}{cc} \underline{\underline{0}} & \nabla\times\underline{\underline{I}} \\ -\nabla\times\underline{\underline{I}} & \underline{\underline{0}} \end{array}\right] \tag{2.4}$$

and $\delta(\underline{r}-\underline{r}')$ being the Dirac delta function. Explicit representations of Green functions are not generally available for anisotropic and bianisotropic materials [28]. However, it suffices for our present purposes to consider the Fourier trans-

form of $\underline{\underline{\mathbf{G}}}_{cm}(\underline{r})$, namely

$$\underline{\underline{\tilde{\mathbf{G}}}}_{cm}(\underline{q}) = \int_{\underline{r}} \underline{\underline{\mathbf{G}}}_{cm}(\underline{r}) \, \exp(-i\underline{q} \cdot \underline{r}) \, d^3\underline{r} \,, \tag{2.5}$$

which is delivered from equation (2.3) as

$$\underline{\underline{\tilde{\mathbf{G}}}}_{cm}(\underline{q}) = \frac{1}{i\omega} \, \left[\underline{\underline{\tilde{\mathbf{A}}}}_{cm}(\underline{q}) \right]^{-1} , \tag{2.6}$$

where

$$\underline{\underline{\tilde{\mathbf{A}}}}_{cm}(\underline{q}) = \left[\begin{array}{cc} \underline{\underline{0}} & (\underline{q}/\omega) \times \underline{\underline{\mathbf{I}}} \\ \\ -(\underline{q}/\omega) \times \underline{\underline{\mathbf{I}}} & \underline{\underline{0}} \end{array} \right] + \underline{\underline{\mathbf{K}}}_{cm} \,. \tag{2.7}$$

Thereby, equation (2.2) yields [2, 3]

$$\underline{\underline{\mathbf{D}}}_{U/cm}(\eta) \;=\; \frac{\eta}{2\pi^2} \int_{\underline{q}} \frac{1}{q^2} \left(\frac{\sin(q\eta)}{q\eta} - \cos(q\eta) \right) \underline{\underline{\tilde{\mathbf{G}}}}_{cm}(\underline{\underline{U}}^{-1} \cdot \underline{q}) \, d^3\underline{q} \,. \tag{2.8}$$

In order to consider the depolarization dydic of a particle of nonzero volume, we express $\underline{\underline{D}}(\eta)$ as the sum (1.27). The two terms on the right side of (1.27) are given by

$$\underline{\underline{\mathbf{D}}}^{>0}_{U/cm}(\eta) = \frac{\eta}{2\pi^2} \int_{\underline{q}} \frac{1}{q^2} \left(\frac{\sin(q\eta)}{q\eta} - \cos(q\eta) \right) \underline{\underline{\tilde{\mathbf{G}}}}^{\eta}_{cm}(\underline{\underline{U}}^{-1} \cdot \underline{q}) \, d^3\underline{q} \,, \tag{2.9}$$

$$\underline{\underline{\mathbf{D}}}^{0}_{U/cm} = \frac{\eta}{2\pi^2} \int_{\underline{q}} \frac{1}{q^2} \left(\frac{\sin(q\eta)}{q\eta} - \cos(q\eta) \right) \underline{\underline{\tilde{\mathbf{G}}}}^{\infty}_{cm}(\underline{\underline{U}}^{-1} \cdot \underline{\hat{q}}) \, d^3\underline{q} \,, \tag{2.10}$$

with

$$\underline{\underline{\tilde{\mathbf{G}}}}^{\eta}_{cm}(\underline{\underline{U}}^{-1} \cdot \underline{q}) \;=\; \underline{\underline{\tilde{\mathbf{G}}}}_{cm}(\underline{\underline{U}}^{-1} \cdot \underline{q}) - \underline{\underline{\tilde{\mathbf{G}}}}^{\infty}_{cm}(\underline{\underline{U}}^{-1} \cdot \underline{\hat{q}}) \,, \tag{2.11}$$

$$\underline{\underline{\tilde{\mathbf{G}}}}^{\infty}_{cm}(\underline{\underline{U}}^{-1} \cdot \underline{\hat{q}}) \;=\; \lim_{q \to \infty} \underline{\underline{\tilde{\mathbf{G}}}}_{cm}(\underline{\underline{U}}^{-1} \cdot \underline{q}) \tag{2.12}$$

$$\;=\; \frac{1}{i\omega \, b(\theta,\phi)} \left[\begin{array}{cc} \alpha_\mu(\theta,\phi) \, \underline{\hat{q}} \, \underline{\hat{q}} & -\alpha_\varsigma(\theta,\phi) \, \underline{\hat{q}} \, \underline{\hat{q}} \\ \\ -\alpha_\xi(\theta,\phi) \, \underline{\hat{q}} \, \underline{\hat{q}} & \alpha_\epsilon(\theta,\phi) \, \underline{\hat{q}} \, \underline{\hat{q}} \end{array} \right] , \tag{2.13}$$

$$\tag{2.14}$$

wherein the scalars

$$\alpha_p(\theta,\phi) = \hat{\underline{q}} \cdot \underline{\underline{U}}^{-1} \cdot \underline{\underline{p}}_{cm} \cdot \underline{\underline{U}}^{-1} \cdot \hat{\underline{q}}\,, \qquad (p = \epsilon, \zeta, \xi, \mu) \tag{2.15}$$

and

$$b(\theta,\phi) = [\alpha_\epsilon(\theta,\phi)\,\alpha_\mu(\theta,\phi)] - [\alpha_\xi(\theta,\phi)\,\alpha_\zeta(\theta,\phi)]\,. \tag{2.16}$$

The volume integral (2.10) simplifies to the η–independent surface integral [2, 3]

$$\underline{\underline{\mathbf{D}}}^0_{U/cm} = \frac{1}{4\pi}\,\underline{\underline{U}}^{-1} \cdot \left(\int_{\phi=0}^{2\pi} \int_{\theta=0}^{\pi} \underline{\underline{\tilde{\mathbf{G}}}}^{\infty}_{cm}(\underline{\underline{U}}^{-1} \cdot \hat{\underline{q}})\ \ \sin\theta\ d\theta\ d\phi \right) \cdot \underline{\underline{U}}^{-1}. \tag{2.17}$$

For certain Lorentz–reciprocal comparison materials, the volume integral (2.9) which yields $\underline{\underline{\mathbf{D}}}^{>0}_{U/cm}(\eta)$ may be reduced to a surface integral, but for a general bianisotropic comparison material no such simplifications are available. The integrals (2.9) and (2.17) may be evaluated using standard numerical techniques [29]. The dyadic $\underline{\underline{\mathbf{D}}}^0_{U/cm}$ represents the depolarization contribution arising from the vanishingly small region of volume $\lim_{\eta\to 0} V_e^\eta$, whereas the dyadic $\underline{\underline{\mathbf{D}}}^{>0}_{U/cm}(\eta)$ provides the depolarization contribution arising from the region of nonzero volume $\left(V_e^\eta - \lim_{\eta\to 0} V_e^\eta\right)$. In homogenization studies, it is common practice to neglect $\underline{\underline{\mathbf{D}}}^{>0}_{U/cm}(\eta)$ and assume that the depolarization dyadic is given by $\underline{\underline{\mathbf{D}}}^0_{U/cm}$ alone [30]. However, studies of isotropic [15, 16, 18, 17, 19] and anisotropic [42] HCMs have emphasized the importance of the nonzero spatial extent of depolarization regions.

2.2.2 Distributional statistics

The distributional statistics of the component phases are as described in (1.3.3). In this Chapter we consider the second–order SPFT in which the two–point covariance function (1.30) is adopted.

2.3 Zeroth and first order SPFT

2.3.1 zeroth order SPFT

The nth order SPFT estimate of the HCM constitutive dyadic, namely $\underline{\underline{\mathbf{K}}}_{HCM}^{[n]}$, is based upon the iterative refinement of the comparison material constitutive dyadic, namely $\underline{\underline{\mathbf{K}}}_{cm}$. To zeroth order and first order, the SPFT permittivity estimate is identical to the comparison material permittivity [8]; i.e.,

$$\underline{\underline{\mathbf{K}}}_{HCM}^{[0]} = \underline{\underline{\mathbf{K}}}_{HCM}^{[1]} = \underline{\underline{\mathbf{K}}}_{cm}. \tag{2.18}$$

The well–known Bruggeman homogenization formalism provides the estimate of $\underline{\underline{\mathbf{K}}}_{cm}$ [8]. That is, $\underline{\underline{\mathbf{K}}}_{cm}$ emerges through solving the nonlinear equations

$$f_a \, \underline{\underline{\boldsymbol{\chi}}}^{a/cm} + f_b \, \underline{\underline{\boldsymbol{\chi}}}^{b/cm} = \underline{\underline{\mathbf{0}}}, \tag{2.19}$$

wherein the polarizability density dyadics

$$\underline{\underline{\boldsymbol{\chi}}}^{\ell/cm} = -i\omega \left(\underline{\underline{\mathbf{K}}}_{\ell} - \underline{\underline{\mathbf{K}}}_{cm} \right) \cdot \left[\underline{\underline{\mathbf{I}}} + i\omega \underline{\underline{\mathbf{D}}}_{U/cm}(\eta) \cdot \left(\underline{\underline{\mathbf{K}}}_{\ell} - \underline{\underline{\mathbf{K}}}_{cm} \right) \right]^{-1}, \tag{2.20}$$

where $\ell = a, b$.

2.3.2 Second order SPFT

The SPFT is most widely implemented at the second order level (also known as the bilocal approximation) which provides the following estimate of the HCM constitutive dyadic [8] (1.40) Thus, the particle size η influences $\underline{\underline{\mathbf{K}}}_{HCM}^{[2]}$ directly through the depolarization dyadic $\underline{\underline{\mathbf{D}}}_{U/cm}(\eta)$ and indirectly through the *mass operator* [22] dyadic term

$$\underline{\underline{\boldsymbol{\Sigma}}}^{[2]} = f_a f_b \left(\underline{\underline{\boldsymbol{\chi}}}^{a/cm} - \underline{\underline{\boldsymbol{\chi}}}^{b/cm} \right) \cdot \underline{\underline{\mathbf{D}}}_{U/cm}^{>0}(L) \cdot \left(\underline{\underline{\boldsymbol{\chi}}}^{a/cm} - \underline{\underline{\boldsymbol{\chi}}}^{b/cm} \right). \tag{2.21}$$

Notice that the correlation length L — which plays a key role in the second order SPFT — does not feature in the zeroth order SPFT.

2.4 Numerical studies

We now apply the theoretical results presented earlier in this Chapter to two specific bianisotropic homogenizations scenarios: in §2.4.1 a biaxial bianisotropic HCM is considered and in §2.4.2 a Faraday chiral material [31, 32] are considered. The HCM in §2.4.1 is Lorentz–reciprocal [33] whereas the HCM in §2.4.2 is not. Numerical studies are presented for representative examples, in order to explore the influence of η in relation to volume fraction, particle eccentricity, particle orientation and correlation length. In view of the vast parameter space associated with bianisotropic materials, only an illustrative selection of graphical results are provided here in this Chapter; further graphical results are presented in Appendix 1. The following calculations were carried using an angular frequency $\omega = 2\pi \times 10^{10}$ rad s^{-1}. Hence, $\lambda_0 = 2\pi/k_0 = 0.030$ m.

2.4.1 Biaxial bianisotropic HCM

The homogenization of (i) a biaxial dielectric material described by the constitutive dyadic

$$\underline{\underline{\mathbf{K}}}_a = \begin{bmatrix} \epsilon_0 \, \mathrm{diag}\,(\epsilon_a^x, \epsilon_a^y, \epsilon_a^z) & \underline{\underline{0}} \\ \underline{\underline{0}} & \mu_0 \, \underline{\underline{I}} \end{bmatrix} \tag{2.22}$$

and (ii) an isotropic chiral material described by the constitutive dyadic

$$\underline{\underline{\mathbf{K}}}_b = \begin{bmatrix} \epsilon_0 \epsilon_b \, \underline{\underline{I}} & i\sqrt{\epsilon_0 \mu_0}\, \xi_b \, \underline{\underline{I}} \\ -i\sqrt{\epsilon_0 \mu_0}\, \xi_b \, \underline{\underline{I}} & \mu_0 \, \mu_b lk \, \underline{\underline{I}} \end{bmatrix} \tag{2.23}$$

is investigated. The constitutive parameters selected for calculations are: $\epsilon_a^x = 4 + i0.12$, $\epsilon_a^y = 3 + i0.1$, $\epsilon_a^z = 1.5 + i0.08$; $\epsilon_b = 2.5 + i0.1$, $\xi_b = 1 + i0.07$ and $\mu_b = 1.75 + i0.09$. The numerical values used for the constitutive parameters of the component materials do not correspond to any one specific material. Instead, these numerical values are representative values, typical of the values that might be encountered for real materials. Also, where possible, the numerical values for the constitutive parameters of the component materials were chosen to allow

direct comparison of my results with results from other published homogenization studies. The shape dyadic of the constituent particles is taken to be

$$\underline{\underline{U}} = \frac{1}{\sqrt[3]{U_x U_y U_z}}\, \underline{\underline{R}}_z(\varphi) \bullet [\,\mathrm{diag}(U_x, U_y, U_z)] \bullet \underline{\underline{R}}_z^T(\varphi), \tag{2.24}$$

with

$$\underline{\underline{R}}_z(\varphi) = \begin{pmatrix} \cos\varphi & \sin\varphi & 0 \\ -\sin\varphi & \cos\varphi & 0 \\ 0 & 0 & 1 \end{pmatrix}. \tag{2.25}$$

Thus, the principal axes of the ellipsoidal particles lie in the xy plane rotated by an angle φ, and along the z axis. The shape parameters selected for calculations are: $U_x = 1+\rho$, $U_y = 1$ and $U_z = 1 - 0.5\rho$; the eccentricity of the ellipsoids is varied through the parameter ρ. The corresponding HCM is a Lorentz–reciprocal, biaxial, bianisotropic material. In this case, the volume integral in (2.9) for $\underline{\underline{\mathbf{D}}}^{>0}(\eta)$ is analogous to one which arises in the development of the second order SPFT [8]. Thus, we may express $\underline{\underline{\mathbf{D}}}^{>0}(\eta)$ as the surface integral

$$\begin{aligned} \underline{\underline{\mathbf{D}}}^{>0}_{U/cm}(\eta) \;=\; & \frac{\omega^3}{8\pi i}\int_{\phi=0}^{2\pi}\int_{\theta=0}^{\pi}\left(\frac{1}{\kappa_+ - \kappa_-}\Big\{\frac{e^{i\eta q}}{q^2}(1 - i\eta q)\Big[\underline{\underline{\mathbf{N}}}(\underline{\underline{U}}^{-1}\bullet\underline{q}) \right. \\ & \left. + \underline{\underline{\mathbf{N}}}(-\underline{\underline{U}}^{-1}\bullet\underline{q})\Big]\Big\}_{q=\sqrt{\kappa_-}}^{q=\sqrt{\kappa_+}} + \frac{2}{\kappa_+ + \kappa_-}\,\underline{\underline{\mathbf{N}}}(\underline{0})\right)\sin\theta\; d\theta\; d\phi\,, \end{aligned} \tag{2.26}$$

with

$$\underline{\underline{\mathbf{N}}}(\underline{\underline{U}}^{-1}\bullet\underline{q}) = \frac{1}{b(\theta,\phi)}\left\{\mathrm{adj}\left[\underline{\underline{\tilde{\mathbf{A}}}}_{cm}(\underline{\underline{U}}^{-1}\bullet\underline{q})\right] - \det\left[\underline{\underline{\tilde{\mathbf{A}}}}_{cm}(\underline{\underline{U}}^{-1}\bullet\underline{q})\right]\underline{\underline{\tilde{\mathbf{G}}}}^{\infty}_{cm}(\underline{\underline{U}}^{-1}\bullet\underline{\hat{q}})\right\} \tag{2.27}$$

and $\kappa_\pm$ being the q^2 roots of $\det\left[\underline{\underline{\tilde{\mathbf{A}}}}_{cm}(\underline{\underline{U}}^{-1}\bullet\underline{q})\right]$.

Particle size and volume fraction

To focus upon the effect of particle size η in relation to volume fraction f_a, we set the eccentricity $\rho = 0$, the orientation angle $\varphi = 0$ and the correlation length

$L = 0$. The corresponding HCM constitutive dyadic has the form

$$\underline{\underline{\mathbf{K}}}_{HCM} = \left[\begin{array}{cc} \epsilon_0 \, \mathrm{diag}\,(\epsilon^x_{HCM}, \epsilon^y_{HCM}, \epsilon^z_{HCM}) & i\sqrt{\epsilon_0\mu_0}\, \mathrm{diag}\,(\xi^x_{HCM}, \xi^y_{HCM}, \xi^z_{HCM}) \\ -i\sqrt{\epsilon_0\mu_0}\, \mathrm{diag}\,(\xi^x_{HCM}, \xi^y_{HCM}, \xi^z_{HCM}) & \mu_0 \, \mathrm{diag}\,(\mu^x_{HCM}, \mu^y_{HCM}, \mu^z_{HCM}) \end{array} \right] . \tag{2.28}$$

In Figure 2.1, the real and imaginary parts of $\epsilon^{x,y,z}_{HCM}$ are plotted against $f_a \in (0,1)$ for $\eta/\lambda_0 \in \{0, 0.05, 0.1\}$. Notice that the HCM parameters are constrained to coincide with those of component phase b in the limit $f_a \to 0$, and those of component phase a in the limit $f_a \to 1$. The influence of η is more obviously observed on the imaginary parts of $\epsilon^{x,y,z}_{HCM}$ than on the real parts. Indeed, the imaginary parts of $\epsilon^{x,y,z}_{HCM}$ for $\eta/\lambda_0 = 0.1$ at mid–range values of f_a are approximately twice as large as they are for $\eta/\lambda_0 = 0$. The corresponding graphs for the HCM magnetoelectric parameters $\xi^{x,y,z}_{HCM}$ and permeability parameters $\mu^{x,y,z}_{HCM}$ are qualitatively similar to those presented for the permeability parameters in Figure 2.1.

Particle size and particle eccentricity

Next we turn to the effect of particle size η in relation to particle eccentricity, as specified by ρ. The volume fraction is fixed at $f_a = 0.5$, the orientation angle at $\varphi = 0$ and the correlation length at $L = 0$. The corresponding HCM constitutive dyadic has the form (2.28). As a typical example of the behaviour of HCM constitutive parameters, the real and imaginary parts of ξ^x_{HCM} are graphed versus $\rho \in (0,1)$ for $\eta/\lambda_0 \in \{0, 0.05, 0.1\}$ in Figure 2.2. Regardless of the value of η, the constitutive parameters vary substantially — particularly their imaginary parts — as ρ increases. Furthermore, there are significant differences in the plots of ξ^x_{HCM} presented for the three values of η. The most striking differences are observed in the plots of the imaginary parts of ξ^x_{HCM}. The corresponding graphs for the constitutive parameters not presented in Figure 2.2 (i.e., $\epsilon^{x,y,z}_{HCM}$, $\xi^{y,z}_{HCM}$ and $\mu^{x,y,z}_{HCM}$) are broadly similar to those given in Figure 2.2.

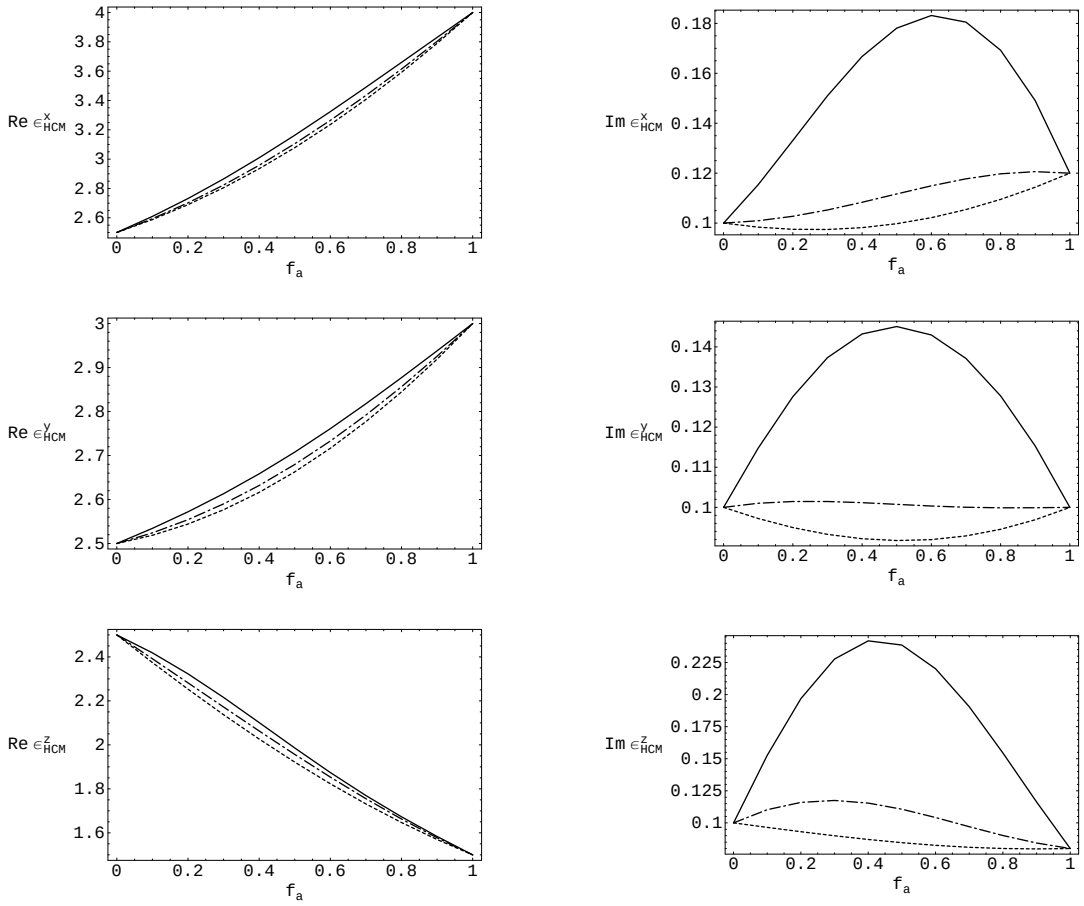

Figure 2.1: Real (left) and imaginary (right) parts of the HCM constitutive parameters $\epsilon^{x,y,z}_{HCM}$ plotted against volume fraction $f_a \in (0,1)$ for $\eta/\lambda_0 = 0$ (dashed curves), $\eta/\lambda_0 = 0.05$ (broken dashed curves) and $\eta/\lambda_0 = 0.1$ (solid curves). The HCM is a biaxial bianisotropic material.

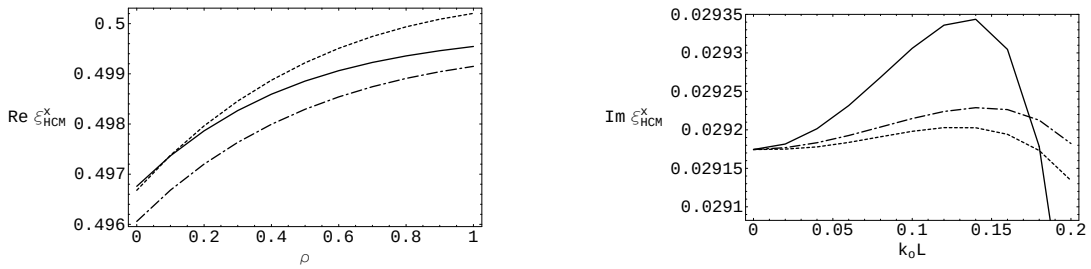

Figure 2.2: Real (left) and imaginary (right) parts of the HCM constitutive parameter ξ^x_{HCM} plotted against the eccentricity parameter $\rho \in (0,1)$ for $\eta/\lambda_0 = 0$ (dashed curves), $\eta/\lambda_0 = 0.05$ (broken dashed curves) and $\eta/\lambda_0 = 0.1$ (solid curves). The HCM is a biaxial bianisotropic material.

Particle size and particle orientation

In order to investigate the effect of particle size η in relation to particle orientation, we fix the volume fraction $f_a = 0.5$, particle eccentricity $\rho = 1$ and the correlation

length $L = 0$. The resulting HCM has a constitutive dyadic of the form

$$\underline{\underline{\mathbf{K}}}_{HCM} = \left[\begin{array}{cc} \epsilon_0 \begin{pmatrix} \epsilon^x_{HCM} & \epsilon^t_{HCM} & 0 \\ \epsilon^t_{HCM} & \epsilon^y_{HCM} & 0 \\ 0 & 0 & \epsilon^z_{HCM} \end{pmatrix} & i\sqrt{\epsilon_0\mu_0} \begin{pmatrix} \xi^x_{HCM} & \xi^t_{HCM} & 0 \\ \xi^t_{HCM} & \xi^y_{HCM} & 0 \\ 0 & 0 & \xi^z_{HCM} \end{pmatrix} \\ -i\sqrt{\epsilon_0\mu_0} \begin{pmatrix} \xi^x_{HCM} & \xi^t_{HCM} & 0 \\ \xi^t_{HCM} & \xi^y_{HCM} & 0 \\ 0 & 0 & \xi^z_{HCM} \end{pmatrix} & \mu_0 \begin{pmatrix} \mu^x_{HCM} & \mu^t_{HCM} & 0 \\ \mu^t_{HCM} & \mu^y_{HCM} & 0 \\ 0 & 0 & \mu^z_{HCM} \end{pmatrix} \end{array} \right] . \tag{2.29}$$

Illustrative numerical results are displayed in Figure 2.3, wherein the real and imaginary parts of $\mu^{y,t}_{HCM}$ are plotted against $\varphi \in (0, \pi/2)$ for $\eta/\lambda_0 \in \{0, 0.05, 0.1\}$. The off–diagonal constitutive parameter μ^t vanishes in the limits $\varphi \to 0$ and $\pi/2$ (as do ϵ^t and ξ^t). Both the real and imaginary parts of μ^t are strongly influenced by the particle size η, especially for mid–range values of φ. The diagonal constitutive parameter μ^y is also clearly sensitive to η. In the case of μ^y, the differences in behaviour for the three values of η are most apparent as φ approaches 0 and $\pi/2$. The graphs of μ^t are symmetric about $\varphi = \pi/4$, but those of μ^y are not. The HCM constitutive parameters that are not represented in Figure 2.3 (i.e., $\epsilon^{x,y,z,t}_{HCM}$, $\xi^{x,y,z,t}_{HCM}$ and $\mu^{x,z}_{HCM}$) exhibit behaviour with respect to φ which is generally similar to that exhibited by $\mu^{y,t}_{HCM}$ in Figure 2.3.

Particle size and correlation length

Lastly in this section, particle size η is considered in relation to correlation length L. To do so, the following parameters are fixed: volume fraction $f_a = 0.5$, orientation angle $\varphi = 0$ and the eccentricity $\rho = 0$. The constitutive dyadic of the HCM which arises has the form (2.28). In Figure 2.4, graphs of the real and imaginary parts of ϵ^x_{HCM} versus $k_0 L \in (0, 0.2)$ are provided for $\eta/L \in \{0, 0.5, 0.95\}$. It is

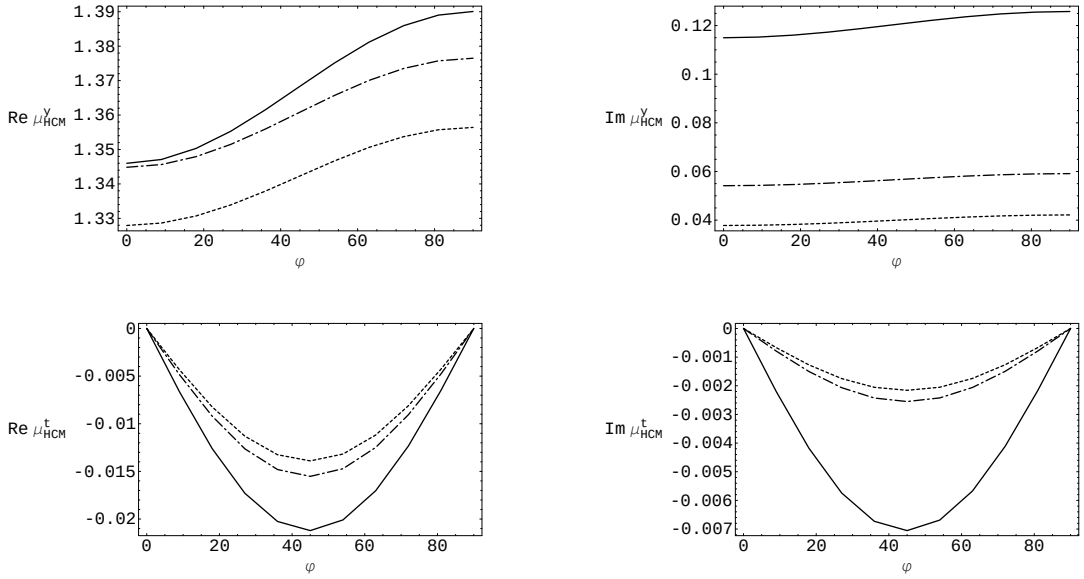

Figure 2.3: Real (left) and imaginary (right) parts of the HCM constitutive parameters $\mu^{y,t}_{HCM}$ plotted against orientation angle $\varphi \in (0, \pi/2)$ for $\eta/\lambda_0 = 0$ (dashed curves), $\eta/\lambda_0 = 0.05$ (broken dashed curves) and $\eta/\lambda_0 = 0.1$ (solid curves). The HCM is a biaxial bianisotropic material.

clear that the imaginary part of ϵ^x_{HCM} is strongly affected by increasing L; the real part of ϵ^x_{HCM} is also affected but to a lesser degree. Furthermore, ϵ^x_{HCM} is much more sensitive to L at larger values of η. The behaviour observed in Figure 2.4 for ϵ^x_{HCM} with respect to L is also generally observed in the HCM constitutive parameters $\epsilon^{y,z}_{HCM}$, $\xi^{x,y,z}_{HCM}$ and $\mu^{x,y,z}_{HCM}$ which are not represented in Figure 2.4.

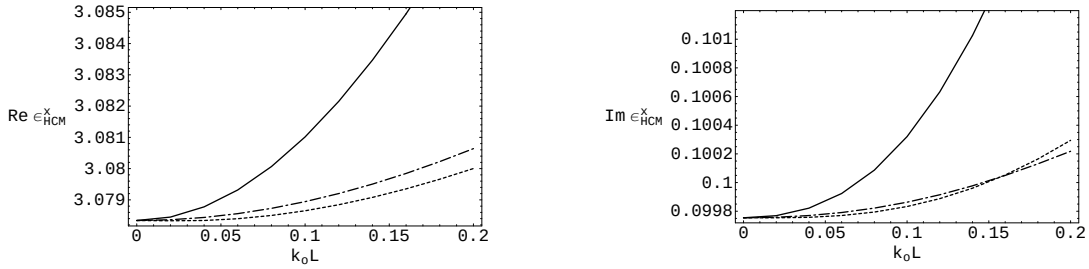

Figure 2.4: Real (left) and imaginary (right) parts of the HCM constitutive parameter ϵ^x_{HCM} plotted against relative correlation length $k_0 L \in (0, 0.2)$ for $\eta/L = 0$ (dashed curves), $\eta/L = 0.5$ (broken dashed curves) and $\eta/L = 0.95$ (solid curves). The HCM is a biaxial bianisotropic material.

2.4.2 Faraday chiral material

For our second homogenization scenario, we explore the homogenization of (i) a gyrotropic magnetic material described by the constitutive dyadic

$$\underline{\underline{\mathbf{K}}}_a = \left[\begin{array}{cc} \epsilon_0\,\epsilon_a\,\underline{\underline{I}} & \underline{\underline{0}} \\ \underline{\underline{0}} & \mu_0 \left(\begin{array}{ccc} \mu_a^x & i\mu_a^g & 0 \\ -i\mu_a^g & \mu_a^x & 0 \\ 0 & 0 & \mu_a^z \end{array} \right) \end{array} \right] \tag{2.30}$$

and (ii) an isotropic chiral material described by the constitutive dyadic (2.23). The constitutive parameters selected for calculations are: $\epsilon_a = 1.2 + i0.02$, $\mu_a^x = 3.5 + i0.08$, $\mu_a^g = 1.8 + i0.05$, $\mu_b^z = 1.4 + i0.04$; $\epsilon_b = 2.5 + i0.1$, $\xi_b = 1 + i0.07$ and $\mu_b = 1.75 + i0.09$. As in §2.4.1, the shape dyadic of the constituent particles is taken to have the form (2.24), with the shape parameters selected for calculations being: $U_x = 1 + \rho$, $U_y = 1$ and $U_z = 1 - 0.5\rho$. The HCM which results is a Faraday chiral material [31, 32, 34]. A HCM of the same form also arises from the homogenization of a magnetically–biased plasma and an isotropic chiral material [44].

Particle size and volume fraction

We begin by considering the effect of particle size η in relation to volume fraction f_a. Accordingly, the eccentricity is fixed at $\rho = 0$, the orientation angle at $\varphi = 0$

and the correlation length at $L = 0$. The HCM constitutive dyadic has the form

$$\underline{\underline{\mathbf{K}}}_{HCM} = \begin{bmatrix} \epsilon_0 \begin{pmatrix} \epsilon^x_{HCM} & i\epsilon^g_{HCM} & 0 \\ -i\epsilon^g_{HCM} & \epsilon^x_{HCM} & 0 \\ 0 & 0 & \epsilon^z_{HCM} \end{pmatrix} & i\sqrt{\epsilon_0\mu_0} \begin{pmatrix} \xi^x_{HCM} & i\xi^g_{HCM} & 0 \\ -i\xi^g_{HCM} & \xi^x_{HCM} & 0 \\ 0 & 0 & \xi^z_{HCM} \end{pmatrix} \\ -i\sqrt{\epsilon_0\mu_0} \begin{pmatrix} \xi^x_{HCM} & i\xi^g_{HCM} & 0 \\ -i\xi^g_{HCM} & \xi^x_{HCM} & 0 \\ 0 & 0 & \xi^z_{HCM} \end{pmatrix} & \mu_0 \begin{pmatrix} \mu^x_{HCM} & i\mu^g_{HCM} & 0 \\ -i\mu^g_{HCM} & \mu^x_{HCM} & 0 \\ 0 & 0 & \mu^z_{HCM} \end{pmatrix} \end{bmatrix}. \tag{2.31}$$

In Figure 2.5, the real and imaginary parts of $\mu^{x,z,g}_{HCM}$ are plotted against $f_a \in (0, 1)$ for $\eta/\lambda_0 \in \{0, 0.05, 0.1\}$. As is the case in Figure 2.1, the HCM constitutive parameters are constrained such that they coincide with those of component phase b and a in the limits $f_a \to 0$ and 1, respectively. The effect of η on the real parts of $\mu^{x,z,g}_{HCM}$ are relatively modest. In contrast, η has a profound effect on the imaginary parts of $\mu^{x,z,g}_{HCM}$, especially for mid–range values of f_a. The pattern of behaviour presented in Figure 2.5 for the HCM permeability parameters $\mu^{x,z,g}_{HCM}$ is mirrored by the HCM permittivity parameters $\epsilon^{x,z,g}_{HCM}$ and magnetoelectric parameters $\xi^{x,z,g}_{HCM}$ which are not displayed in Figure 2.5.

Particle size and particle eccentricity

The effect of particle size η in relation to particle eccentricity is considered next. We set the volume fraction $f_a = 0.5$, orientation angle $\varphi = 0$ and the correlation

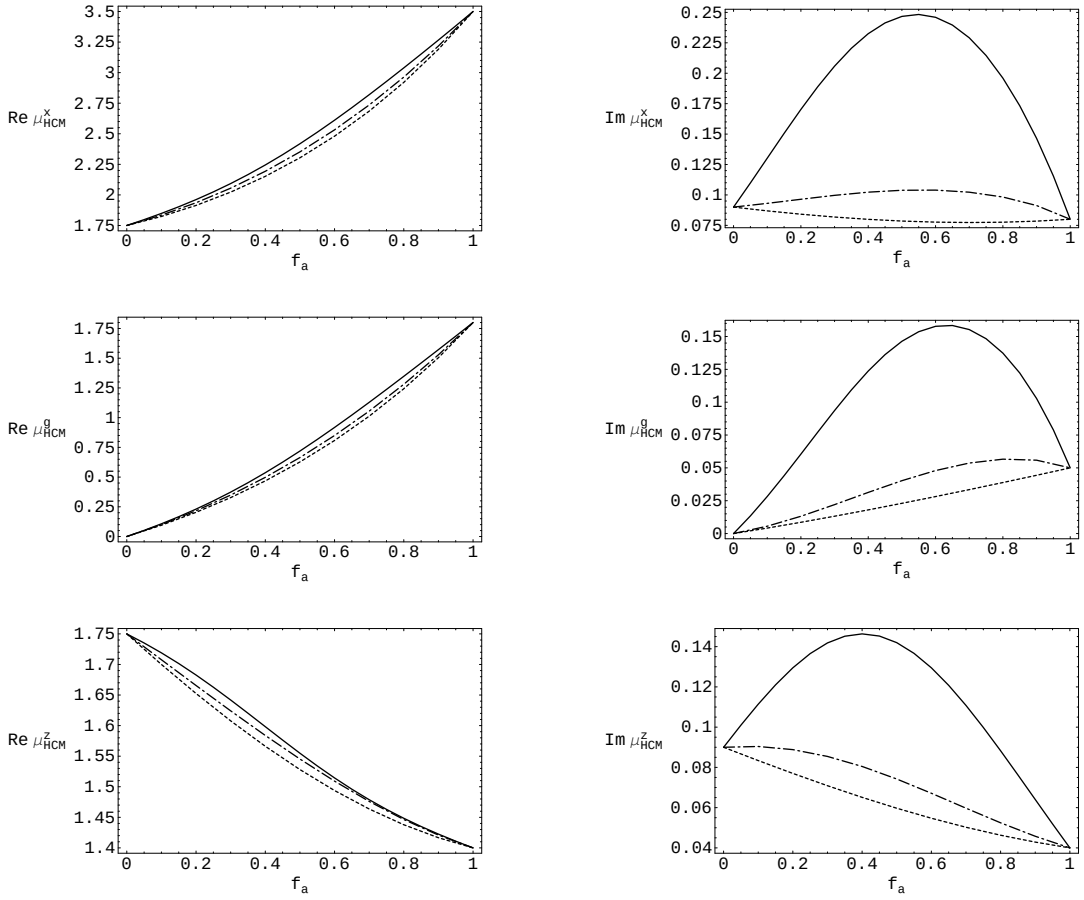

Figure 2.5: Real (left) and imaginary (right) parts of the HCM constitutive parameters $\mu^{x,z,g}_{HCM}$ plotted against volume fraction $f_a \in (0,1)$ for $\eta/\lambda_0 = 0$ (dashed curves), $\eta/\lambda_0 = 0.05$ (broken dashed curves) and $\eta/\lambda_0 = 0.1$ (solid curves). The HCM is a Faraday chiral material.

length $L = 0$. The HCM constitutive dyadic then has the form

$$\underline{\underline{\mathbf{K}}}_{HCM} =$$

$$\begin{bmatrix} \epsilon_0 \begin{pmatrix} \epsilon^x_{HCM} & i\epsilon^g_{HCM} & 0 \\ -i\epsilon^g_{HCM} & \epsilon^y_{HCM} & 0 \\ 0 & 0 & \epsilon^z_{HCM} \end{pmatrix} & i\sqrt{\epsilon_0\mu_0} \begin{pmatrix} \xi^x_{HCM} & i\xi^{g1}_{HCM} & 0 \\ -i\xi^{g2}_{HCM} & \xi^y_{HCM} & 0 \\ 0 & 0 & \xi^z_{HCM} \end{pmatrix} \\ -i\sqrt{\epsilon_0\mu_0} \begin{pmatrix} \xi^x_{HCM} & i\xi^{g2}_{HCM} & 0 \\ -i\xi^{g1}_{HCM} & \xi^y_{HCM} & 0 \\ 0 & 0 & \xi^z_{HCM} \end{pmatrix} & \mu_0 \begin{pmatrix} \mu^x_{HCM} & i\mu^g_{HCM} & 0 \\ -i\mu^g_{HCM} & \mu^y_{HCM} & 0 \\ 0 & 0 & \mu^z_{HCM} \end{pmatrix} \end{bmatrix}, \tag{2.32}$$

which is rather more general than the form (2.31). As a representative example, graphs of the real and imaginary parts of ξ^z_{HCM} versus $\rho \in (0,1)$ are exhibited in Figure 2.6 for $\eta/\lambda_0 \in \{0, 0.05, 0.1\}$. The real part of ξ^z_{HCM} is a strong function of ρ, whereas the imaginary part varies less as ρ increases. The sensitivity of both the real and imaginary parts of ξ^z_{HCM} to ρ is clearly influenced by the value of η. Patterns of behaviour with respect to ρ that are qualitatively similar to those displayed in Figure 2.6 are found for the HCM constitutive parameters $\epsilon^{x,y,z,g}_{HCM}$, $\xi^{x,y,g1,g2}_{HCM}$ and $\mu^{x,y,z,g}_{HCM}$ which are not represented in Figure 2.6.

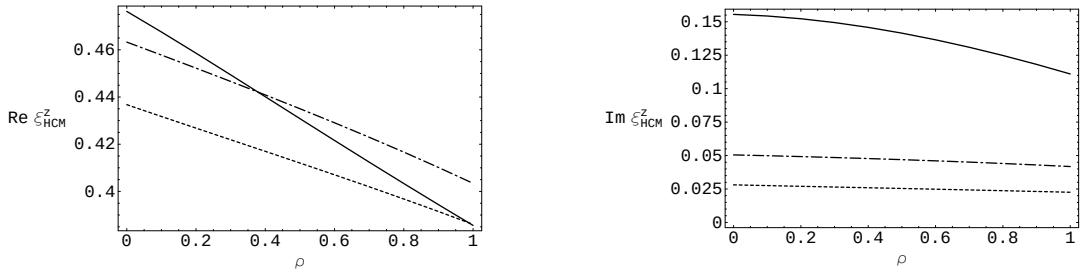

Figure 2.6: Real (left) and imaginary (right) parts of the HCM constitutive parameter ξ^z_{HCM} plotted against the eccentricity parameter $\rho \in (0,1)$ for $\eta/\lambda_0 = 0$ (dashed curves), $\eta/\lambda_0 = 0.05$ (broken dashed curves) and $\eta/\lambda_0 = 0.1$ (solid curves). The HCM is a Faraday chiral material.

Particle size and particle orientation

Now we turn to effect of particle size η in relation to particle orientation. Let us fix the following parameters: volume fraction $f_a = 0.5$, particle eccentricity $\rho = 1$ and the correlation length $L = 0$. Consequently, the HCM constitutive dyadic

has the form

$$\underline{\underline{\mathbf{K}}}_{HCM} = \left[\begin{array}{cc} \epsilon_0 \begin{pmatrix} \epsilon^x_{HCM} & i\epsilon^{g1}_{HCM} & 0 \\ -i\epsilon^{g2}_{HCM} & \epsilon^y_{HCM} & 0 \\ 0 & 0 & \epsilon^z_{HCM} \end{pmatrix} & i\sqrt{\epsilon_0\mu_0} \begin{pmatrix} \xi^x_{HCM} & i\xi^{g1}_{HCM} & 0 \\ -i\xi^{g2}_{HCM} & \xi^y_{HCM} & 0 \\ 0 & 0 & \xi^z_{HCM} \end{pmatrix} \\ -i\sqrt{\epsilon_0\mu_0} \begin{pmatrix} \zeta^x_{HCM} & i\zeta^{g1}_{HCM} & 0 \\ -i\zeta^{g2}_{HCM} & \zeta^y_{HCM} & 0 \\ 0 & 0 & \xi^z_{HCM} \end{pmatrix} & \mu_0 \begin{pmatrix} \mu^x_{HCM} & i\mu^{g1}_{HCM} & 0 \\ -i\mu^{g2}_{HCM} & \mu^y_{HCM} & 0 \\ 0 & 0 & \mu^z_{HCM} \end{pmatrix} \end{array}\right], \tag{2.33}$$

which is more general than (2.31) and (2.32). As illustrative examples, the the real and imaginary parts of $\epsilon^{x,g1}_{HCM}$ are plotted in Figure 2.7 against $\varphi \in (0, \pi/2)$ for $\eta/\lambda_0 \in \{0, 0.05, 0.1\}$. The particle size η has a strong influence on the real and imaginary parts of ϵ^{g1}_{HCM}, as well as on the imaginary part of ϵ^x_{HCM}. The influence on the real part of ϵ^x_{HCM} is smaller by comparison, but still significant. The graphs for ϵ^{g1}_{HCM} are symmetric about the line $\varphi = \pi/4$ whereas those for ϵ^x_{HCM} are not. Broadly similar behaviour is exhibited by the HCM constitutive parameters not plotted in Figure 2.7, namely, $\epsilon^{y,z,g2}_{HCM}$, $\xi^{x,y,z,g1,g2}_{HCM}$, $\zeta^{x,y,g1,g2}_{HCM}$ and $\mu^{x,y,z,g1,g2}_{HCM}$.

Particle size and correlation length

Finally, to focus upon the effect of particle size η in relation to correlation length L, the volume fraction is fixed at $f_a = 0.5$, the orientation angle at $\varphi = 0$ and the eccentricity parameter at $\rho = 0$. The corresponding HCM constitutive dyadic has the form (2.31). In Figure 2.8, the real and imaginary parts of μ^g_{HCM} are plotted against $k_0 L \in (0, 0.2)$ for $\eta/L \in \{0, 0.5, 0.95\}$. The pattern of behaviour with respect to L is similar to that presented in Figure 2.4 for the biaxial bi-isotropic HCM. That is, the imaginary part of μ^g_{HCM} is more obviously sensitive to inceasing L than is the real part. In addition, both the real and imaginary

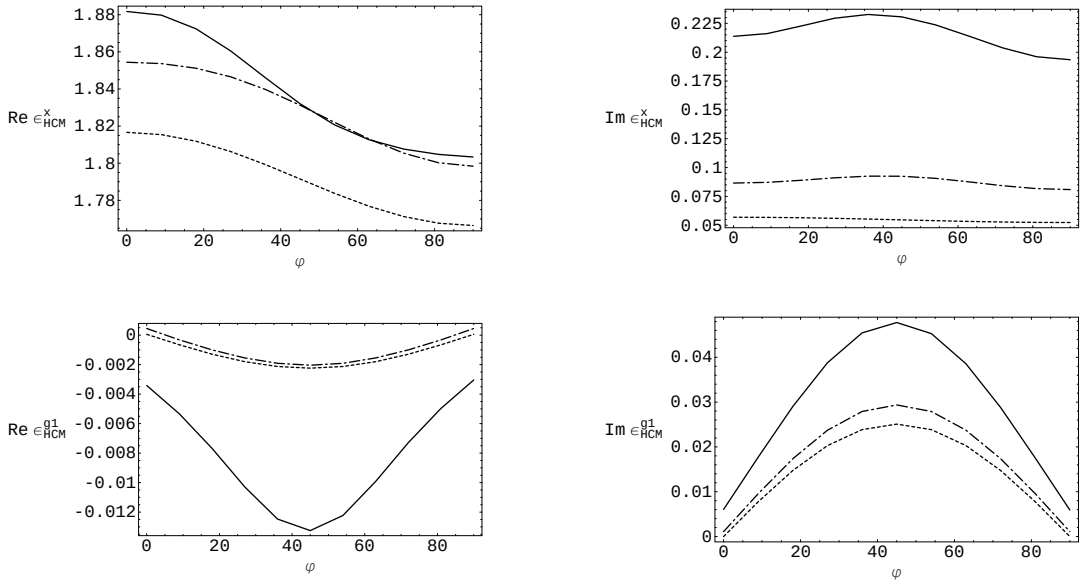

Figure 2.7: Real (left) and imaginary (right) parts of the HCM constitutive parameters $\epsilon^{x,g1}_{HCM}$ plotted against orientation angle $\varphi \in (0, \pi/2)$ for $\eta/\lambda_0 = 0$ (dashed curves), $\eta/\lambda_0 = 0.05$ (broken dashed curves) and $\eta/\lambda_0 = 0.1$ (solid curves). The HCM is a Faraday chiral material.

parts of μ^{g}_{HCM} are more sensitive to L at larger values of η. The other HCM constitutive parameters, namely $\epsilon^{x,z,g}_{HCM}$, $\xi^{x,z,g}_{HCM}$ and $\mu^{x,z}_{HCM}$, respond in a generally similar manner as L increases for the three values of η considered here.

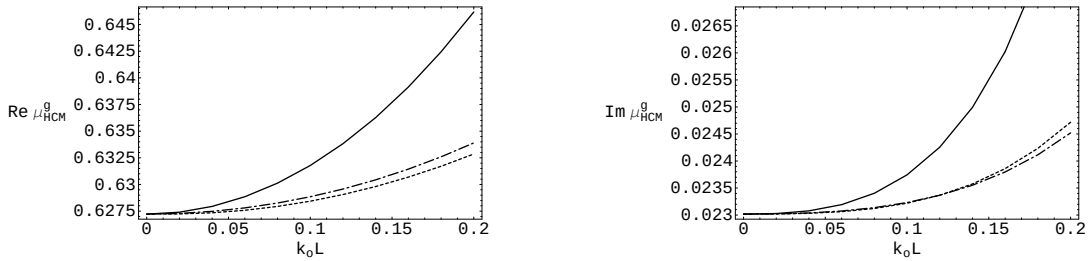

Figure 2.8: Real (left) and imaginary (right) parts of the HCM constitutive parameter μ^{g}_{HCM} plotted against relative correlation length $k_0L \in (0, 0.2)$ for $\eta/L = 0$ (dashed curves), $\eta/L = 0.5$ (broken dashed curves) and $\eta/L = 0.95$ (solid curves). The HCM is a Faraday chiral material.

2.5 Concluding remarks

Homogenization formalisms, such as the widely-used Maxwell Garnett and Bruggeman formalisms, often inadequately take into account the distributional statistics and sizes of the component phase particles. The SPFT — through describing the distributional statistics of the component phases in terms of a hierarchy of spatial correlation functions — provides a conspicuous exception. In the preceding sections, an extension to the SPFT for the most general linear class of HCM is developed, in which a nonzero volume is attributed to the component phase particles. By means of extensive numerical calculations, based on Lorentz–reciprocal and Lorentz–nonreciprocal HCMs, it is demonstrated that estimates of the HCM constitutive parameters in relation to volume fraction, particle eccentricity, particle orientation and correlation length are all significantly influenced by the size of the component phase particles. It is particularly noteworthy that the influence of the particle size is generally stronger on the imaginary parts of the HCM constitutive parameters than it is on the corresponding real parts. In this respect, the effect of η is reminiscent of the effect of the correlation length in the second order SPFT [25]. Increasing the correlation length for the second order SPFT generally results in an increase in the degree of dissipation associated with the HCM. This dissipative loss is attributed to radiative scattering losses from the macroscopic coherent field [8, 35]. It may be observed in Figures (2.4) and (2.8) (and in other Figures presented in Appendix 1) that the effects of particle size and correlation length on the estimates of the imagine the HCM constitutive parameters are generally cumulative. This suggests that coherent scattering losses associated with the HCM become greater as the particle size increases. A similar finding was reported for anisotropic dielectric HCMs [42]. In conclusion, the importance of incorporating microstructural details, such component particle size and spatial distribution, within homogenization formalisms is further emphasized by this study.

Chapter 3

Weakly nonlinear anisotropic composites

3.1 Overview

An implementation of the strong–permittivity–fluctuation theory (SPFT) is presented in order to estimate the constitutive parameters of a homogenized composite material (HCM) which is both cubically nonlinear and anisotropic. Unlike conventional approaches to homogenization, the particles which comprise the component material phases are herein assumed to be small but not vanishingly small. The influence of particle size on the estimates of the HCM constitutive parameters is illustrated by means of a representative numerical example. It is observed that, by taking the nonzero particle size into consideration, attenuation is predicted and nonlinear enhancement is somewhat diminished. In these respects, the effect of particle size is similar to that of correlation length within the bilocally–approximated SPFT.

3.1.1 Homogenization preliminaries

The homogenization of two component material phases, namely phase a and phase b, is considered. Each component phase is an isotropic dielectric material; and, in general, each is cubically nonlinear. Thus, the permittivities of the component

material phases are expressed as

$$\epsilon_\ell = \epsilon_{\ell 0} + \chi_\ell \, | \, \underline{E}_\ell \, |^2, \qquad\qquad (\ell = a, b), \tag{3.1}$$

with $\epsilon_{\ell 0}$ being the linear permittivity, χ_ℓ the nonlinear susceptibility, and $\underline{E}_\ell$ is the electric field developed inside a region of phase ℓ by illumination of the composite material. The assumption of weak nonlinearity ensures that $| \, \epsilon_{\ell 0} \, | \gg | \, \chi_\ell \, | \, | \, \underline{E}_\ell \, |^2$. Notice that nonlinear permittivities of the form (3.1) describe electrostrictive materials which can induce stimulated Brillouin scattering [50].

The component material phases a and b are made up of ellipsoidal particles. The particles all have the same shape and orientation, as specified by the shape dyadic (2.24). The distributional statistics of the component phases are as described in (1.3.3). In this Chapter we consider the second–order SPFT in which the two–point covariance function (1.30) is adopted.

$$\underline{r}^e(\theta, \phi) = \eta \, \underline{\underline{U}} \cdot \underline{\hat{r}} \, (\theta, \phi), \tag{3.2}$$

where $\underline{\hat{r}} \, (\theta, \phi)$ is the radial unit vector specified by the spherical polar coordinates θ and ϕ. The size parameter η provides a measure of the linear dimensions of the ellipsoidal particles. It is assumed that η is much smaller than the electromagnetic wavelengths, but not vanishingly small.

The component phase particles are randomly distributed throughout a region of volume V, which is partitioned into the disjoint regions of volume V_a and V_b containing phase a and b, respectively. Thus, the component phase distributions are characterized in terms of statistical moments of the characteristic functions

$$\Phi_\ell(\underline{r}) = \begin{cases} 1, & \underline{r} \in V_\ell, \\ \\ 0, & \underline{r} \notin V_\ell, \end{cases} \qquad\qquad (\ell = a, b). \tag{3.3}$$

In order for V to be completely filled by either phase a or b material, the size parameter η should be interpreted as providing a measure of the particle size on average. The first statistical moment of Φ_ℓ delivers the volume fraction of

phase ℓ, i.e., $\langle\, \Phi_\ell(\underline{r})\,\rangle = f_\ell$. Plainly, $f_a + f_b = 1$. The two–point covariance function which constitutes the second statistical moment of Φ_ℓ is taken as the physically–motivated form [27]

$$\langle\, \Phi_\ell(\underline{r})\, \Phi_\ell(\underline{r}')\,\rangle = \begin{cases} \langle\, \Phi_\ell(\underline{r})\,\rangle\langle \Phi_\ell(\underline{r}')\,\rangle\,, & |\, \underline{\underline{U}}^{-1} \cdot (\underline{r} - \underline{r}')\,| > L\,, \\ \\ \langle\, \Phi_\ell(\underline{r})\,\rangle\,, & |\, \underline{\underline{U}}^{-1} \cdot (\underline{r} - \underline{r}')\,| \leq L\,, \end{cases} \tag{3.4}$$

where $L > 0$ is the correlation length. Within the SPFT, the estimates of HCM constitutive parameters are largely insensitive to the specific form of the covariance function, as has been shown by comparative studies [46, 26].

3.1.2 Depolarization dyadic

Let us focus our attention on a single component phase particle of volume V^e, characterized by the shape dyadic $\underline{\underline{U}}$ and size parameter η. Suppose that this particle is embedded in a comparison material. In consonance with the ellipsoidal geometry of the component phase particles and the weakly nonlinear permittivities of the component material phases, the comparison material is a weakly nonlinear, anisotropic, dielectric material characterized by the permittivity dyadic

$$\begin{aligned} \underline{\underline{\epsilon}}_{cm} &= \underline{\underline{\epsilon}}_{cm0} + \underline{\underline{\chi}}_{cm}\, |\, \underline{E}_{HCM}\,|^2 \\ &= \mathrm{diag}\,(\epsilon^x_{cm0},\, \epsilon^y_{cm0},\, \epsilon^z_{cm0}) + \mathrm{diag}\,(\chi^x_{cm},\, \chi^y_{cm},\, \chi^z_{cm})\;|\, \underline{E}_{HCM}\,|^2, \end{aligned} \tag{3.5}$$

where $\underline{E}_{HCM}$ denotes the spatially–averaged electric field in the HCM. The eigenvectors of $\underline{\underline{\epsilon}}_{cm}$ are aligned with those of $\underline{\underline{U}}$.

The depolarization dyadic [2] (1.26) provides the electromagnetic response of the ellipsoidal particle embedded in the comparison material. Here, the dyadic Green function of the comparison material, namely $\underline{\underline{G}}_{cm}(\underline{r})$, satisfies the nonhomogeneous vector Helmholtz equation (2.3) An explicit representation of $\underline{\underline{G}}_{cm}(\underline{r})$ is not generally available [28], but its Fourier transform,

$$\underline{\underline{\tilde{G}}}_{cm}(\underline{q}) = \int_{\underline{r}} \underline{\underline{G}}_{cm}(\underline{r})\, \exp(-i\underline{q} \cdot \underline{r})\, d^3\underline{r}, \tag{3.6}$$

may be deduced from (2.3) as

$$\underline{\underline{\tilde{G}}}_{cm}(\underline{q}) = -i\omega\mu_0 \left(\underline{q} \times \underline{q} \times \underline{\underline{I}} + \omega^2 \mu_0 \, \underline{\underline{\epsilon}}_{cm} \right)^{-1}. \tag{3.7}$$

By combining (1.26), (3.6) and (3.7),

$$\underline{\underline{D}} = \frac{\eta}{2\pi^2} \int_{\underline{q}} \frac{1}{q^2} \left[\frac{\sin(q\eta)}{q\eta} - \cos(q\eta) \right] \underline{\underline{\tilde{G}}}_{cm}(\underline{\underline{U}}^{-1} \cdot \underline{q}) \, d^3\underline{q} \tag{3.8}$$

is obtained, after some simplification [2, 3]. In this Chapter, for reasons of clarity, we omit the subscripts on $\underline{\underline{D}}$. It is to be understood here that $\underline{\underline{D}} \equiv \underline{\underline{D}}_{U/cm}$.

3.1.3 Depolarization contributions from regions of nonzero volume

As in [42], we express the depolarization dyadic as the sum

$$\underline{\underline{D}} = \underline{\underline{D}}^{\eta=0} + \underline{\underline{D}}^{\eta>0}, \tag{3.9}$$

where the dyadic (2.10) represents the depolarization contribution arising from the region of vanishingly small volume $\lim_{\eta\to 0} V^e$, whereas the dyadic (2.9) provides the depolarization contribution arising from the region of nonzero volume $\left(V^e - \lim_{\eta\to 0} V^e \right)$.

Depolarization dyadics associated with vanishingly small regions have been studied extensively [49, 3]. The volume integral (2.10) reduces to the η–independent surface integral [2]

$$\underline{\underline{D}}^{\eta=0} = \frac{1}{4\pi i\omega} \int_{\phi=0}^{2\pi} \int_{\theta=0}^{\pi} \left[\frac{1}{\mathrm{tr}\left(\underline{\underline{\epsilon}}_{cm} \cdot \underline{\underline{A}} \right)} \underline{\underline{A}} \right] \sin\theta \, d\theta \, d\phi, \tag{3.10}$$

with

$$\underline{\underline{A}} = \mathrm{diag} \left(\frac{\sin^2\theta \, \cos^2\phi}{U_x^2}, \frac{\sin^2\theta \, \sin^2\phi}{U_y^2}, \frac{\cos^2\theta}{U_z^2} \right). \tag{3.11}$$

An elliptic function representation for $\underline{\underline{D}}^{\eta=0}$ is available [53] (which simplifies to a hyperbolic function representation in the case of a spheroidal depolarization

region [2]), but for our present purposes the integral representation (3.10) is more convenient.

Depolarization dyadics associated with small regions of nonzero volume have lately come under scrutiny for anisotropic [42] and bianisotropic [51] HCMs. As described elsewhere [48, 42], by the calculus of residues the anisotropic dielectric specialization of (2.9) reduces to

$$\underline{\underline{D}}^{\eta>0} = \frac{1}{4\pi i\omega}\,\underline{\underline{W}}(\eta), \tag{3.12}$$

where the dyadic function

$$\begin{aligned}\underline{\underline{W}}(\eta) &= \eta^3 \int_{\phi=0}^{2\pi}\int_{\theta=0}^{\pi} \frac{\sin\theta}{3\,\Delta} \\ &\left\{ \left[\frac{3\,(\kappa_+ - \kappa_-)}{2\eta} + i\left(\kappa_+^{\frac{3}{2}} - \kappa_-^{\frac{3}{2}}\right)\right]\underline{\underline{\alpha}} + i\omega^2\mu_0\,\left(\kappa_+^{\frac{1}{2}} - \kappa_-^{\frac{1}{2}}\right)\underline{\underline{\beta}} \right\}\, d\theta\, d\phi\end{aligned} \tag{3.13}$$

is introduced. Herein, the dyadics

$$\begin{aligned}\underline{\underline{\alpha}} &= \left[2\,\underline{\underline{\epsilon}}_{cm} - \mathrm{tr}\left(\underline{\underline{\epsilon}}_{cm}\right)\,\underline{\underline{I}}\right]\,\cdot\underline{\underline{A}} \\ &- \mathrm{tr}\left(\underline{\underline{\epsilon}}_{cm}\cdot\underline{\underline{A}}\right)\,\underline{\underline{I}} - \frac{\mathrm{tr}\left(\underline{\underline{\epsilon}}_{cm}^{adj}\cdot\underline{\underline{A}}\right) - \left[\mathrm{tr}\left(\underline{\underline{\epsilon}}_{cm}^{adj}\right)\,\mathrm{tr}\left(\underline{\underline{A}}\right)\right]}{\mathrm{tr}\left(\underline{\underline{\epsilon}}_{cm}\cdot\underline{\underline{A}}\right)}\,\underline{\underline{A}},\end{aligned}$$

$$\underline{\underline{\beta}} = \underline{\underline{\epsilon}}_{cm}^{adj} - \frac{\det\left(\underline{\underline{\epsilon}}_{cm}\right)}{\mathrm{tr}\left(\underline{\underline{\epsilon}}_{cm}\cdot\underline{\underline{A}}\right)}\,\underline{\underline{A}}$$

and the scalars

$$\Delta = \sqrt{t_B^2 - 4t_A t_C}, \tag{3.14}$$

$$\kappa_\pm = \mu_0\omega^2\frac{-t_B \pm \Delta}{2t_C}, \tag{3.15}$$

with

$$\left.\begin{aligned} t_A &= \det\left(\underline{\underline{\epsilon}}_{cm}\right) \\ t_B &= \mathrm{tr}\left(\underline{\underline{\epsilon}}_{cm}^{adj}\cdot\underline{\underline{A}}\right) - \left[\mathrm{tr}\left(\underline{\underline{\epsilon}}_{cm}^{adj}\right)\,\mathrm{tr}\left(\underline{\underline{A}}\right)\right] \\ t_C &= \mathrm{tr}\left(\underline{\underline{\epsilon}}_{cm}\cdot\underline{\underline{A}}\right)\,\mathrm{tr}\left(\underline{\underline{A}}\right)\end{aligned}\right\}. \tag{3.16}$$

Often the approximation $\underline{\underline{D}} \approx \underline{\underline{D}}^{\eta=0}$ is implemented in homogenization studies [30]. However, studies of isotropic [15, 16, 18, 37, 17, 19], anisotropic [42] and bianisotropic [51] HCMs have emphasized the importance of the nonzero spatial extent of depolarization regions.

3.1.4 Linear and weakly nonlinear depolarization contributions

We exploit the fact that the comparison material permittivity (3.5) is the sum of a linear part and a weakly nonlinear part to similarly express

$$\begin{aligned} \underline{\underline{D}} &= \underline{\underline{D}}_0 + \underline{\underline{D}}_1 \,|\, \underline{E}_{HCM} \,|^2 \\ &= \underline{\underline{D}}_0^{\eta=0} + \underline{\underline{D}}_0^{\eta>0} + \left(\underline{\underline{D}}_1^{\eta=0} + \underline{\underline{D}}_1^{\eta>0} \right) |\, \underline{E}_{HCM} \,|^2, \end{aligned} \tag{3.17}$$

where

$$\underline{\underline{D}}^{\eta\geq 0} = \underline{\underline{D}}_0^{\eta\geq 0} + \underline{\underline{D}}_1^{\eta\geq 0} \,|\, \underline{E}_{HCM} \,|^2. \tag{3.18}$$

The linear and weakly nonlinear contributions to $\underline{\underline{D}}^{\eta=0}$ have been derived earlier [48]; these are

$$\underline{\underline{D}}_0^{\eta=0} = \frac{1}{4\pi i\omega} \int_{\phi=0}^{2\pi} \int_{\theta=0}^{\pi} \left[\frac{1}{\mathrm{tr}\left(\underline{\underline{\epsilon}}_{cm0} \cdot \underline{\underline{A}} \right)} \underline{\underline{A}} \right] \sin\theta \; d\theta \, d\phi, \tag{3.19}$$

$$\underline{\underline{D}}_1^{\eta=0} = -\frac{1}{4\pi i\omega} \int_{\phi=0}^{2\pi} \int_{\theta=0}^{\pi} \left\{ \frac{\mathrm{tr}\left(\underline{\underline{\chi}}_{cm} \cdot \underline{\underline{A}} \right)}{\left[\mathrm{tr}\left(\underline{\underline{\epsilon}}_{cm0} \cdot \underline{\underline{A}} \right) \right]^2} \underline{\underline{A}} \right\} \sin\theta \; d\theta \, d\phi. \tag{3.20}$$

The linear and weakly nonlinear contributions to $\underline{\underline{D}}^{\eta>0}$ — and, equivalently, $\underline{\underline{W}}(\eta)$ — follow from corresponding contributions for an expression analogous to (3.13) which crops up in the bilocally–approximated SPFT [8, 48]. Thus, we have

$$\underline{\underline{W}}(\eta) = \underline{\underline{W}}_0(\eta) + \underline{\underline{W}}_1(\eta) \,|\, \underline{E}_{HCM} \,|^2 \tag{3.21}$$

with

$$\underline{\underline{W}}_0(\eta) = \eta^3 \int_{\phi=0}^{2\pi} \int_{\theta=0}^{\pi} \frac{\sin\theta}{3\,\Delta_0} \left[\tau_\alpha(\eta) \, \underline{\underline{\alpha}}_0 + \tau_\beta \, \underline{\underline{\beta}}_0 \right] \, d\theta \, d\phi \tag{3.22}$$

and

$$\underline{\underline{W}}_1(\eta) = \eta^3 \int_{\phi=0}^{2\pi} \int_{\theta=0}^{\pi} \frac{\sin\theta}{3\,\Delta_0} \Bigg\{ \tau_\alpha(\eta) \left(\underline{\underline{\alpha}}_1 - \frac{\Delta_1}{\Delta_0} \underline{\underline{\alpha}}_0 \right) + \tau_\beta \left(\underline{\underline{\beta}}_1 - \frac{\Delta_1}{\Delta_0} \underline{\underline{\beta}}_0 \right)$$

$$+ \frac{3}{2} \Big[\left(\frac{1}{\eta} + i\kappa_{0+}^{\frac{1}{2}} \right) \kappa_{1+} - \left(\frac{1}{\eta} + i\kappa_{0-}^{\frac{1}{2}} \right) \kappa_{1-} \Big] \underline{\underline{\alpha}}_0 + \frac{i}{2} \left(\frac{\kappa_{1+}}{\kappa_{0+}^{\frac{1}{2}}} - \frac{\kappa_{1-}}{\kappa_{0-}^{\frac{1}{2}}} \right) \underline{\underline{\beta}}_0 \Bigg\}$$

$$d\theta\, d\phi, \tag{3.23}$$

where

$$\left.\begin{aligned} \tau_\alpha(\eta) &= \frac{3\left(\kappa_{0+} - \kappa_{0-}\right)}{2\eta} + i\left(\kappa_{0+}^{\frac{3}{2}} - \kappa_{0-}^{\frac{3}{2}}\right) \\ \tau_\beta &= i\omega^2\mu_0 \left(\kappa_{0+}^{\frac{1}{2}} - \kappa_{0-}^{\frac{1}{2}}\right) \end{aligned}\right\}. \tag{3.24}$$

The dyadics $\underline{\underline{\alpha}}_0$ and $\underline{\underline{\beta}}_0$, and scalars $\kappa_{0\pm}$ and Δ_0, herein represent the linear parts of their counterpart dyadics $\underline{\underline{\alpha}}$ and $\underline{\underline{\beta}}$, and scalars $\kappa_\pm$ and Δ, as per [48]

$$\begin{aligned} \underline{\underline{\alpha}}_0 &= \left[2\,\underline{\underline{\epsilon}}_{cm0} - \mathrm{tr}\left(\underline{\underline{\epsilon}}_{cm0}\right) \underline{\underline{I}} \right] \cdot \underline{\underline{A}} - \mathrm{tr}\left(\underline{\underline{\epsilon}}_{cm0} \cdot \underline{\underline{A}}\right) \underline{\underline{I}} \\ &- \frac{\mathrm{tr}\left(\underline{\underline{\epsilon}}_{cm0}^{adj} \cdot \underline{\underline{A}}\right) - \left[\mathrm{tr}\left(\underline{\underline{\epsilon}}_{cm0}^{adj}\right) \mathrm{tr}\left(\underline{\underline{A}}\right) \right]}{\mathrm{tr}\left(\underline{\underline{\epsilon}}_{cm0} \cdot \underline{\underline{A}}\right)} \underline{\underline{A}}, \\ \underline{\underline{\beta}}_0 &= \underline{\underline{\epsilon}}_{cm0}^{adj} - \frac{\det\left(\underline{\underline{\epsilon}}_{cm0}\right)}{\mathrm{tr}\left(\underline{\underline{\epsilon}}_{cm0} \cdot \underline{\underline{A}}\right)} \underline{\underline{A}}, \\ \kappa_{0\pm} &= \mu_0\omega^2 \frac{-t_{B0} \pm \Delta_0}{2t_{C0}}, \\ \Delta_0 &= \sqrt{t_{B0}^2 - 4t_{A0}t_{C0}}, \end{aligned} \tag{3.25}$$

with

$$\left.\begin{aligned} t_{A0} &= \det\left(\underline{\underline{\epsilon}}_{cm0}\right) \\ t_{B0} &= \mathrm{tr}\left(\underline{\underline{\epsilon}}_{cm0}^{adj} \cdot \underline{\underline{A}}\right) - \left[\mathrm{tr}\left(\underline{\underline{\epsilon}}_{cm0}^{adj}\right) \mathrm{tr}\left(\underline{\underline{A}}\right) \right] \\ t_{C0} &= \mathrm{tr}\left(\underline{\underline{\epsilon}}_{cm0} \cdot \underline{\underline{A}}\right) \mathrm{tr}\left(\underline{\underline{A}}\right) \end{aligned}\right\}. \tag{3.26}$$

Moreover, the weakly nonlinear contributions to $\underline{\underline{\alpha}}$, $\underline{\underline{\beta}}$, $\kappa_{\pm}$ and Δ are provided as [48]

$$\begin{aligned}
\underline{\underline{\alpha}}_1 &= \left[2\,\underline{\underline{\chi}}_{cm} - \frac{t_{B1}t_{C0} - t_{B0}t_{C1}}{t_{C0}\,\mathrm{tr}\left(\underline{\underline{\epsilon}}_{cm0}\cdot\underline{\underline{A}}\right)} - \mathrm{tr}\left(\underline{\underline{\chi}}_{cm}\right)\,\underline{\underline{I}} \right]\cdot\underline{\underline{A}} - \\
&\quad \mathrm{tr}\left(\underline{\underline{\chi}}_{cm}\cdot\underline{\underline{A}}\right)\,\underline{\underline{I}}\,, \\
\underline{\underline{\beta}}_1 &= \underline{\underline{\Upsilon}} - \frac{t_{B1}t_{C0} - t_{B0}t_{C1}}{t_{C0}\,\mathrm{tr}\left(\underline{\underline{\epsilon}}_{cm0}\cdot\underline{\underline{A}}\right)}\,\underline{\underline{A}}\,, \\
\kappa_{1\pm} &= \frac{\omega^2\,(\,-t_{B1} \pm \Delta_1\,) - 2t_{C1}\,\kappa_{0\pm}}{2\,t_{C0}}\,, \\
\Delta_1 &= \frac{t_{B0}t_{B1} - 2\,(\,t_{A1}t_{C0} + t_{A0}t_{C1}\,)}{\Delta_0}\,,
\end{aligned} \tag{3.27}$$

with

$$\left.\begin{aligned}
t_{A1} &= \chi^x_{cm}\,\epsilon^y_{cm0}\,\epsilon^z_{cm0} + \epsilon^x_{cm0}\,\chi^y_{cm}\,\epsilon^z_{cm0} + \epsilon^x_{cm0}\,\epsilon^y_{cm0}\,\chi^z_{cm} \\
t_{B1} &= \mathrm{tr}\left(\underline{\underline{\Upsilon}}\cdot\underline{\underline{A}}\right) - \left[\,\mathrm{tr}\left(\underline{\underline{\Upsilon}}\right)\,\mathrm{tr}\left(\underline{\underline{A}}\right)\right] \\
t_{C1} &= \mathrm{tr}\left(\underline{\underline{A}}\right)\,\mathrm{tr}\left(\underline{\underline{\chi}}_{cm}\cdot\underline{\underline{A}}\right)
\end{aligned}\right\}, \tag{3.28}$$

and

$$\underline{\underline{\Upsilon}} = \mathrm{diag}\,(\,\chi^y_{cm}\,\epsilon^z_{cm0} + \epsilon^y_{cm0}\,\chi^z_{cm},\ \chi^z_{cm}\,\epsilon^x_{cm0} + \epsilon^z_{cm0}\,\chi^x_{cm},\ \chi^x_{cm}\,\epsilon^y_{cm0} + \epsilon^x_{cm0}\,\chi^y_{cm}\,)\,. \tag{3.29}$$

3.2 SPFT estimate of HCM permittivity

Now that the linear and nonlinear contributions to the depolarization dyadic have been established for depolarization regions of nonzero volume, we can amalgamate these expressions with the SPFT for weakly nonlinear anisotropic dielectric HCMs — which is presented elsewhere [48] — and thereby estimate the HCM permittivity. Notice that the SPFT estimate of the HCM constitutive parameters is developed under the assumption that the correlation length L is much smaller than the electromagnetic wavelengths. In turn, the correlation length is required to be larger than the particle size parameter η.

As a precursor, an estimate of permittivity dyadic of the comparison material

must first be computed. The Bruggeman homogenization formalism (which is, in fact, equivalent to the lowest–order SPFT [8]) is used for this purpose. Thus, $\underline{\underline{\epsilon}}_{cm}$ is found by solving the nonlinear equations

$$f_a \, \underline{\underline{X}}_{a\mathrm{j}} + f_b \, \underline{\underline{X}}_{b\mathrm{j}} = \underline{\underline{0}}, \qquad (\mathrm{j} = 0, 1), \tag{3.30}$$

where

$$\left.\begin{aligned} \underline{\underline{X}}_{\ell 0} &= -i\,\omega \left(\epsilon_{\ell 0}\, \underline{\underline{I}} - \underline{\underline{\epsilon}}_{cm0} \right) \cdot \underline{\underline{\Gamma}}_{\ell 0}^{-1} \\ \underline{\underline{X}}_{\ell 1} &= -i\,\omega \left[\left(g_\ell \, \chi_\ell \, \underline{\underline{I}} - \underline{\underline{\chi}}_{cm} \right) \cdot \underline{\underline{\Gamma}}_{\ell 0}^{-1} + \left(\epsilon_{\ell 0}\, \underline{\underline{I}} - \underline{\underline{\epsilon}}_{cm0} \right) \cdot \underline{\underline{\Lambda}}_{\ell} \right] \end{aligned}\right\}, \qquad (\ell = a, b), \tag{3.31}$$

are the linear and nonlinear parts, respectively, of the corresponding polarizability dyadics. Herein,

$$\begin{aligned} \underline{\underline{\Lambda}}_{\ell} &= \frac{1}{\det\left(\underline{\underline{\Gamma}}_{\ell 0} \right)} \\ &\left[\mathrm{diag}\left(\Gamma^y_{\ell 1}\Gamma^z_{\ell 0} + \Gamma^y_{\ell 0}\Gamma^z_{\ell 1},\, \Gamma^z_{\ell 1}\Gamma^x_{\ell 0} + \Gamma^z_{\ell 0}\Gamma^x_{\ell 1},\, \Gamma^y_{\ell 1}\Gamma^x_{\ell 0} + \Gamma^y_{\ell 0}\Gamma^x_{\ell 1} \right) - \rho_\ell \, \underline{\underline{\Gamma}}_{\ell 0}^{-1} \right], \end{aligned} \tag{3.32}$$

with

$$\rho_\ell = \Gamma^x_{\ell 0}\Gamma^y_{\ell 0}\Gamma^z_{\ell 1} + \Gamma^x_{\ell 0}\Gamma^y_{\ell 1}\Gamma^z_{\ell 0} + \Gamma^x_{\ell 1}\Gamma^y_{\ell 0}\Gamma^z_{\ell 0}, \tag{3.33}$$

are expressed in terms of components of the dyadics

$$\left.\begin{aligned} \underline{\underline{\Gamma}}_{\ell 0} &= \underline{\underline{I}} + i\omega \, \underline{\underline{D}}_0 \cdot \left(\epsilon_{\ell 0}\, \underline{\underline{I}} - \underline{\underline{\epsilon}}_{cm0} \right) = \mathrm{diag}\left(\Gamma^x_{\ell 0},\, \Gamma^y_{\ell 0},\, \Gamma^z_{\ell 0} \right) \\ \underline{\underline{\Gamma}}_{\ell 1} &= i\omega \left[\underline{\underline{D}}_0 \cdot \left(g_\ell \, \chi_\ell \, \underline{\underline{I}} - \underline{\underline{\chi}}_{cm} \right) + \underline{\underline{D}}_1 \cdot \left(\epsilon_{\ell 0}\, \underline{\underline{I}} - \underline{\underline{\epsilon}}_{cm0} \right) \right] \\ &= \mathrm{diag}\left(\Gamma^x_{\ell 1},\, \Gamma^y_{\ell 1},\, \Gamma^z_{\ell 1} \right) \end{aligned}\right\}; \tag{3.34}$$

and the local field factor is estimated by [54]

$$g_\ell = \left| \frac{1}{3} \left[\mathrm{tr}\left(\underline{\underline{\Gamma}}_{\ell 0}^{-1} \right) \right] \right|^2. \tag{3.35}$$

Estimates of the $\underline{\underline{\epsilon}}_{cm0}$ and $\underline{\underline{\chi}}_{cm}$ may be straightforwardly extracted from (3.30) by recursive schemes; see [48] for details.

Finally, the bilocally–approximated SPFT estimate of the HCM permittivity dyadic, namely

$$\underline{\underline{\epsilon}}_{\Omega} = \underline{\underline{\epsilon}}_{\Omega 0} + \underline{\underline{\chi}}_{\Omega} \, | \, \underline{E}_{HCM} \, |^2 = \mathrm{diag} \, (\epsilon^x_{\Omega 0}, \, \epsilon^y_{\Omega 0}, \, \epsilon^z_{\Omega 0}) + \mathrm{diag} \, (\chi^x_{\Omega}, \, \chi^y_{\Omega}, \, \chi^z_{\Omega}) \, | \, \underline{E}_{HCM} \, |^2, \tag{3.36}$$

is given as [8]

$$\left. \begin{array}{l} \underline{\underline{\epsilon}}_{\Omega 0} = \underline{\underline{\epsilon}}_{cm0} - \dfrac{1}{i \, \omega} \, \underline{\underline{Q}}^{-1} \cdot \underline{\underline{\Sigma}}_0 \\ \underline{\underline{\chi}}_{\Omega} = \underline{\underline{\chi}}_{cm} - \dfrac{1}{i \, \omega} \left(\underline{\underline{Q}}^{-1} \cdot \underline{\underline{\Sigma}}_1 + \underline{\underline{\Pi}} \cdot \underline{\underline{\Sigma}}_0 \right) \end{array} \right\} . \tag{3.37}$$

Herein, the linear and nonlinear parts of the mass operator are represented, respectively, by the dyadics

$$\left. \begin{array}{rl} \underline{\underline{\Sigma}}_0 = & \dfrac{f_a f_b}{4 \pi i \omega} \left(\underline{\underline{X}}_{a0} - \underline{\underline{X}}_{b0} \right) \cdot \underline{\underline{W}}_0(L) \cdot \left(\underline{\underline{X}}_{a0} - \underline{\underline{X}}_{b0} \right) \\ \underline{\underline{\Sigma}}_1 = & \dfrac{f_a f_b}{4 \pi i \omega} \Big[2 \left(\underline{\underline{X}}_{a0} - \underline{\underline{X}}_{b0} \right) \cdot \underline{\underline{W}}_0(L) \cdot \left(\underline{\underline{X}}_{a1} - \underline{\underline{X}}_{b1} \right) \\ & + \left(\underline{\underline{X}}_{a0} - \underline{\underline{X}}_{b0} \right) \cdot \underline{\underline{W}}_1(L) \cdot \left(\underline{\underline{X}}_{a0} - \underline{\underline{X}}_{b0} \right) \Big] \end{array} \right\} ; \tag{3.38}$$

and the dyadic

$$\underline{\underline{\Pi}} = \frac{1}{\det \left(\underline{\underline{Q}}_0 \right)} \, \left[\mathrm{diag} \left(Q^y_1 Q^z_0 + Q^y_0 Q^z_1, \, Q^z_1 Q^x_0 + Q^z_0 Q^x_1, \, Q^y_1 Q^x_0 + Q^y_0 Q^x_1 \right) - \nu \, \underline{\underline{Q}}^{-1}_0 \right] , \tag{3.39}$$

with

$$\nu = Q^x_0 Q^y_0 Q^z_1 + Q^x_0 Q^y_1 Q^z_0 + Q^x_1 Q^y_0 Q^z_0, \tag{3.40}$$

is expressed in terms of the components of

$$\left. \begin{array}{l} \underline{\underline{Q}}_0 = \underline{\underline{I}} + \underline{\underline{\Sigma}}_0 \cdot \underline{\underline{D}}_0 = \mathrm{diag} \, (Q^x_0, \, Q^y_0, \, Q^z_0) \\ \underline{\underline{Q}}_1 = \underline{\underline{\Sigma}}_0 \cdot \underline{\underline{D}}_1 + \underline{\underline{\Sigma}}_1 \cdot \underline{\underline{D}}_0 = \mathrm{diag} \, (Q^x_1, \, Q^y_1, \, Q^z_1) \end{array} \right\} . \tag{3.41}$$

3.3 Numerical studies

The SPFT estimates (3.37) of the HCM linear permittivity and nonlinear susceptibility are represented by mathematically complicated expressions. In order to discern the influence of the size parameter η, parametric numerical studies are called for. To this end, we investigate the following representative example of a homogenization scenario. Let component phase a be a cubically nonlinear material with linear permittivity $\epsilon_{a0} = 2\epsilon_0$ and nonlinear susceptibility $\chi_a = 9.07571 \times 10^{-12}\epsilon_0\,\mathrm{m^2V^{-2}}$ ($\equiv 6.5 \times 10^{-4}$ esu); and component phase b be a linear material with permittivity $\epsilon_b \equiv \epsilon_{b0} = 12\epsilon_0$. The value of the nonlinear susceptibility χ_a is that of gallium arsenide [50]. The eccentricities of the ellipsoidal component phase particles are specified by $U_x = 1$, $U_y = 3$ and $U_z = 15$. These choices of parameter values facilitate direct comparisons with a previous investigation in which the effects of the size parameter η were not included [48]. Results are presented for an angular frequency of $\omega = \pi \times 10^{15}\mathrm{rad\ s^{-1}}$ (equivalent to a free–space wavelength of 600 nm).

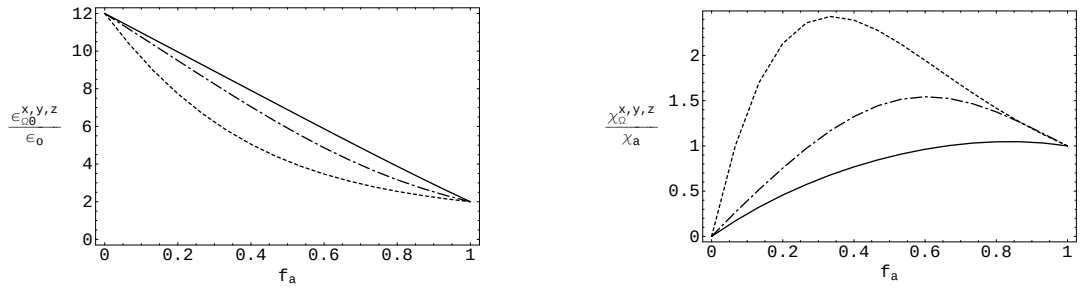

Figure 3.1: The HCM relative linear permittivity and nonlinear susceptibility parameters plotted against f_a, calculated for $\eta = L = 0$. Key: $\epsilon^x_{\Omega 0}/\epsilon_0$ and χ^x_Ω/χ_a dashed curves; $\epsilon^y_{\Omega 0}/\epsilon_0$ and χ^y_Ω/χ_a broken dashed curves; and $\epsilon^z_{\Omega 0}/\epsilon_0$ and χ^z_Ω/χ_a solid curves. Component phase parameter values: $\epsilon_{a0} = 2\epsilon_0$, $\chi_a = 9.07571 \times 10^{-12}\epsilon_0\,\mathrm{m^2V^{-2}}$, $\epsilon_b \equiv \epsilon_{b0} = 12\epsilon_0$, $U_x = 1$, $U_y = 3$ and $U_z = 15$.

We begin with the relatively straightforward case where neither the size parameter nor the correlation length is taken into account; i.e. $\eta = L = 0$. In this case, the SPFT estimates of the constitutive parameters are equivalent to those of the conventional Bruggeman formalism for weakly nonlinear, anisotropic, dielectric HCMs [54]. In Fig. 3.1, the HCM linear and nonlinear constitutive parameters are plotted against volume fraction f_a. The HCM linear permittivity parameters

$\epsilon_{\Omega 0}^{x,y,z}$ uniformly decrease from ϵ_{b0} at $f_a = 0$ to ϵ_{a0} at $f_a = 1$. In contrast, the HCM nonlinear susceptibility parameter χ_{Ω}^{x}, and to a lesser extent χ_{Ω}^{y}, exceeds the nonlinear susceptibility of component phase a for a wide range of values of f_a. This *nonlinear enhancement* phenomenon, and its potential for technological exploitation, have been reported on previously for both isotropic [45, 47, 55, 56] and anisotropic [48, 54] HCMs. The anisotropy reflected by the constitutive parameters, and the nonlinear enhancement, stem from the ellipsoidal geometry of the component phase particles.

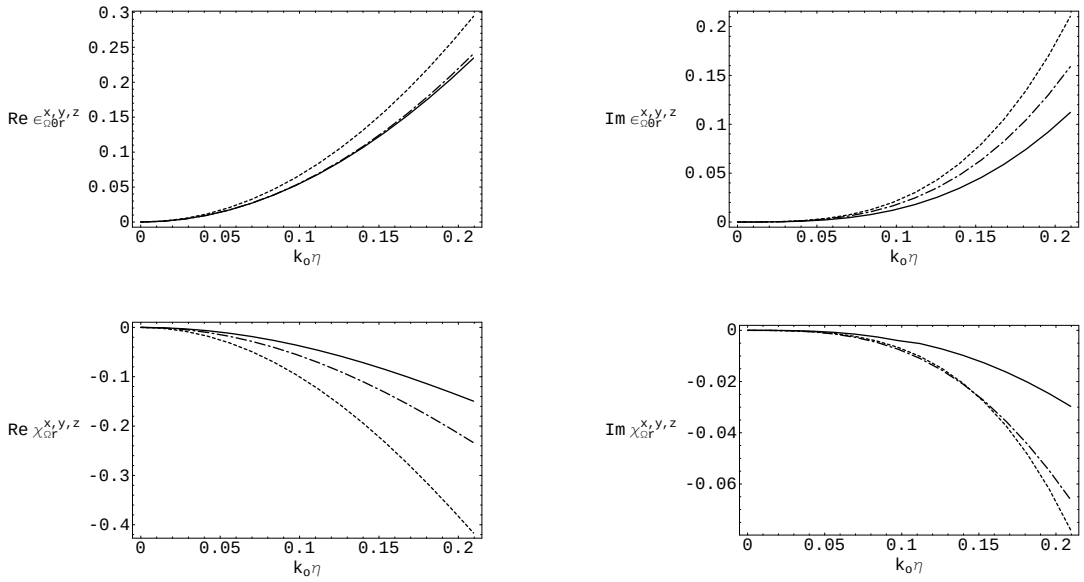

Figure 3.2: Real and imaginary parts of the HCM linear permittivity and nonlinear susceptibility parameters plotted against η (in nm), calculated for $L = 0$ and $f_a = 0.3$. Key: $\epsilon_{\Omega 0r}^{x}$ and $\chi_{\Omega r}^{x}$ dashed curves; $\epsilon_{\Omega 0r}^{y}$ and $\chi_{\Omega r}^{y}$ broken dashed curves; and $\epsilon_{\Omega 0r}^{z}$ and $\chi_{\Omega r}^{z}$ solid curves. Component phase parameter values as in Fig. 3.1.

How does the size parameter η influence the estimates of the HCM constitutive parameters? To answer this question, we fix the volume fraction at $f_a = 0.3$ and calculate the HCM constitutive parameters for $0 < \eta < 20$ nm with $L = 0$. The presentation of results is aided by the introduction of the relative constitutive

parameters

$$\left.\begin{aligned} \epsilon_{\Omega 0r}^{n} &= \frac{\epsilon_{\Omega 0}^{n} - \left(\epsilon_{\Omega 0}^{n}|_{\eta=L=0}\right)}{\epsilon_{0}} \\ \chi_{\Omega r}^{n} &= \frac{\chi_{\Omega}^{n} - \left(\chi_{\Omega}^{n}|_{\eta=L=0}\right)}{\chi_{a}} \end{aligned}\right\}, \qquad (n = x, y, z), \tag{3.42}$$

which measure the difference between the SPFT estimates calculated for $\eta, L \neq 0$ and $\eta = L = 0$. That is, the relative parameters represented by (3.42) highlight the effects of $\eta > 0$ and $L > 0$. The results are plotted in Fig. 3.2. It is notable that the HCM constitutive parameters have nonzero imaginary parts whereas the component material phases are specified by real–valued constitutive parameters. As previously described for linear HCMs [42], the presence of nonzero imaginary parts for the HCM constitutive parameters may be attributed to radiative scattering losses associated with the nonzero size of the component phase particles. Plainly, increasing the size parameter η has the effect of increasing the real and imaginary parts of the HCM linear permittivity, but decreasing the real and imaginary parts of the HCM nonlinear susceptibility. In fact, the influence of the size parameter is very similar to the influence of the correlation length, as has been noted for linear HCMs [48].

Fig. 3.2 reveals that by taking into consideration the nonzero size of the component phase particles — but not the correlation length — the predicted nonlinear enhancement is somewhat diminished. We now consider the estimates of the HCM constitutive parameters when both the size parameter and the correlation length are taken into account. In Fig. 3.3, the HCM relative constitutive parameters are plotted against both L and η/L with the volume fraction fixed at $f_a = 0.3$. the results for $\epsilon_{\Omega 0}^{x}$ and χ_{Ω}^{x} are presented; the corresponding plots for $\epsilon_{\Omega 0}^{y,z}$ and $\chi_{\Omega}^{y,z}$ are similar and are provided in Appendix 2. It may be observed in Fig. 3.3 that the effects of η and L are cumulative insofar as the increase in the real and imaginary parts of $\epsilon_{\Omega 0}^{x,y,z}$, and the decrease in the real and imaginary parts of $\chi_{\Omega}^{x,y,z}$, which occur as η increases, become steadily more exaggerated as L increases.

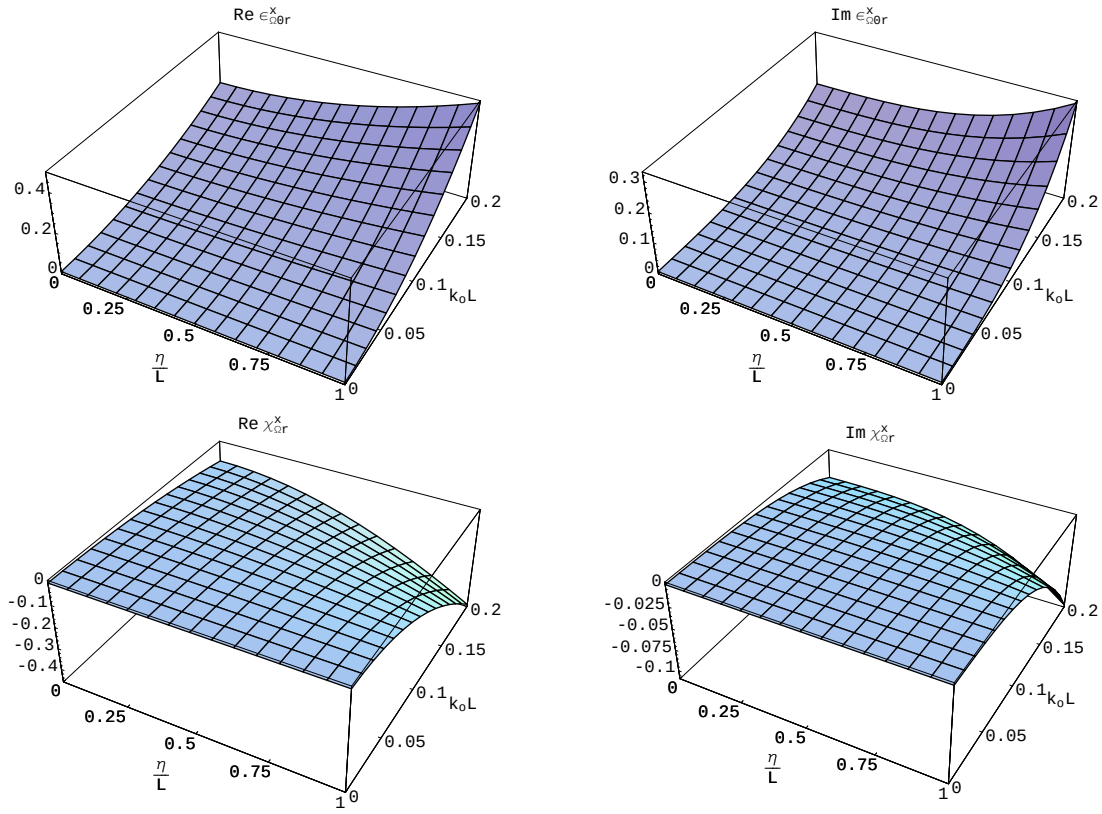

Figure 3.3: Real and imaginary parts of the HCM linear permittivity and nonlinear susceptibility parameters $\epsilon^x_{\Omega 0 r}$ and $\chi^x_{\Omega r}$ plotted against L (in nm) and η/L, calculated for $f_a = 0.3$. Component phase parameter values as in Fig. 3.1.

3.4 Conclusion

The size of the component phase particles can have a significant bearing upon the estimated constitutive parameters of weakly nonlinear bianisotropic HCMs, within the bilocally-approximated SPFT. Most obviously, by taking nonzero particle size into consideration, attenuation is predicted and the degree of nonlinear enhancement is somewhat dilimished. In repect of both of these effects, the influence of particle size is similar to the influence of the correlation length. Furthermore, the effects of particle size and correlation length on both linear and nonlinear HCM constitutive parameters are found to be cumulative.

Chapter 4

Third order considerations

4.1 Overview

The strong–property–fluctuation theory (SPFT) provides a sophisticated means of estimating the effective constitutive parameters of a homogenized composite material (HCM), which takes account of the statistical distribution of the component particles. We present an extended version of the third–order SPFT in which the component particles are represented as depolarization regions of nonzero volume. Numerical results are provided for a bianisotropic homogenization scenario wherein the HCM is a Faraday chiral material. Thereby, convergence of the extended SPFT at the second–order level of approximation is demonstrated within the long–wavelength regime.

4.2 Strong–property–fluctuation theory

4.2.1 Component materials

Two particulate component materials are considered. The particles which comprise each component material are assumed to be spherical. The distributional statistics of the component phases are as described in (1.3.3) with $\underline{\underline{U}} = \underline{\underline{I}}$. In this Chapter we consider the third–order SPFT in which the two–point covariance function (1.30) and the three–point covariance function (1.31) are adopted.

4.2.2 Homogenised composite material

The constitutive dyadic of the HCM, as estimated by the nth–order SPFT, is given by [8] (1.40) Herein, the constitutive dyadic $\underline{\underline{\mathbf{K}}}_{cm}$ characterizes a comparison material whose constitutive parameters are provided by the Bruggeman homogenization formalism.

The depolarization dyadic $\underline{\underline{\mathbf{D}}}_{I/cm}(\eta)$ in (1.40) represents the electromagnetic response of a spherical particle of radius η, immersed in the comparison material. It is defined as (1.27) with $\underline{\underline{\mathbf{G}}}_{cm}(\underline{r})$ being the dyadic Green function of the comparison material [2, 3, 42]. For convenience, $\underline{\underline{\mathbf{D}}}_{I/cm}(\eta)$ is expressed as the sum of two parts [51]: (1.27) where $\underline{\underline{\mathbf{D}}}^{0}_{I/cm}$ represents the contribution to the depolarization arising from component particles in the limit $\eta \to 0$, whereas $\underline{\underline{\mathbf{D}}}^{>0}_{I/cm}(\eta)$ represents the depolarization contribution arising from the nonzero volume of the component particles. Often in homogenization studies the $\underline{\underline{\mathbf{D}}}^{>0}_{I/cm}(\eta)$ contribution is neglected, but recent studies have highlighted the significance of this contribution, particularly in the context of scattering losses [51, 52]. The conventional SPFT incorporates $\underline{\underline{\mathbf{D}}}^{0}_{I/cm}$ only as the depolarization dyadic, whereas the extended SPFT accommodates both $\underline{\underline{\mathbf{D}}}^{0}_{I/cm}$ and $\underline{\underline{\mathbf{D}}}^{>0}_{I/cm}(\eta)$. The mathematical expressions for $\underline{\underline{\mathbf{D}}}^{0}_{I/cm}$ and $\underline{\underline{\mathbf{D}}}^{>0}_{I/cm}(\eta)$ are complicated, especially for bianisotropic HCMs, but integral representations are available which can be straightforwardly evaluated using standard numerical techniques [29]. These integral representations are provided in the Appendix.

The mass operator term $\underline{\underline{\mathbf{\Sigma}}}^{[n]}(\eta, L)$ appearing in (1.40) vanishes for the zeroth– and first–order versions of the SPFT [4] ; i.e.,

$$\underline{\underline{\mathbf{\Sigma}}}^{[0]} = \underline{\underline{\mathbf{\Sigma}}}^{[1]} = \underline{\underline{\mathbf{0}}}. \tag{4.1}$$

By implementing the two–point covariance function (1.30), the second–order mass operator term is given by [8] (2.21) with the polarizability density dyadics

$$\underline{\underline{\boldsymbol{\chi}}}_{\ell}(\eta) \;=\; -i\omega \left(\underline{\underline{\mathbf{K}}}_{\ell} - \underline{\underline{\mathbf{K}}}_{cm} \right) \cdot \left[\underline{\underline{\mathbf{I}}} + i\omega \underline{\underline{\mathbf{D}}}_{I/cm}(\eta) \cdot \left(\underline{\underline{\mathbf{K}}}_{\ell} - \underline{\underline{\mathbf{K}}}_{cm} \right) \right]^{-1}, \tag{4.2}$$

where $\ell = a, b$. The three–point covariance function (1.31) yields the third–order

mass operator term [25]

$$\underline{\underline{\mathbf{\Sigma}}}^{[3]}(\eta, L) = \underline{\underline{\mathbf{\Sigma}}}^{[2]}(\eta, L) + \frac{f_a(1-2f_a)}{3(1-f_a)^2}\, \underline{\underline{\boldsymbol{\chi}}}_a(\eta) \cdot \Big[\underline{\underline{\mathbf{V}}}(\eta) \cdot \underline{\underline{\boldsymbol{\chi}}}_a(\eta) \cdot \underline{\underline{\mathbf{D}}}^{>0}_{I/cm}(L) + \underline{\underline{\mathbf{D}}}^{>0}_{I/cm}(L) \cdot \underline{\underline{\boldsymbol{\chi}}}_a(\eta) \cdot \underline{\underline{\mathbf{V}}}(\eta) + \underline{\underline{\mathbf{D}}}^{>0}_{I/cm}(L) \cdot \underline{\underline{\boldsymbol{\chi}}}_a(\eta) \cdot \underline{\underline{\mathbf{D}}}^{>0}_{I/cm}(L) \Big] \cdot \underline{\underline{\boldsymbol{\chi}}}_a(\eta), \tag{4.3}$$

where

$$\underline{\underline{\mathbf{V}}}(\eta) = \frac{1}{i\omega}\, \underline{\underline{\mathbf{K}}}^{-1}_{cm} - \underline{\underline{\mathbf{D}}}_{I/cm}(\eta). \tag{4.4}$$

4.3 Numerical studies

We now apply the extended third–order SPFT presented in §4.2 to a specific bianisotropic homogenization scenario. The constitutive parameters of the HCM are provided by evaluating (1.40) with (4.1) for the zeroth–order (and first–order) SPFT, (2.21) for the second–order SPFT, and (4.3) for the third–order SPFT. As an illustrative example, let us consider the homogenization of (i) a magnetically–biased ferrite material described by the constitutive dyadic [38]

$$\underline{\underline{\mathbf{K}}}_a = \delta \begin{bmatrix} \epsilon_0\, \epsilon_a\, \underline{\underline{I}} & \underline{\underline{0}} \\ \underline{\underline{0}} & \mu_0 \begin{pmatrix} \mu_a^x & i\mu_a^g & 0 \\ -i\mu_a^g & \mu_a^x & 0 \\ 0 & 0 & \mu_a^z \end{pmatrix} \end{bmatrix} \tag{4.5}$$

and (ii) an isotropic chiral material described by the constitutive dyadic [17] (2.23) The parameter δ in (4.5) provides a means of varying the constitutive contrast between the component material phases. The constitutive relations of the resulting HCM — which is known as a Faraday chiral material — are rigorously established [31, 32]. The constitutive dyadic of the HCM, as estimated by the nth–order SPFT, has the general form (2.31) An HCM of the same form also arises from the homogenization of a magnetically–biased plasma and an isotropic chiral material [34, 44]. Bearing in mind that the third–order SPFT is established only for

bianisotropic materials which are weakly anisotropic [25], we select the following representative values for the constitutive parameters of the component material phases: $\epsilon_a = 1.2 + i0.02$, $\mu_a^x = 3.5 + i0.08$, $\mu_a^g = 0.7 + i0.005$, $\mu_a^z = 3.0 + i0.06$; $\epsilon_b = 2.5 + i0.1$, $\xi_b = 1 + i0.07$ and $\mu_b = 1.75 + i0.09$. Results which are qualitatively similar to those presented here were observed — in further studies not reported here — when different values were selected for the constitutive parameters of the component materials.

In the following numerical studies, the correlation length L is fixed[1] for each value of δ considered, while the particle size parameter η varies from 0 to $L/2$. In order to conform to the long–wavelength regime under which the SPFT estimates of the HCM parameters are derived, the value of L is selected such that the scalar $Q \ll 1$, where

$$Q = \frac{\max\{|\gamma_1|, |\gamma_2|, |\gamma_3|, |\gamma_4|\}}{2\pi} L, \tag{4.6}$$

with $\{\gamma_i \,|\, i = 1, \ldots, 4\}$ being the four independent wavenumbers supported by the HCM. For simplicity, we choose the wavenumbers associated with propagation along the Cartesian z axis [42]; i.e.,

$$\left.\begin{aligned}
\gamma_1 &= k_0 \left(\sqrt{\epsilon_{HCM}^x + \epsilon_{HCM}^g} \sqrt{\mu_{HCM}^x + \mu_{HCM}^g} - \xi_{HCM}^x - \xi_{HCM}^g \right) \\
\gamma_2 &= k_0 \left(-\sqrt{\epsilon_{HCM}^x + \epsilon_{HCM}^g} \sqrt{\mu_{HCM}^x + \mu_{HCM}^g} - \xi_{HCM}^x - \xi_{HCM}^g \right) \\
\gamma_3 &= k_0 \left(\sqrt{\epsilon_{HCM}^x - \epsilon_{HCM}^g} \sqrt{\mu_{HCM}^x - \mu_{HCM}^g} + \xi_{HCM}^x - \xi_{HCM}^g \right) \\
\gamma_4 &= k_0 \left(-\sqrt{\epsilon_{HCM}^x - \epsilon_{HCM}^g} \sqrt{\mu_{HCM}^x - \mu_{HCM}^g} + \xi_{HCM}^x - \xi_{HCM}^g \right)
\end{aligned}\right\}. \tag{4.7}$$

All numerical calculations were carried out using an angular frequency $\omega = 2\pi \times 10^{10}$ rad s^{-1} with the volume fraction fixed at $f_a = 0.3$. Only a selection of representative numerical results are presented here in this Chapter; further graphical results are presented in Appendix 3.

The zeroth–, second– and third–order SPFT estimates of the HCM constitutive parameters μ_{HCM}^x, μ_{HCM}^g and μ_{HCM}^z are plotted against the size parameter η in Figure 4.1 for the case where $\delta = 10$. Here, the correlation length is set at

[1] This applies to the second–order and third–order SPFT calculations; L does not feature in the zeroth–order SPFT.

$L = 0.45$ mm, in order that $Q = 0.1$ at $\eta = L/2$. The third–order estimates of the real and imaginary parts of μ^x_{HCM}, μ^g_{HCM} and μ^z_{HCM} increase steadily as η is increased, as do the zeroth–order and second–order estimates, but the difference between the third–order estimates and the second–order estimates remains very small for all values of η. In contrast, there are plainly significant differences between the second–order and zeroth–order estimates. Furthermore, the difference between the zeroth– and second–order estimates increases in magnitude slightly as the the size parameter η increases. The corresponding graphs for the permittivity and magnetoelectric constitutive parameters of the HCM are qualitatively similar to those graphs presented in Figure 4.1. Accordingly, these are not displayed here.

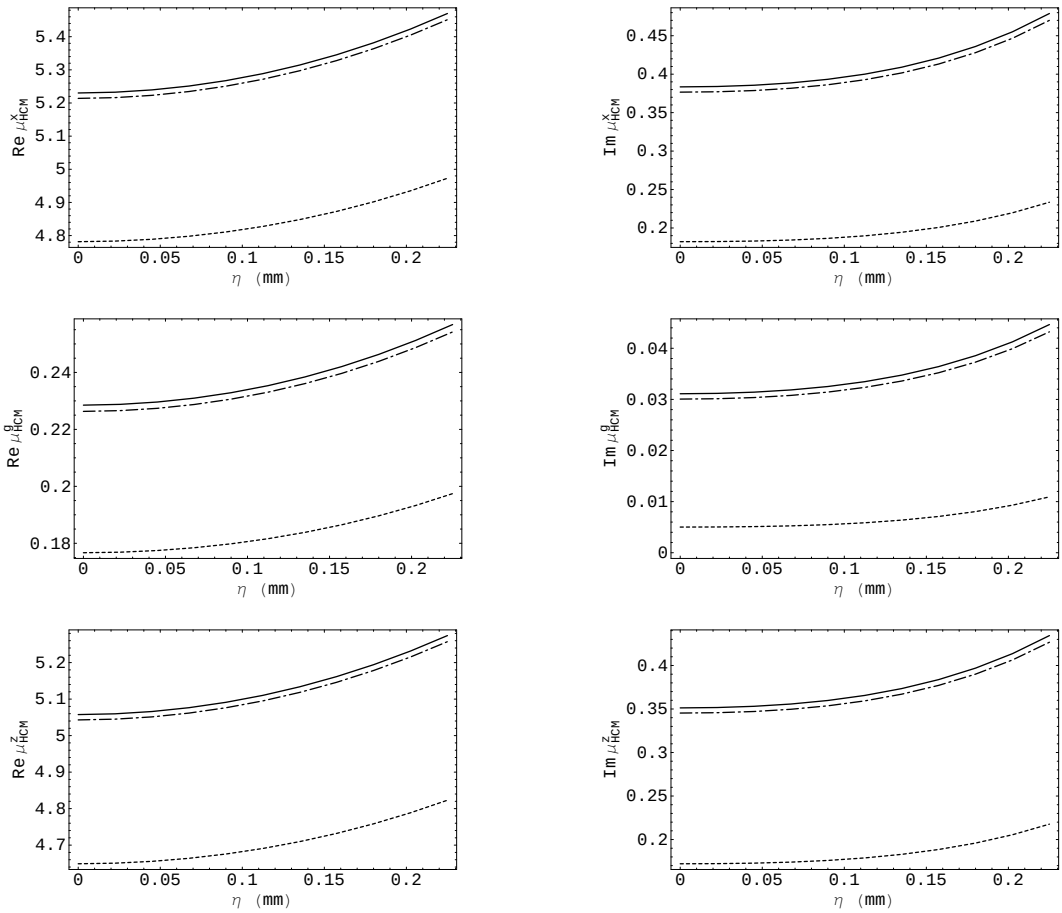

Figure 4.1: Real (left) and imaginary (right) parts of the HCM constitutive parameters $\mu^{x,z,g}_{HCM}$ plotted against η (mm) for $\delta = 10$. Key: dashed curve is the zeroth–order SPFT estimate; broken dashed curve is the second–order SPFT estimate; and solid curve is the third–order SPFT estimate.

Plots of μ^x_{HCM}, μ^g_{HCM} and μ^z_{HCM} versus η for the cases where $\delta = 20$ and 30 are shown in Figures 4.2 and 4.3, respectively. The correlation lengths $L = 0.34$ and 0.28 mm were used for the calculations of Figures 4.2 and 4.3, respectively, thereby resulting in $Q = 0.1$ at $\eta = L/2$. As is the case for $\delta = 10$, the second–order estimates are plainly different to the zeroth–order estimates for $\delta = 20$ and 30. The differences between second–order and third–order estimates of the real and imaginary parts of the HCM constitutive parameters increase slightly as δ increases, but they remain small for all values of η. The corresponding permittivity and magnetoelectric constitutive parameters of the HCM exhibit trends which are qualitatively similar to those shown in Figures 4.2 and 4.3 for the HCM magnetic constitutive parameters.

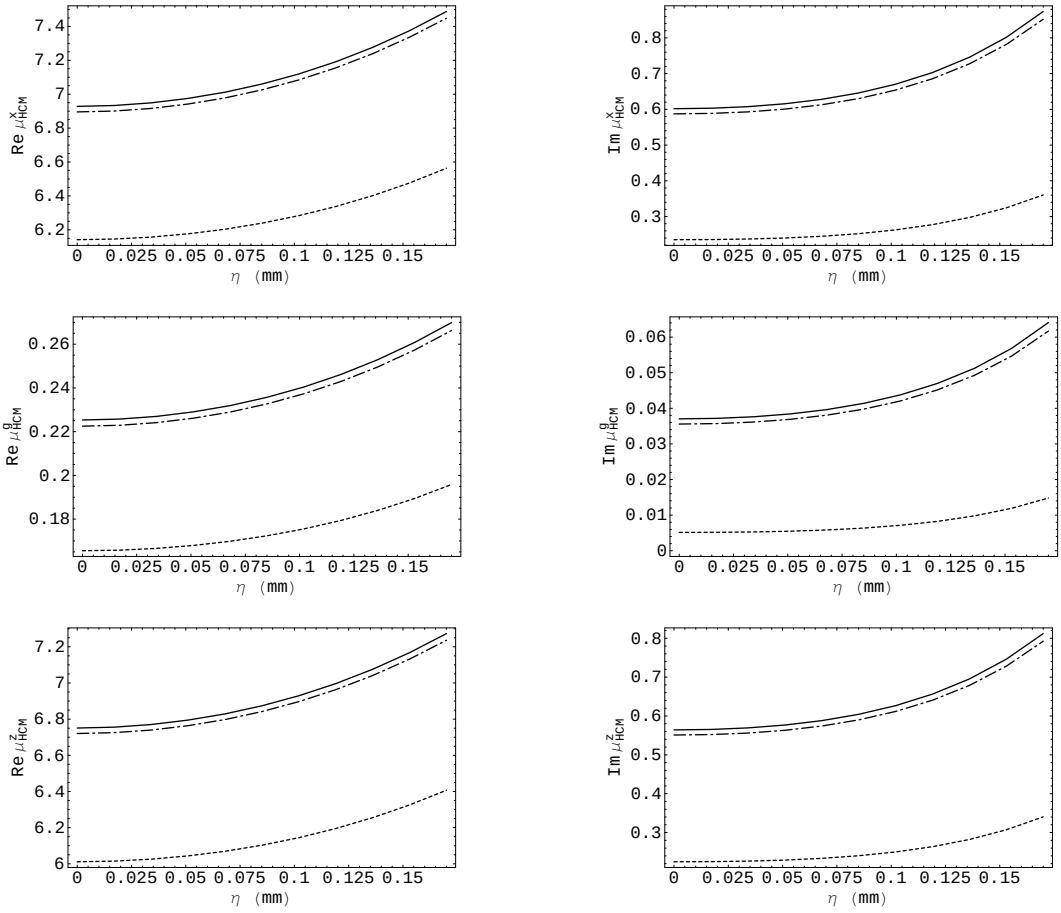

Figure 4.2: As Figure 4.1 but for $\delta = 20$.

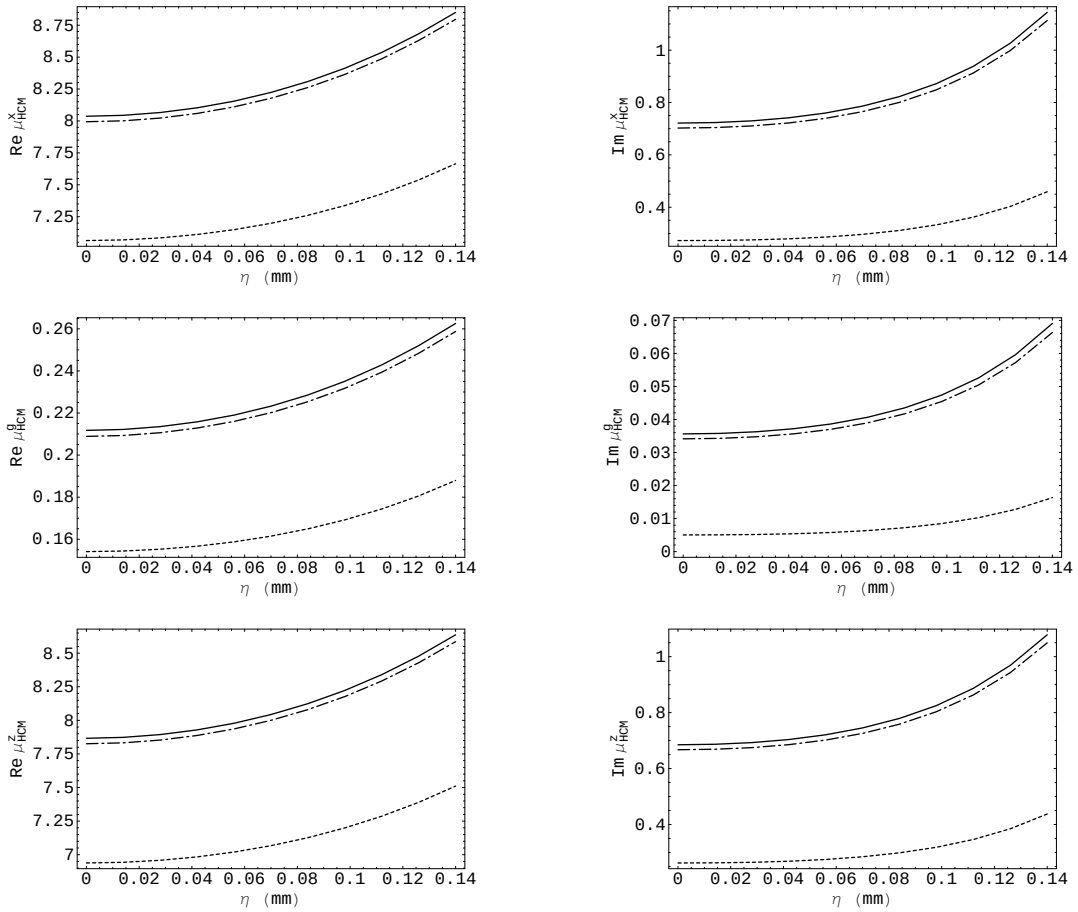

Figure 4.3: As Figure 4.1 but for $\delta = 30$.

4.4 Concluding remarks

It is demonstrated by our numerical studies in §4.3 (and in further studies not presented here) that the extended SPFT at the third–order level of approximation does not add significantly to the HCM estimates yielded by the second–order extended SPFT. The differences between second–order and third–order estimates of the HCM constitutive parameters are very small for all values of the size parameter investigated, even when the constitutive contrast between the component materials is as large as a factor of 30. Significant differences between the second– and third–order estimates arise only when (i) the correlation length and/or size parameter become similar in magnitude to the electromagnetic wavelength(s); and/or (ii) the constitutive contrast between the component materials becomes enormous. In the case of (i) the bounds imposed by the long–wavelength regime are exceeded, while in the case of (ii) the contrast between the polarizability

density dyadics $\underline{\underline{\boldsymbol{\chi}}}_a$ and $\underline{\underline{\boldsymbol{\chi}}}_b$ is likely to become strong. In either scenario the basic assumptions underlying the long–wavelength SPFT are violated [8, 25]. We therefore conclude that the extended SPFT converges at the second–order level of approximation for bianisotropic HCMs which are weakly anisotropic.

Chapter 5

Conclusions and further work

Recent advances in the science and engineering of materials and metamaterials [39] serve to further emphasize the pressing need for accurate and convenient theoretical methods to estimate the effective constitutive parameters of complex materials. In this regard, the SPFT represents an important step forward as it takes into account details of the statistical distribution of the constituent particles, unlike more conventional approaches to homogenization. In this thesis, the SPFT is developed further through the incorporation of depolarization dyadics which represent particles of small, but not vanishingly small, spatial extent.

It has been demonstrated that depolarization regions of nonzero volume can have a significant influence in linear bianisotropic HCMs and weakly nonlinear HCMs. The effect for linear HCMs is generally an increase the predicted losses associated with the HCM, which manifests itself as an increase in the magnitude of the imaginary parts of the HCM constitutive parameters. For weakly nonlinear HCMs, the degree of nonlinear enhancement is somewhat diminished by taking the size of the depolarization region into account. Furthermore, it has been demonstrated for a wide class of complex HCMs, that convergence of the SPFT is achieved at the second–order level of approximation when nonzero depolarization volumes are taken into account.

Several possible topics for future work are suggested by the work of this thesis, both in terms of further theoretical developments and applications. On the theoretical side, convergence of the SPFT for weakly nonlinear HCMs has yet to

be established, even in the case where depolarization volumes are taken to be vanishingly small. On the side of applications, it would be of interest to consider the effect of nonzero depolarization volume for exotic HCM–based metamaterials which exhibit negative refraction. Some initial studies have already been reported in this area [57].

Appendix A

Linear bianisotropic composites

In this Appendix we provide additional graphs to supplement those already presented in Chapter 2. See Chapter 2 for a discussion of these.

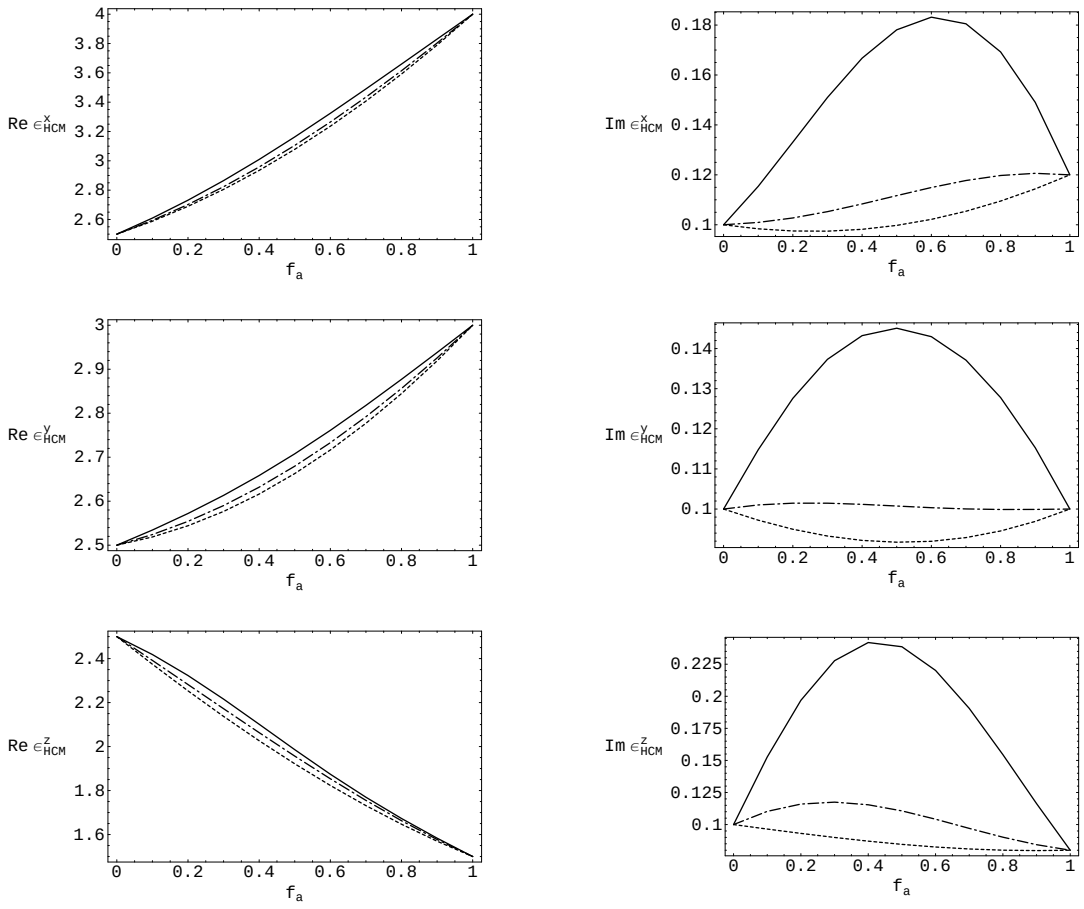

Figure A.1: Real (left) and imaginary (right) parts of the HCM constitutive parameters $\epsilon^{x,y,z}_{HCM}, \xi^{x,y,z}_{HCM}, \mu^{x,y,z}_{HCM}$ plotted against volume fraction $f_a \in (0,1)$ for $\eta/\lambda_0 = 0$ (dashed curves), $\eta/\lambda_0 = 0.05$ (broken dashed curves) and $\eta/\lambda_0 = 0.1$ (solid curves). The HCM is a biaxial bianisotropic material.

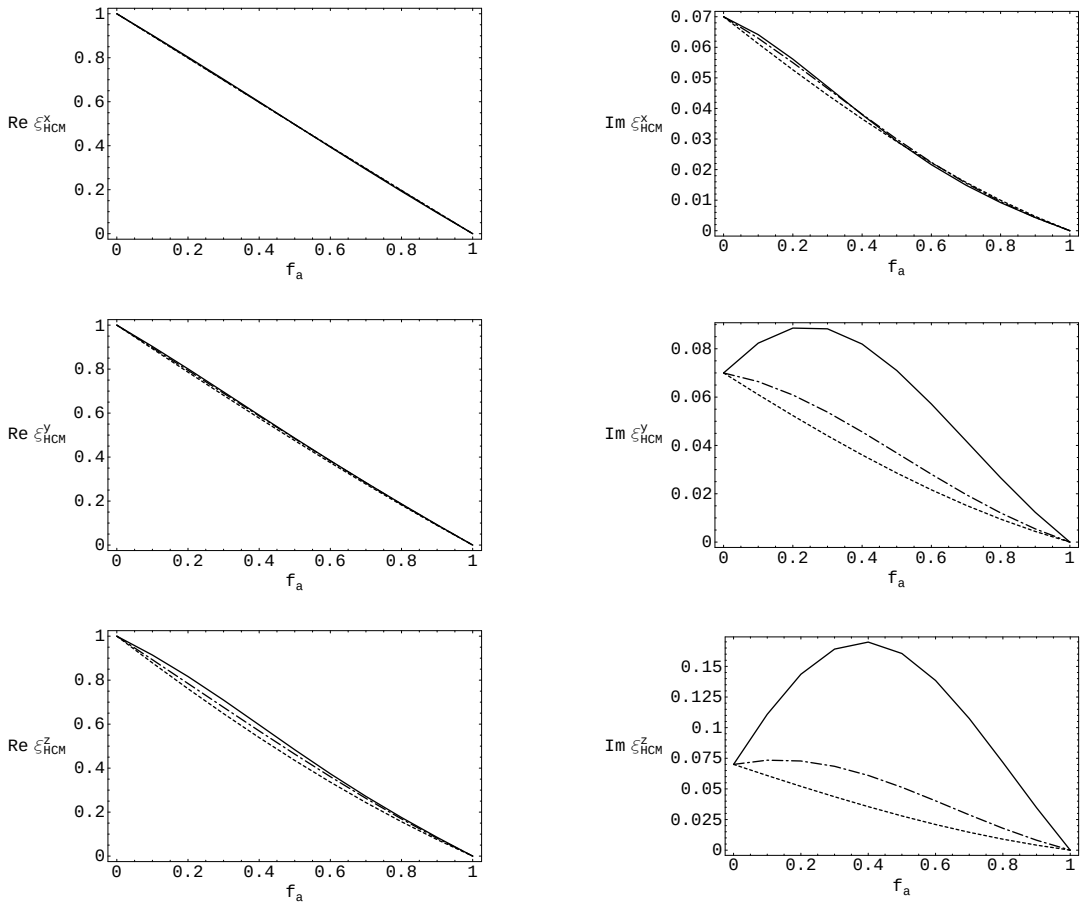

Figure A.1: continued

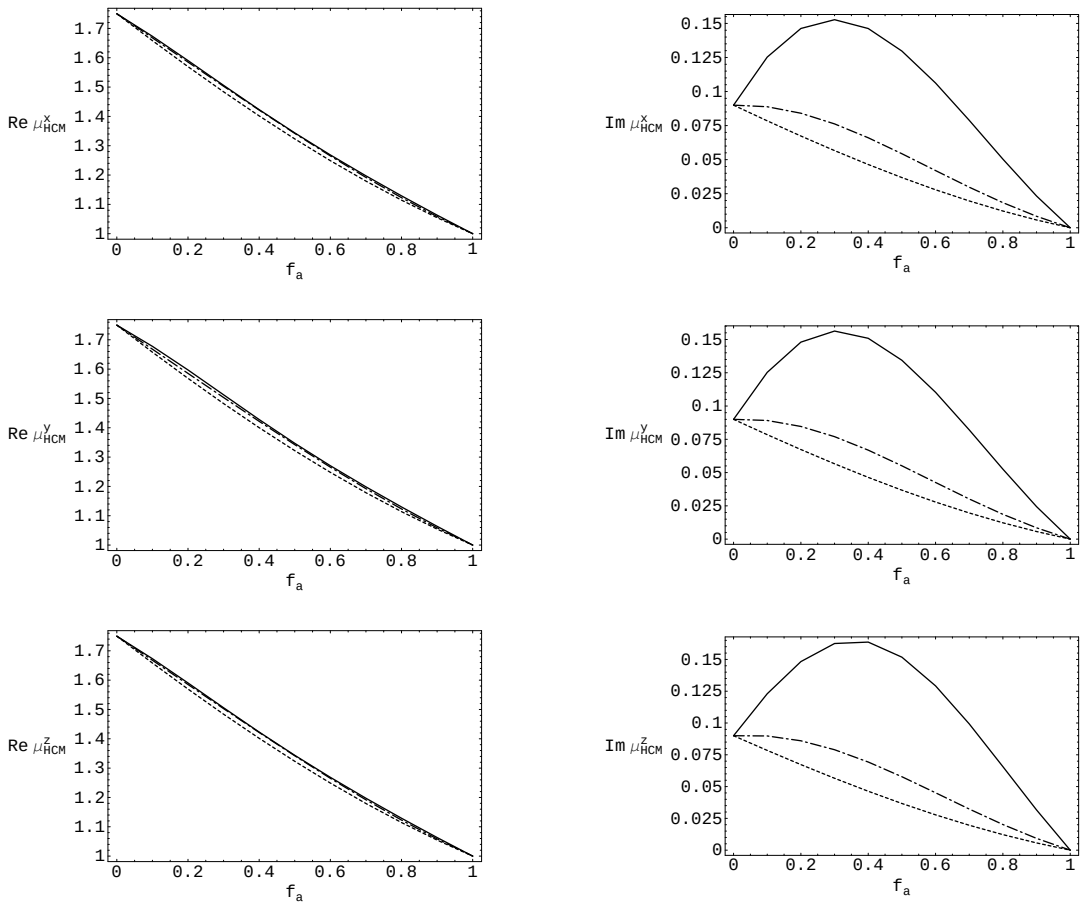

Figure A.1: continued

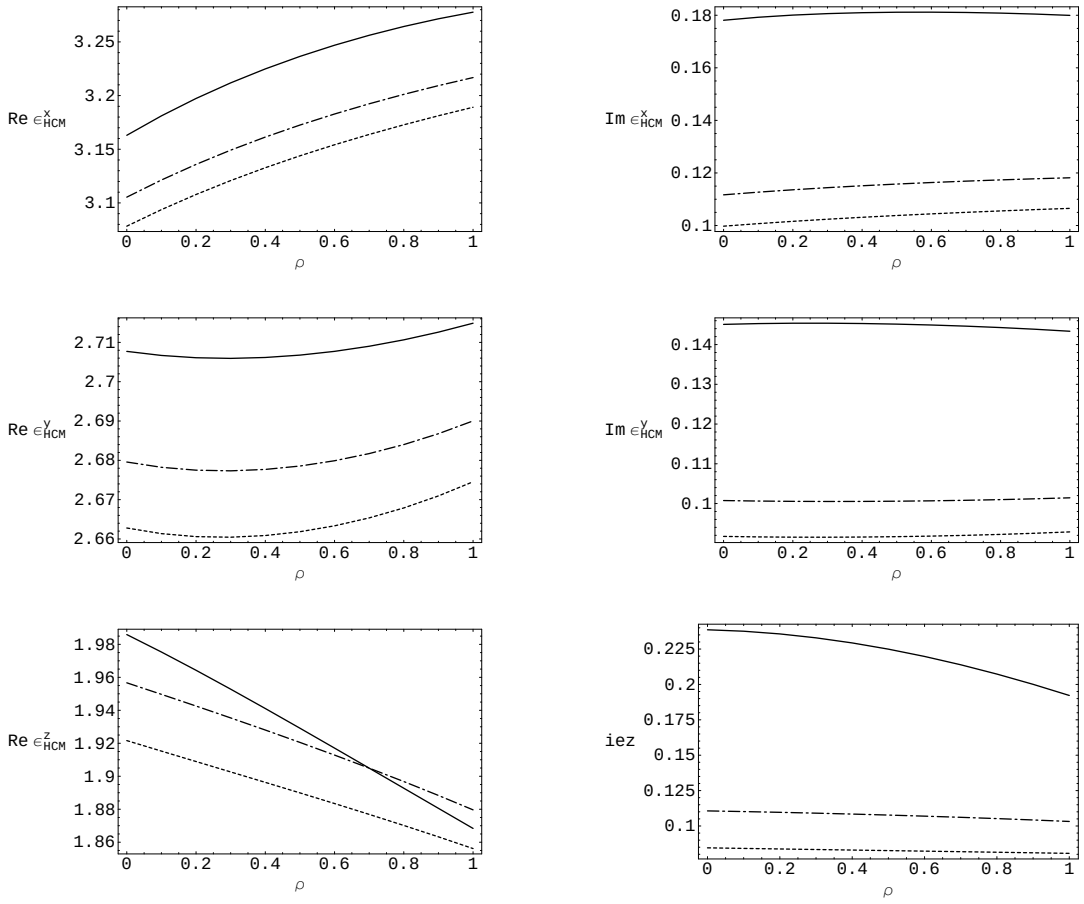

Figure A.2: Real (left) and imaginary (right) parts of the HCM constitutive parameters $\epsilon^{x,y,z}_{HCM}, \xi^{x,y,z}_{HCM}, \mu^{x,y,z}_{HCM}$ plotted against eccentricity parameter $\rho \in (0,1)$ for $\eta/\lambda_0 = 0$ (dashed curves), $\eta/\lambda_0 = 0.05$ (broken dashed curves) and $\eta/\lambda_0 = 0.1$ (solid curves). The HCM is a biaxial bianisotropic material.

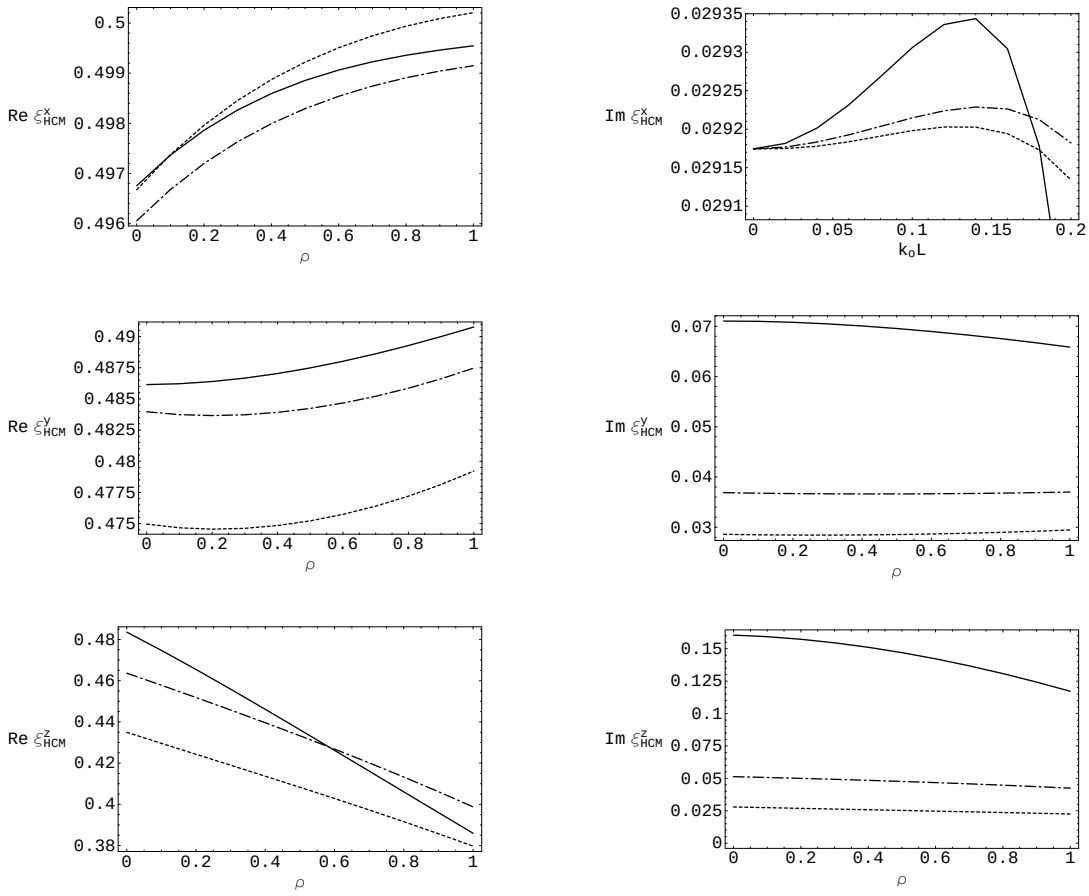

Figure A.2: continued

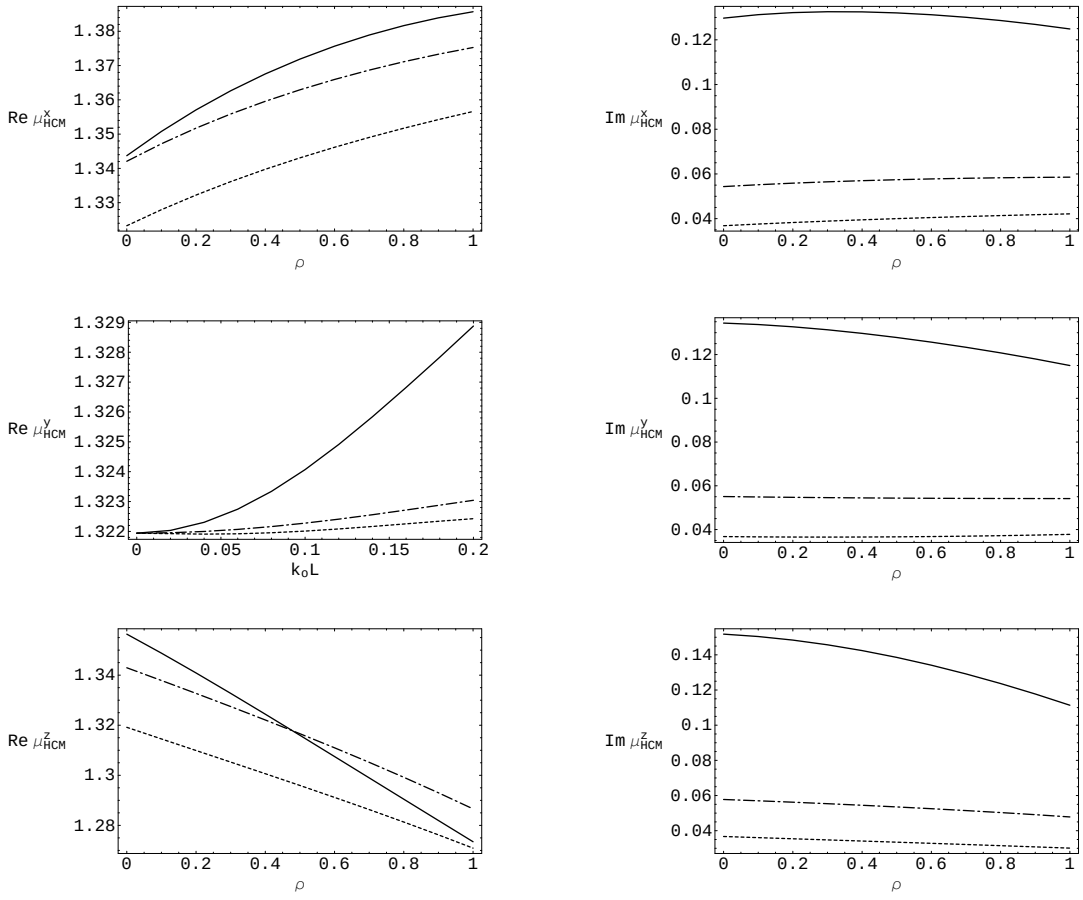

Figure A.2: continued

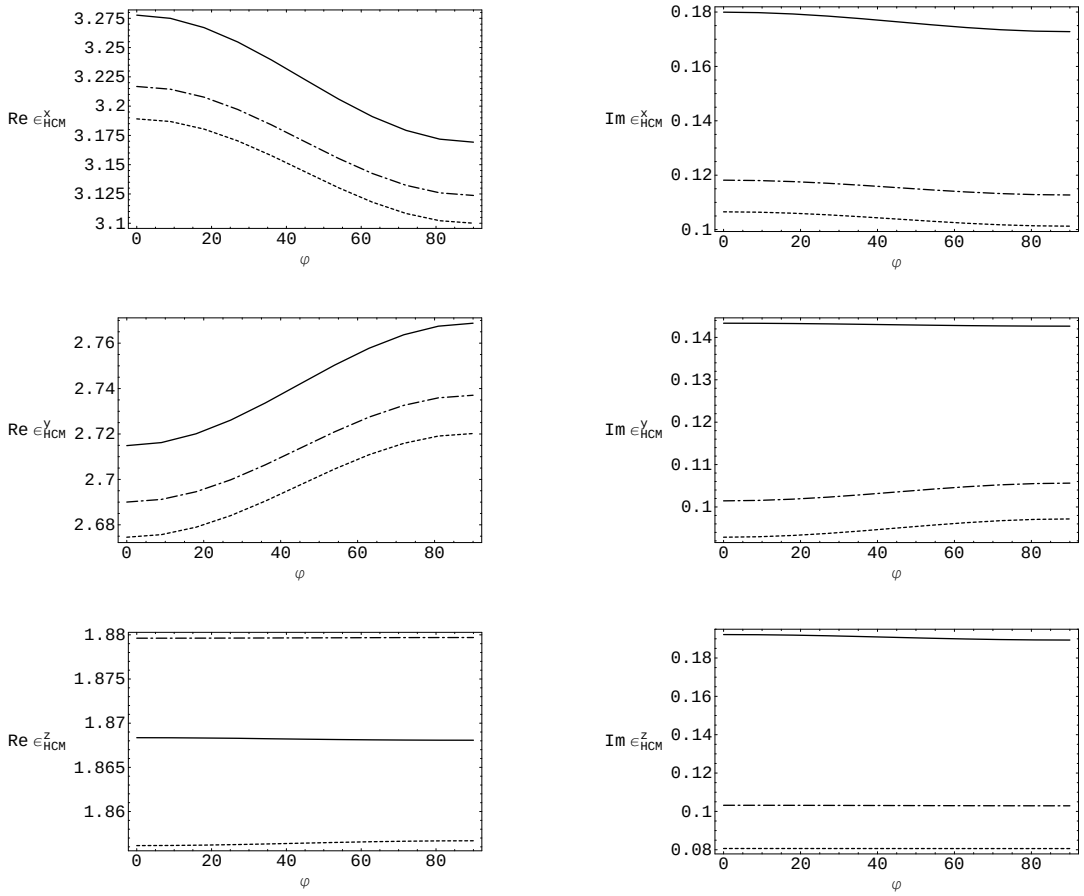

Figure A.3: Real (left) and imaginary (right) parts of the HCM constitutive parameters $\epsilon^{x,y,z}_{HCM}, \xi^{x,y,z}_{HCM}, \mu^{x,y,z}_{HCM}$ plotted against orientation angle $\varphi \in (0, \pi/2)$ for $\eta/\lambda_0 = 0$ (dashed curves), $\eta/\lambda_0 = 0.05$ (broken dashed curves) and $\eta/\lambda_0 = 0.1$ (solid curves). The HCM is a biaxial bianisotropic material.

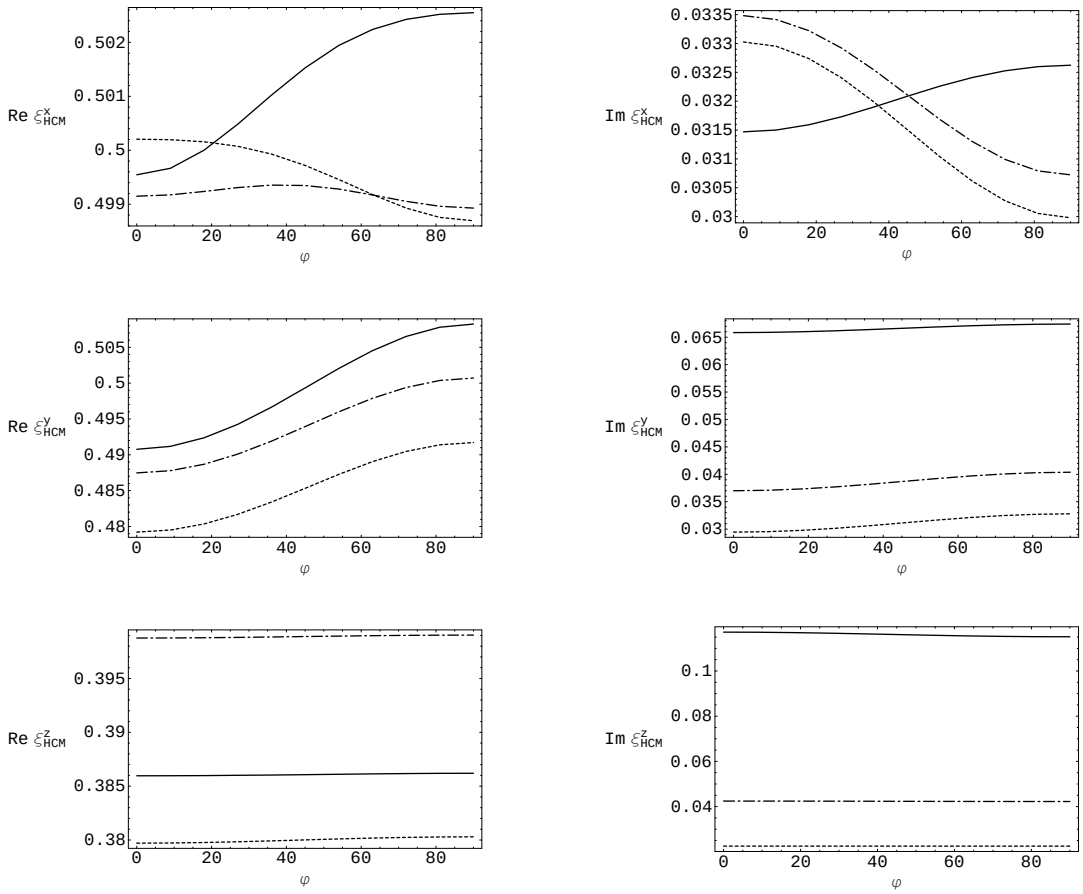

Figure A.3: continued

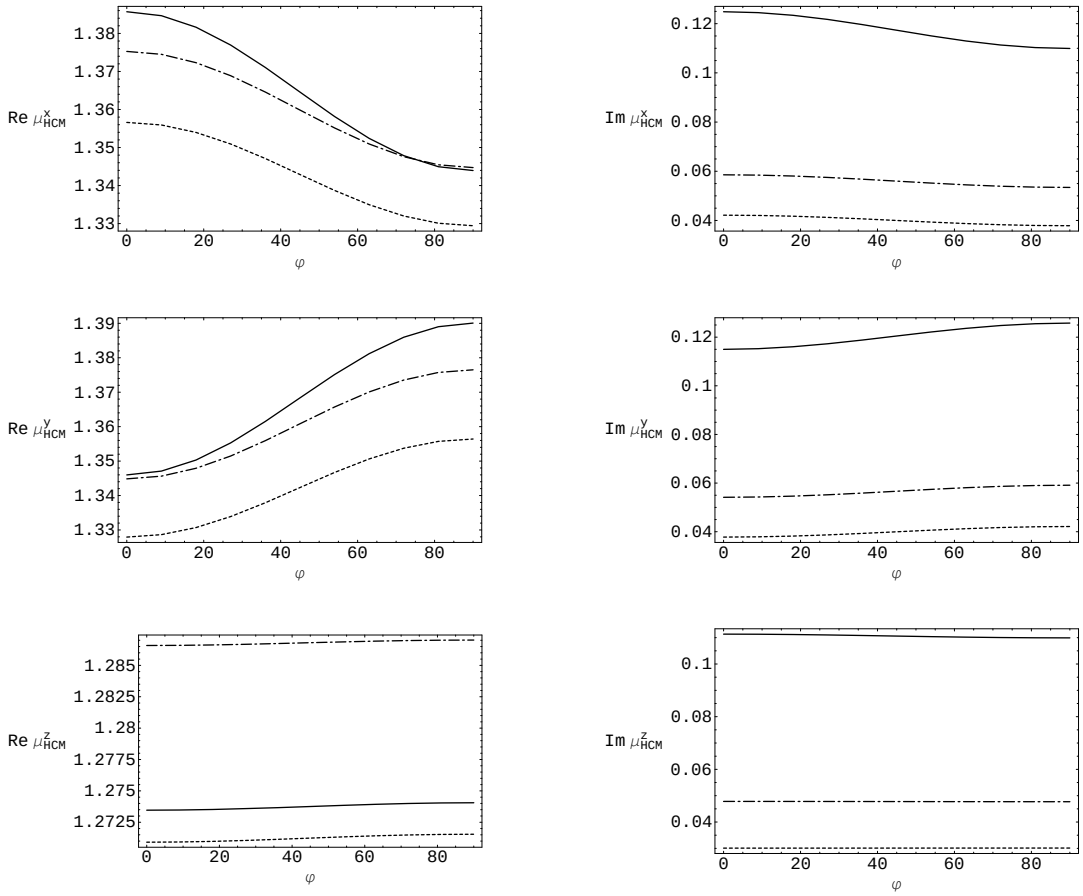

Figure A.3: continued

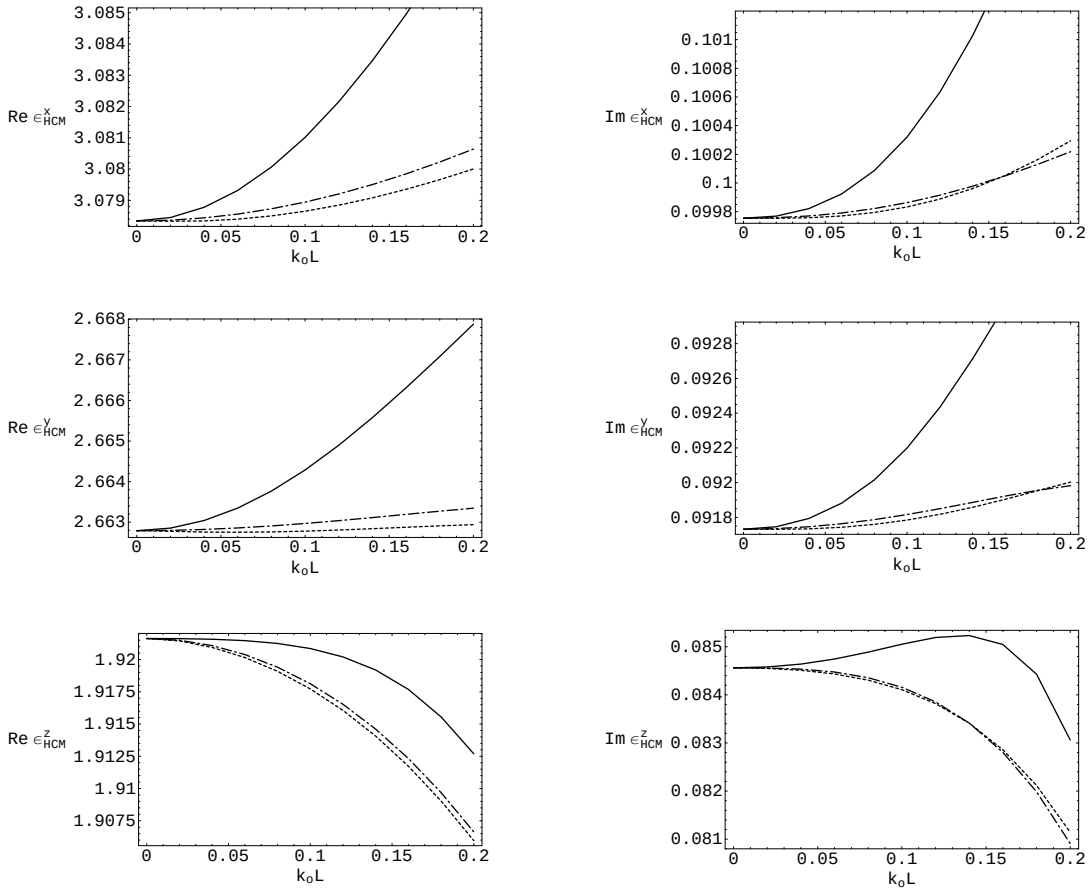

Figure A.4: Real (left) and imaginary (right) parts of the HCM constitutive parameters $\epsilon^{x,y,z}_{HCM}, \xi^{x,y,z}_{HCM}, \mu^{x,y,z}_{HCM}$ plotted against relative correlation length $k_0L \in (0, 0.2)$ for $\eta/L = 0$ (dashed curves), $\eta/L = 0.5$ (broken dashed curves) and $\eta/L = 0.95$ (solid curves). The HCM is a biaxial bianisotropic material.

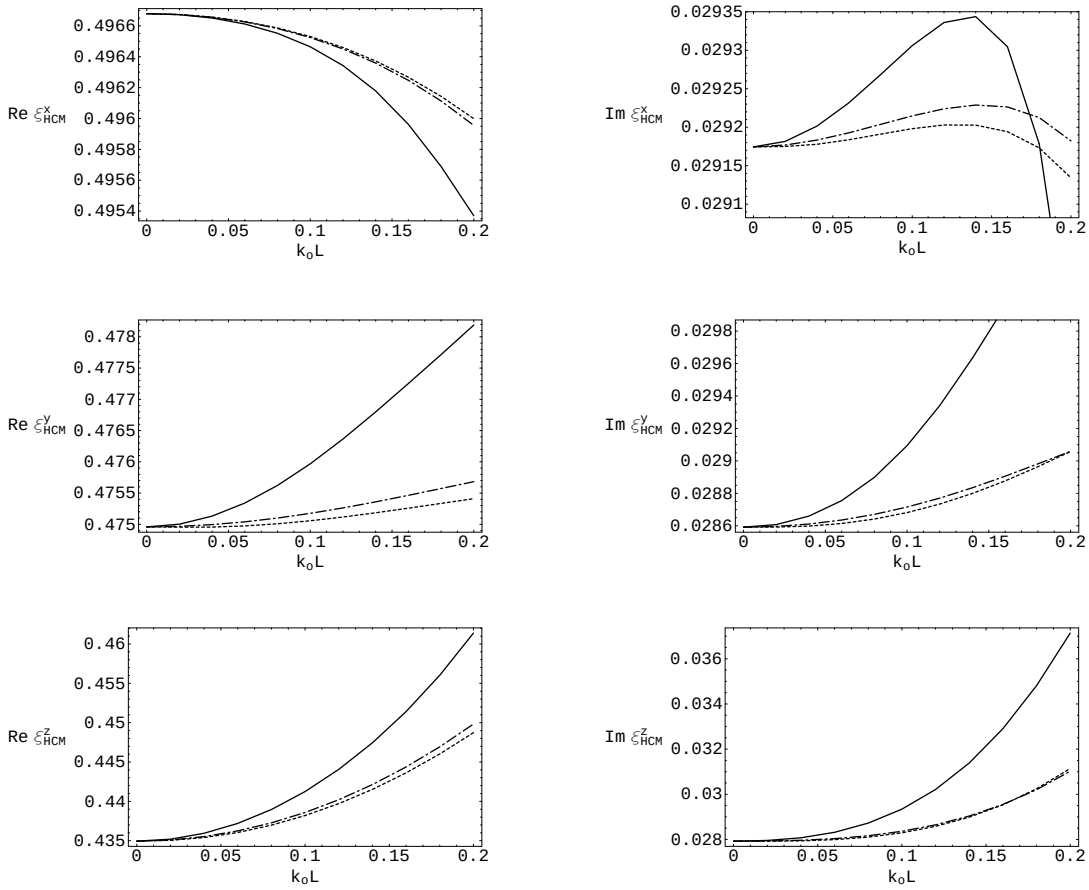

Figure A.4: continued

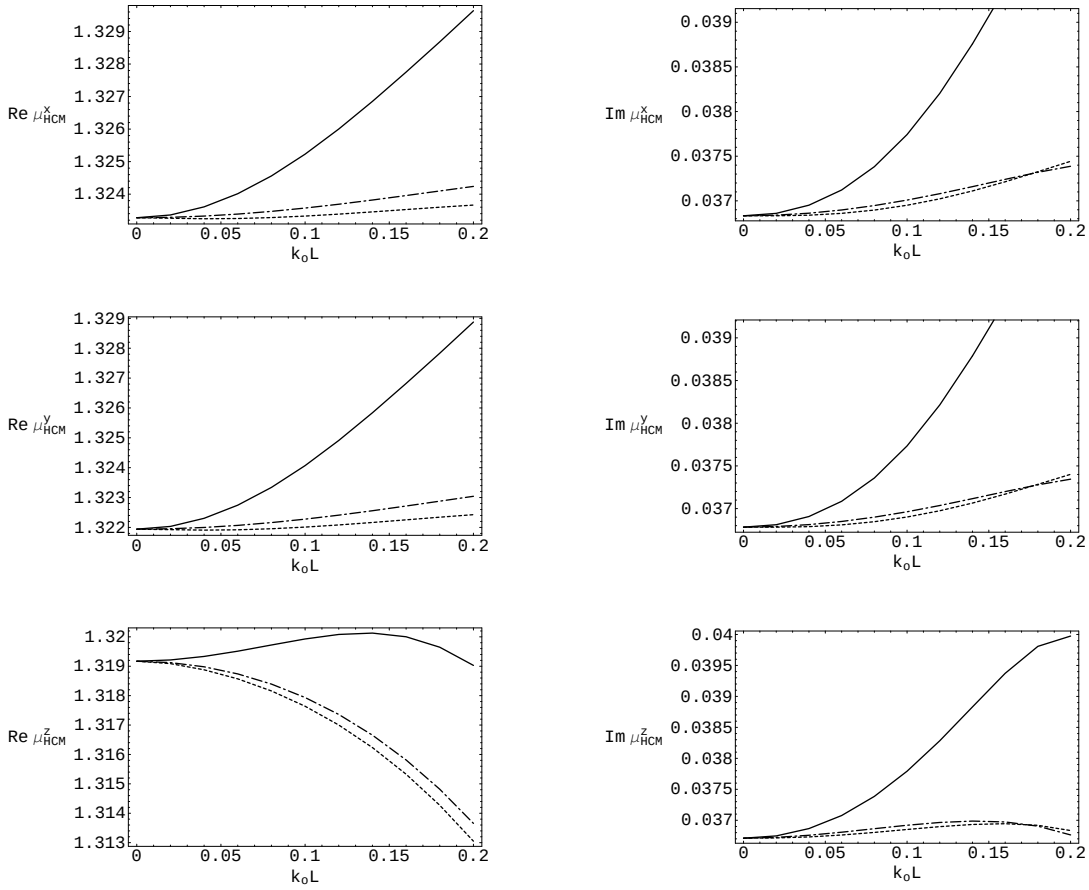

Figure A.4: continued

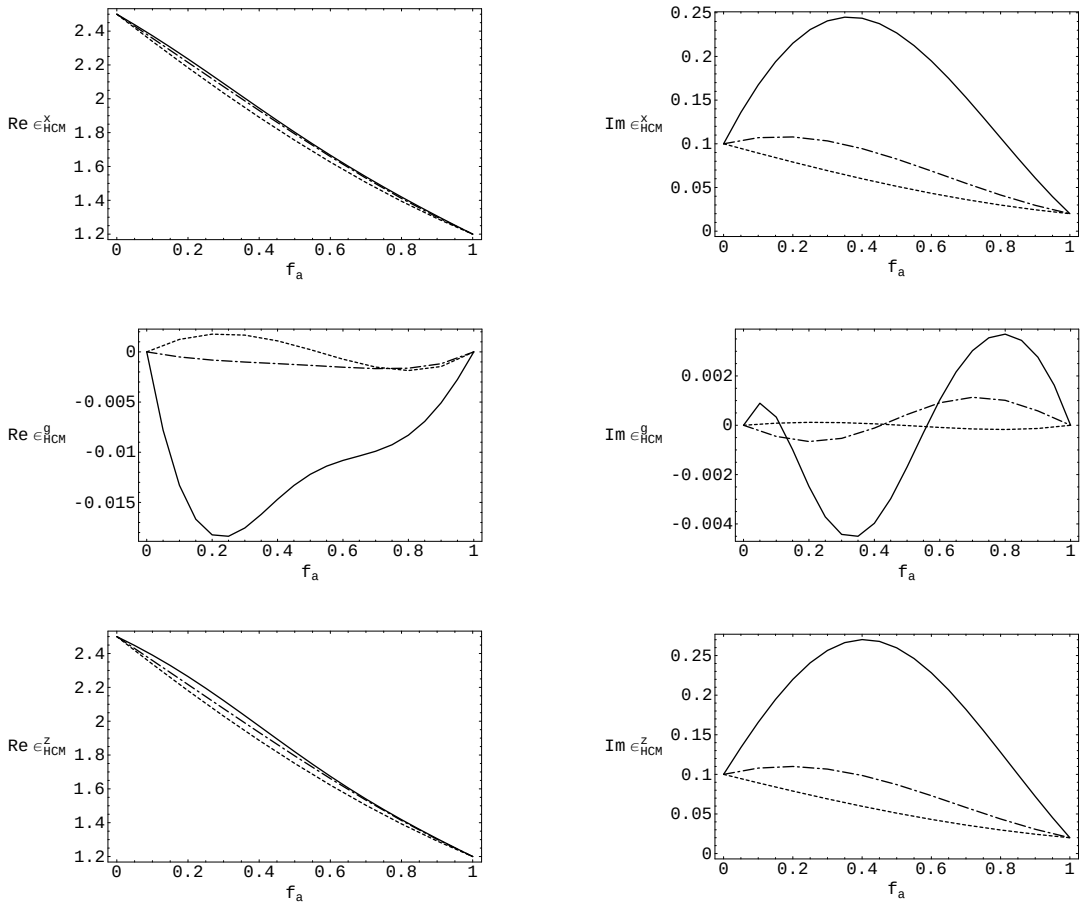

Figure A.5: Real (left) and imaginary (right) parts of the HCM constitutive parameters $\epsilon^{x,y,z}_{HCM}, \xi^{x,y,z}_{HCM}, \mu^{x,y,z}_{HCM}$ plotted against volume fraction $f_a \in (0,1)$ for $\eta/\lambda_0 = 0$ (dashed curves), $\eta/\lambda_0 = 0.05$ (broken dashed curves) and $\eta/\lambda_0 = 0.1$ (solid curves). The HCM is a Faraday chiral material.

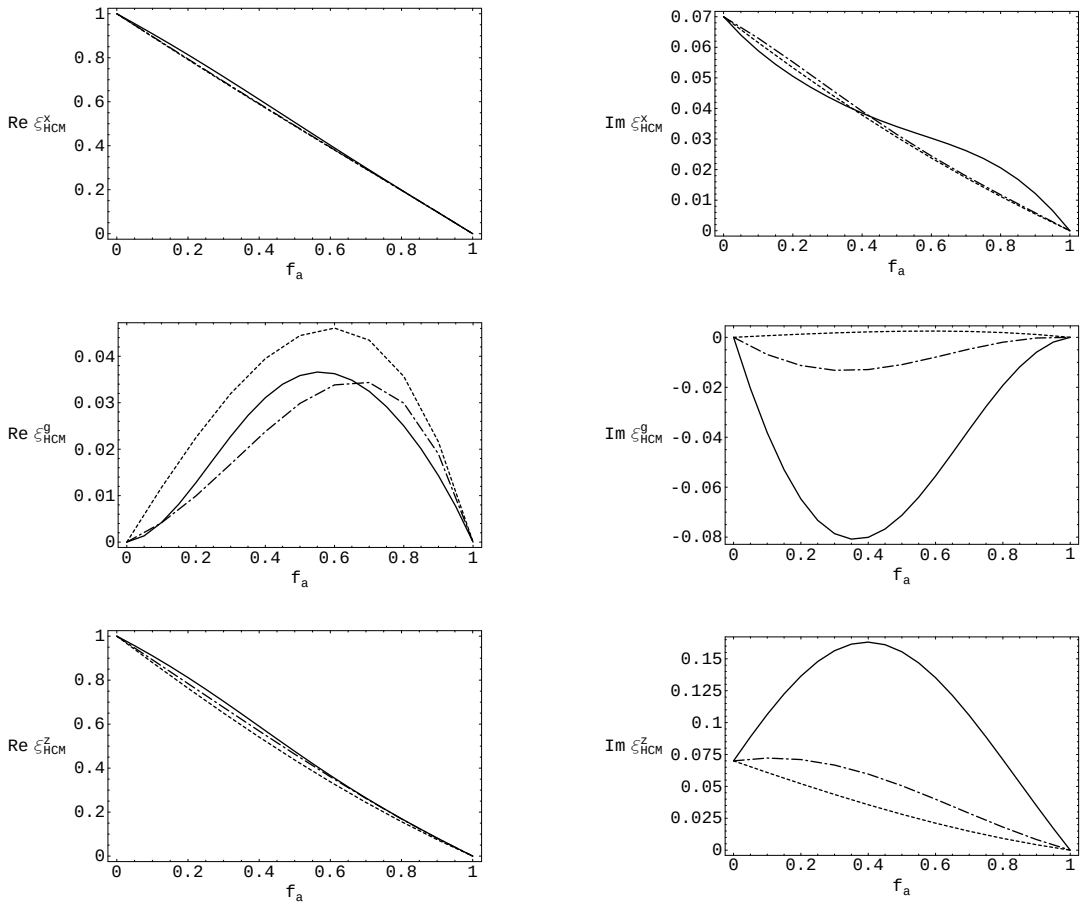

Figure A.5: continued

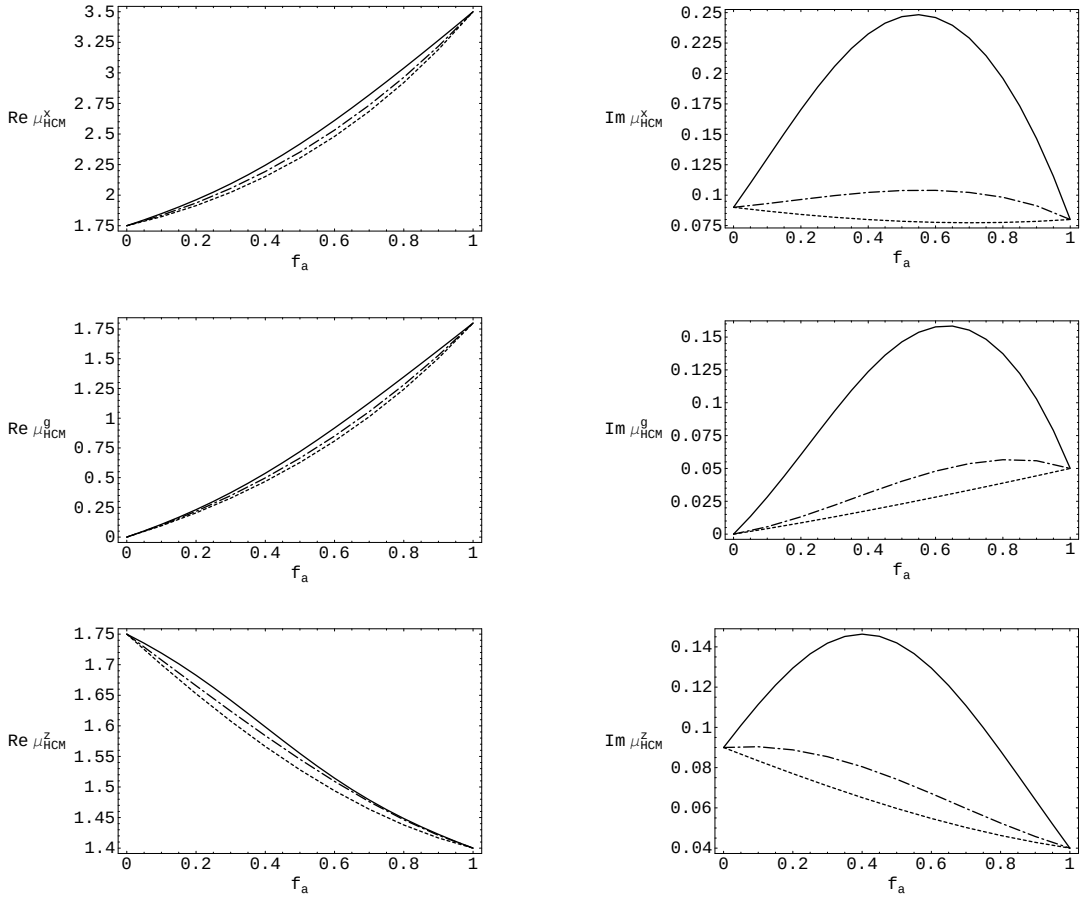

Figure A.5: continued

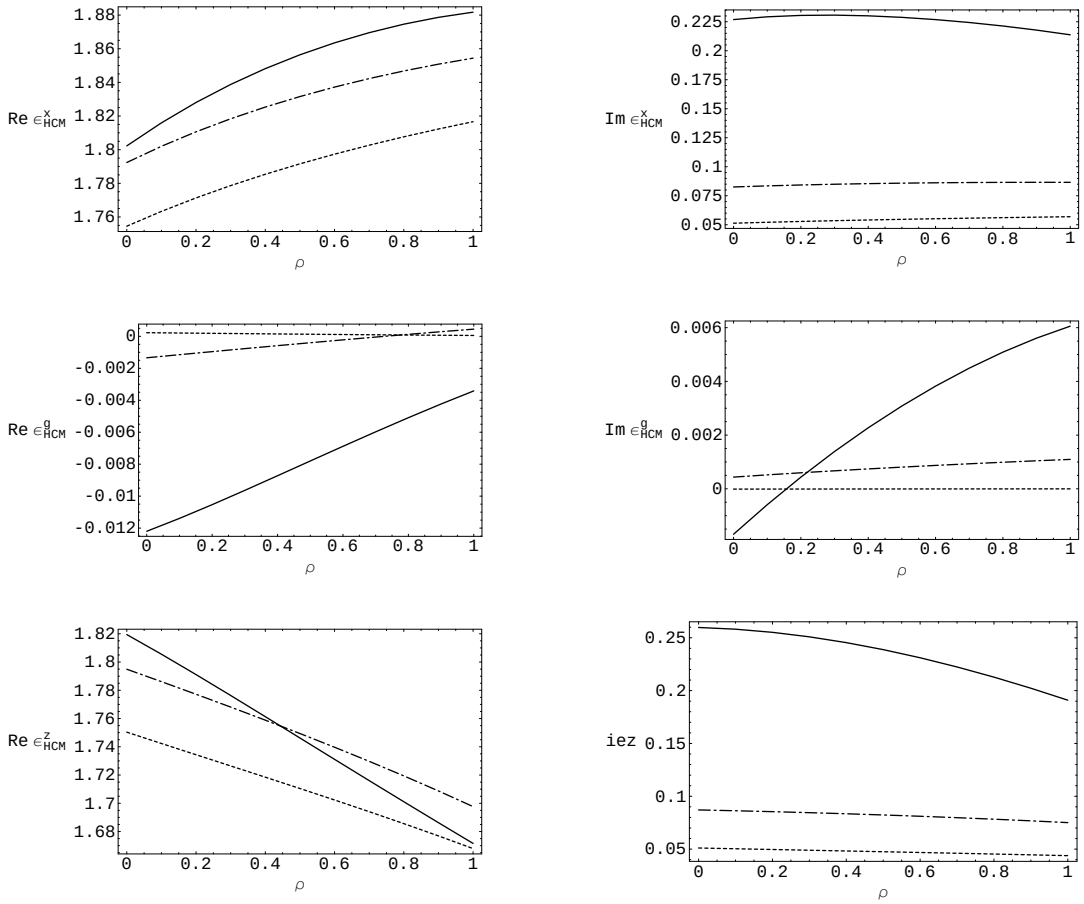

Figure A.6: Real (left) and imaginary (right) parts of the HCM constitutive parameters $\epsilon^{x,y,z}_{HCM}, \xi^{x,y,z}_{HCM}, \mu^{x,y,z}_{HCM}$ plotted against eccentricity parameter $\rho \in (0,1)$ for $\eta/\lambda_0 = 0$ (dashed curves), $\eta/\lambda_0 = 0.05$ (broken dashed curves) and $\eta/\lambda_0 = 0.1$ (solid curves). The HCM is a Faraday chiral material.

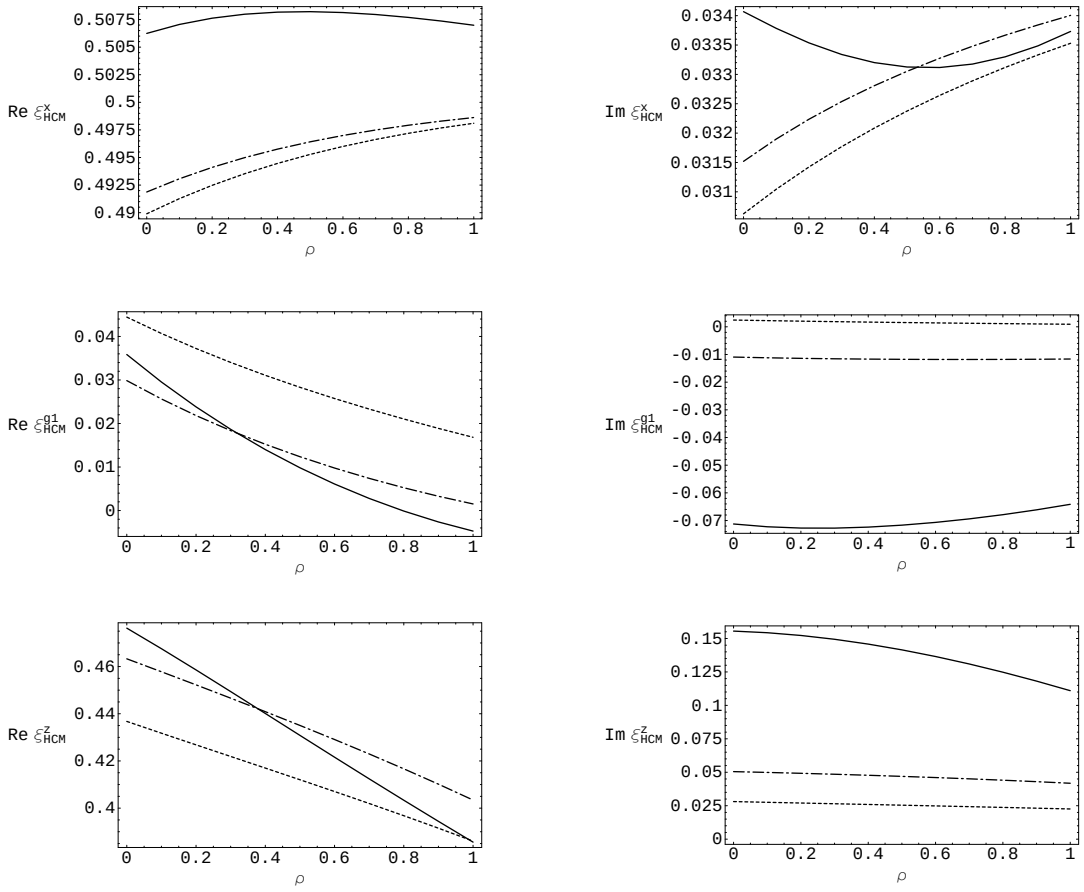

Figure A.6: continued

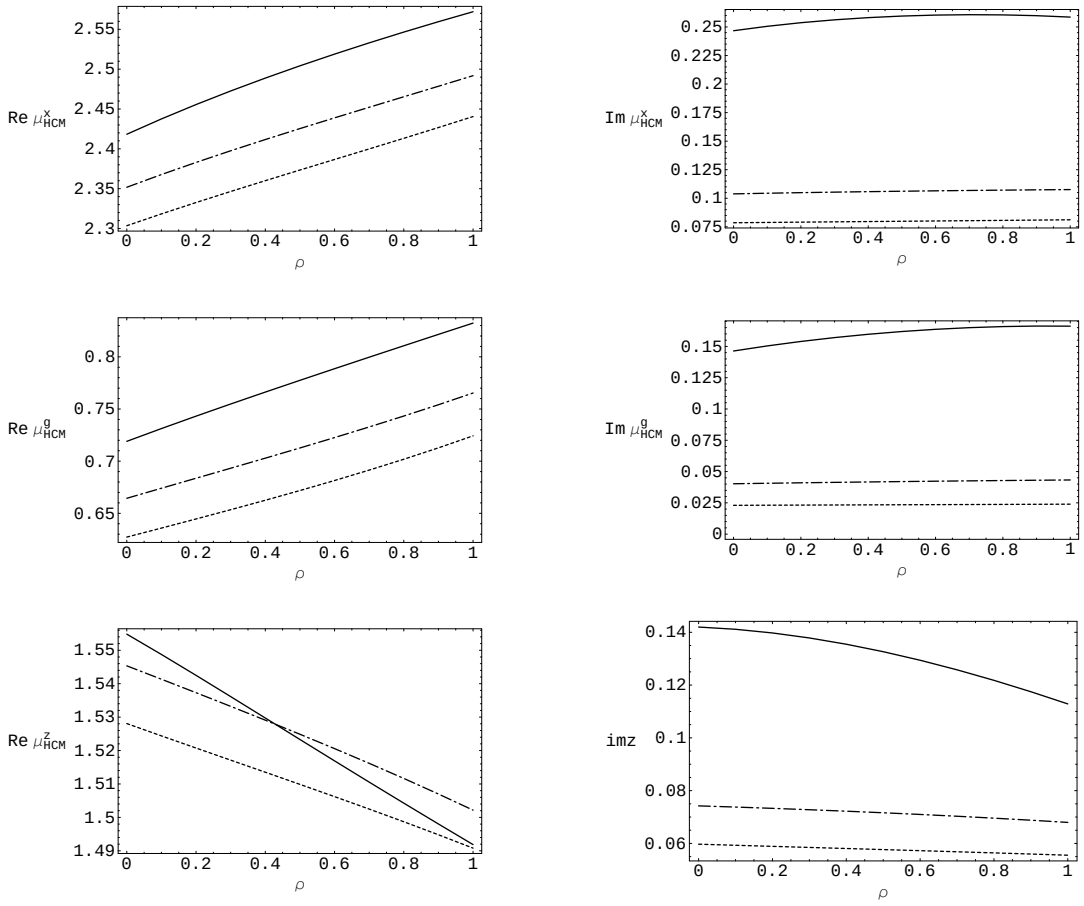

Figure A.6: continued

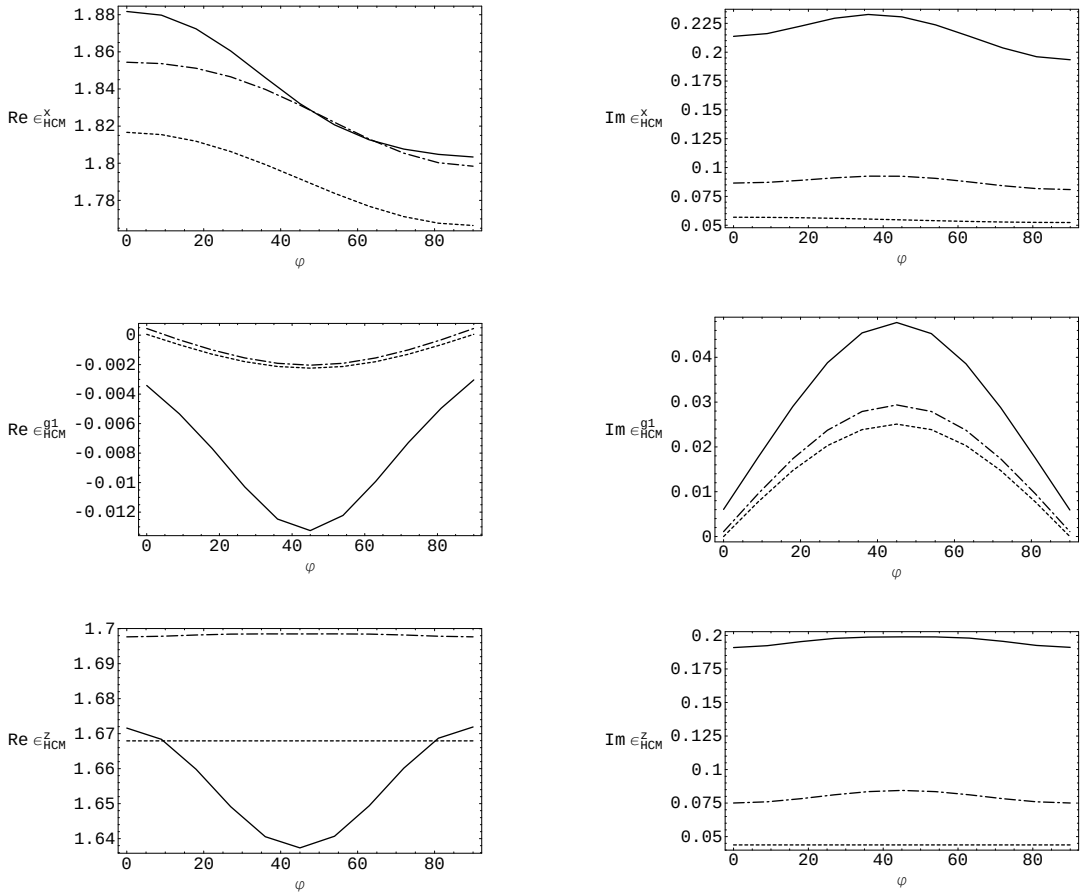

Figure A.7: Real (left) and imaginary (right) parts of the HCM constitutive parameters $\epsilon^{x,y,z}_{HCM}, \xi^{x,y,z}_{HCM}, \mu^{x,y,z}_{HCM}$ plotted against orientation angle $\varphi \in (0, \pi/2)$ for $\eta/\lambda_0 = 0$ (dashed curves), $\eta/\lambda_0 = 0.05$ (broken dashed curves) and $\eta/\lambda_0 = 0.1$ (solid curves). The HCM is a Faraday chiral material.

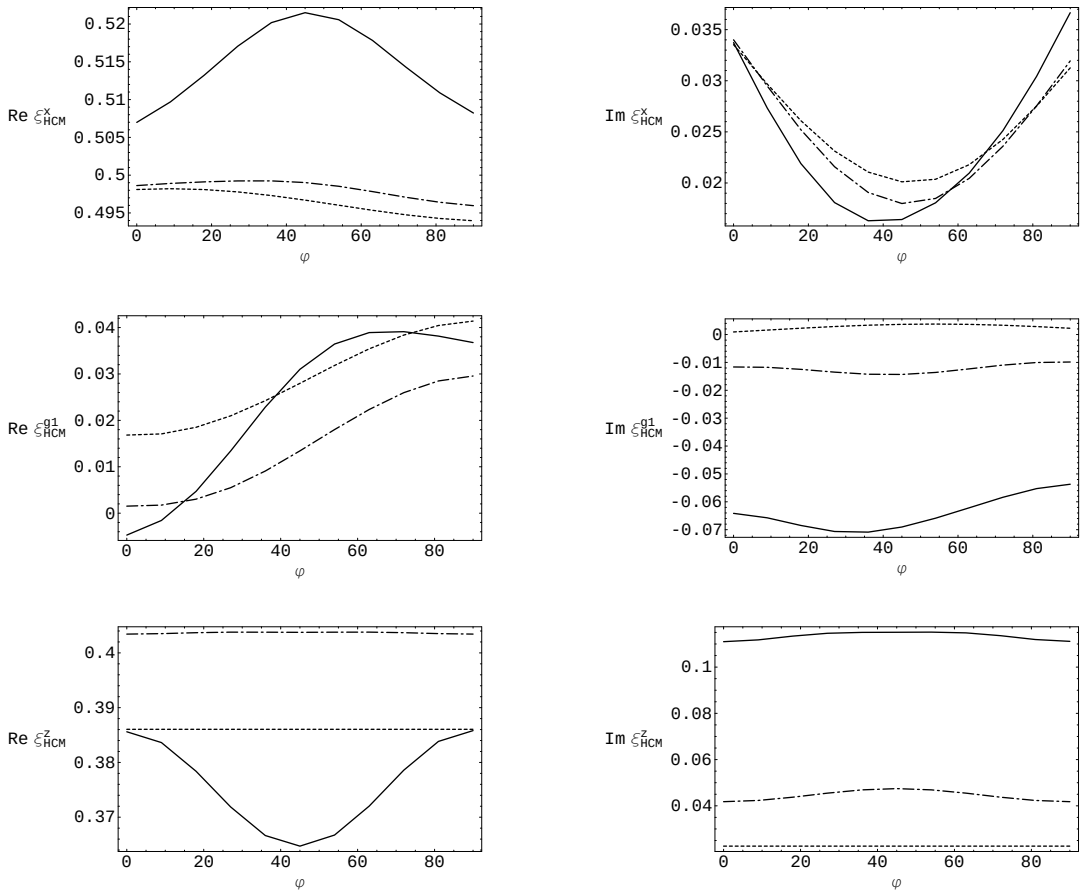

Figure A.7: continued

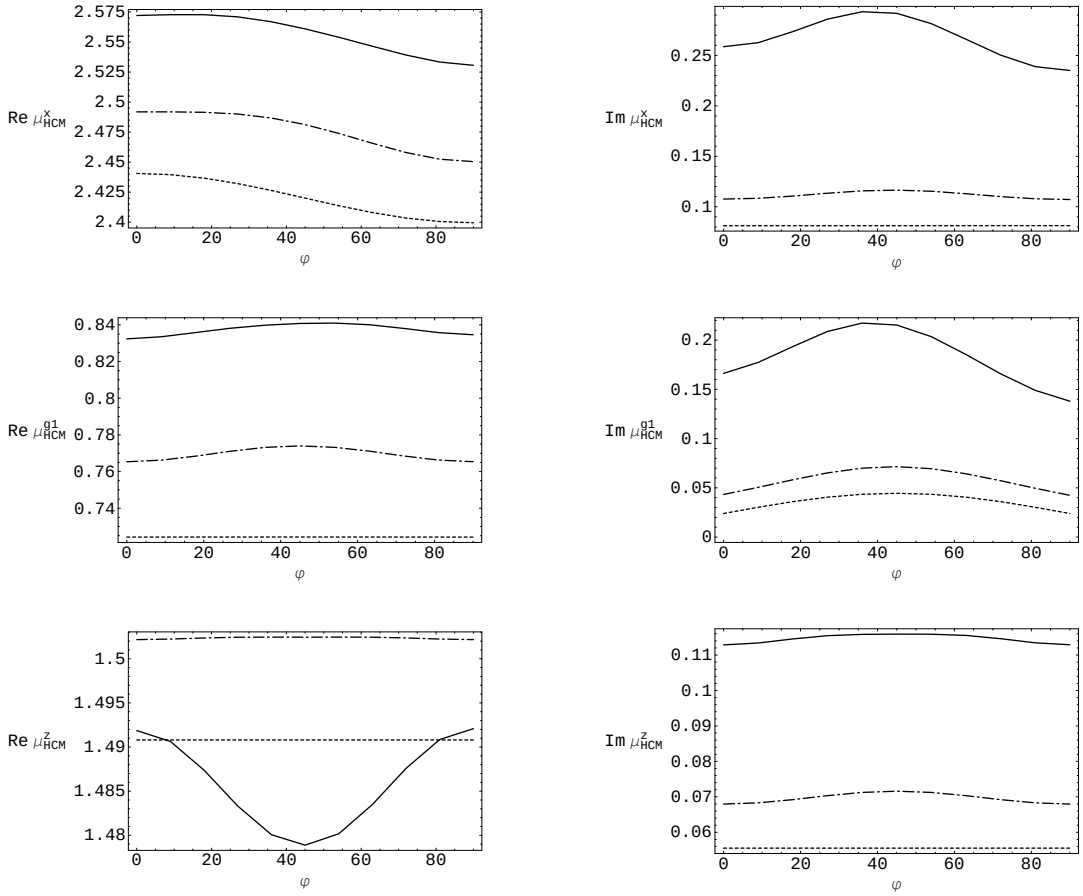

Figure A.7: continued

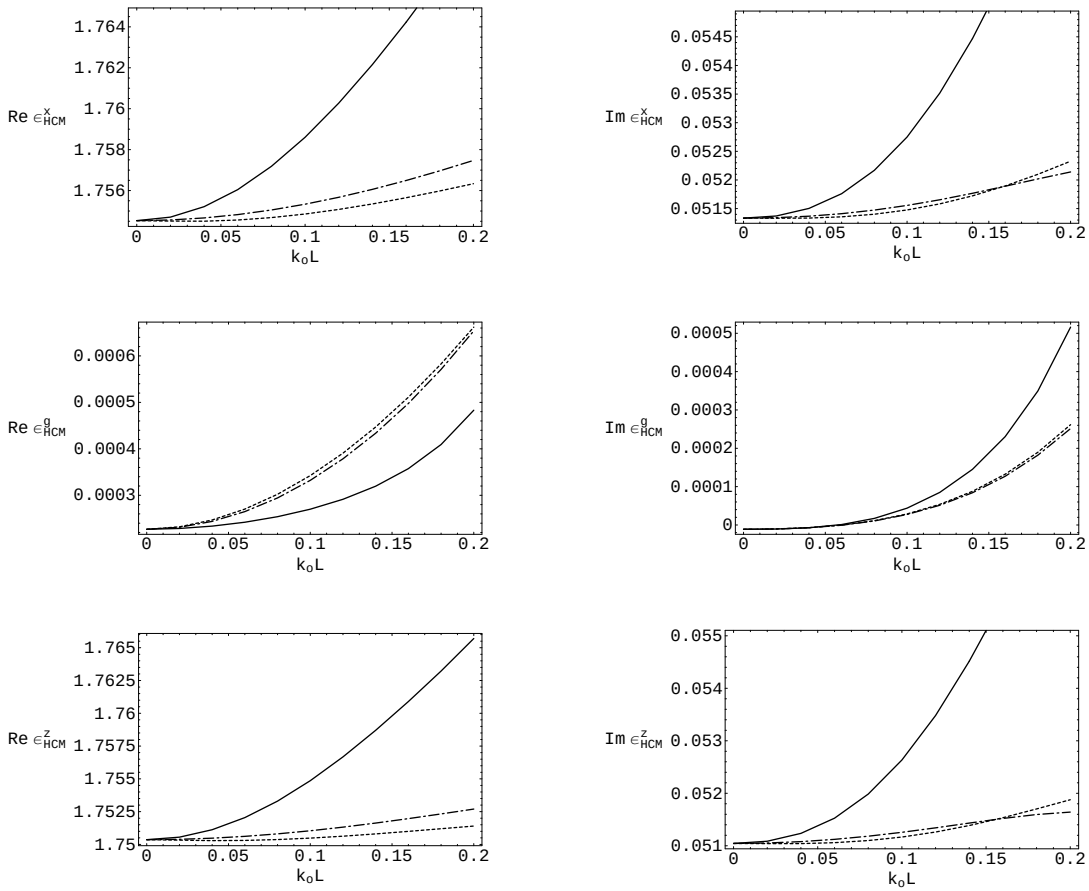

Figure A.8: Real (left) and imaginary (right) parts of the HCM constitutive parameters $\epsilon^{x,y,z}_{HCM}, \xi^{x,y,z}_{HCM}, \mu^{x,y,z}_{HCM}$ plotted against relative correlation length $k_0L \in (0, 0.2)$ for $\eta/L = 0$ (dashed curves), $\eta/L = 0.5$ (broken dashed curves) and $\eta/L = 0.95$ (solid curves). The HCM is a Faraday chiral material.

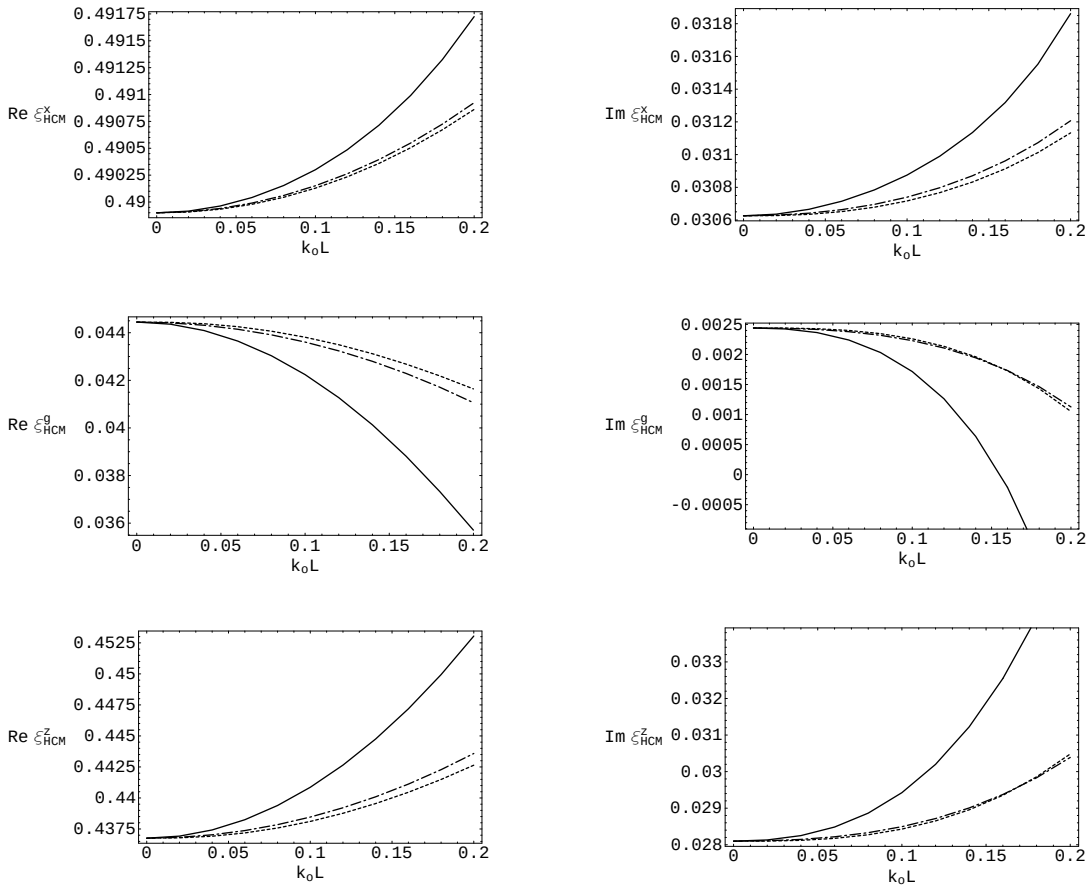

Figure A.8: continued

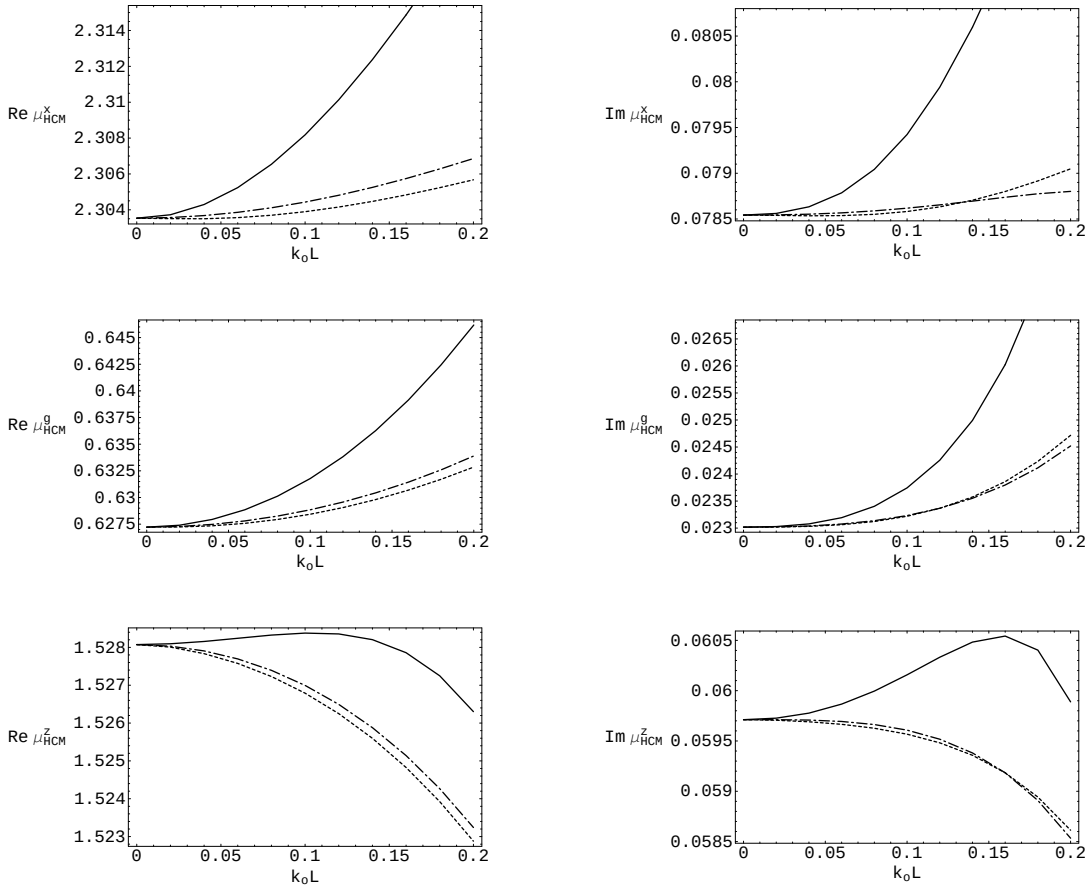

Figure A.8: continued

Appendix B

Weakly nonlinear anisotropic composites

In this Appendix we provide additional graphs to supplement those already presented in Chapter 3. See Chapter 3 for a discussion of these.

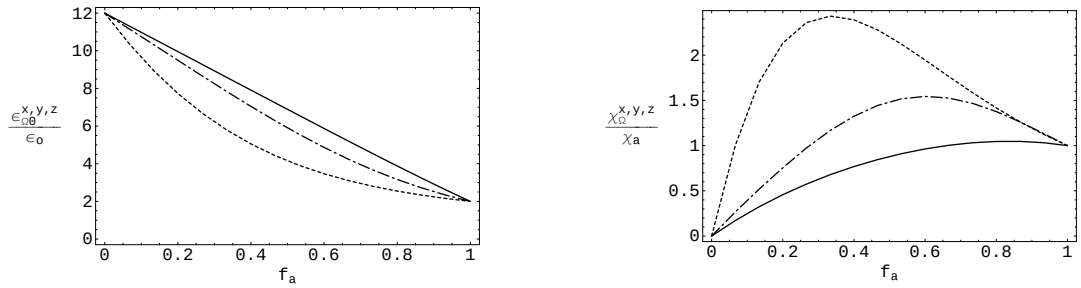

Figure B.1: The HCM relative linear permittivity and nonlinear susceptibility parameters plotted against f_a, calculated for $\eta = L = 0$. Key: $\epsilon^x_{\Omega 0}/\epsilon_0$ and χ^x_Ω/χ_a dashed curves; $\epsilon^y_{\Omega 0}/\epsilon_0$ and χ^y_Ω/χ_a broken dashed curves; and $\epsilon^z_{\Omega 0}/\epsilon_0$ and χ^z_Ω/χ_a solid curves. Component phase parameter values: $\epsilon_{a0} = 2\epsilon_0$, $\chi_a = 9.07571 \times 10^{-12}\epsilon_0\,\mathrm{m^2V^{-2}}$, $\epsilon_b \equiv \epsilon_{b0} = 12\epsilon_0$, $U_x = 1$, $U_y = 3$ and $U_z = 15$.

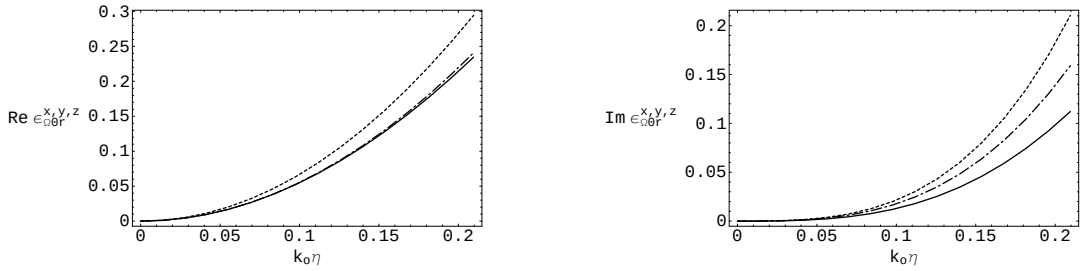

Figure B.2: Real and imaginary parts of the HCM linear permittivity and nonlinear susceptibility parameters plotted against η (in nm), calculated for $L = 0$ and $f_a = 0.3$. Key: $\epsilon^x_{\Omega 0r}$ and $\chi^x_{\Omega r}$ dashed curves; $\epsilon^y_{\Omega 0r}$ and $\chi^y_{\Omega r}$ broken dashed curves; and $\epsilon^z_{\Omega 0r}$ and $\chi^z_{\Omega r}$ solid curves. Component phase parameter values as in Fig. 3.1.

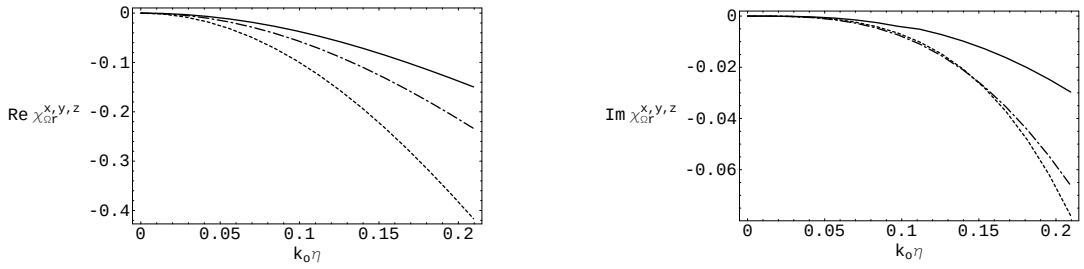

Figure B.2: continued

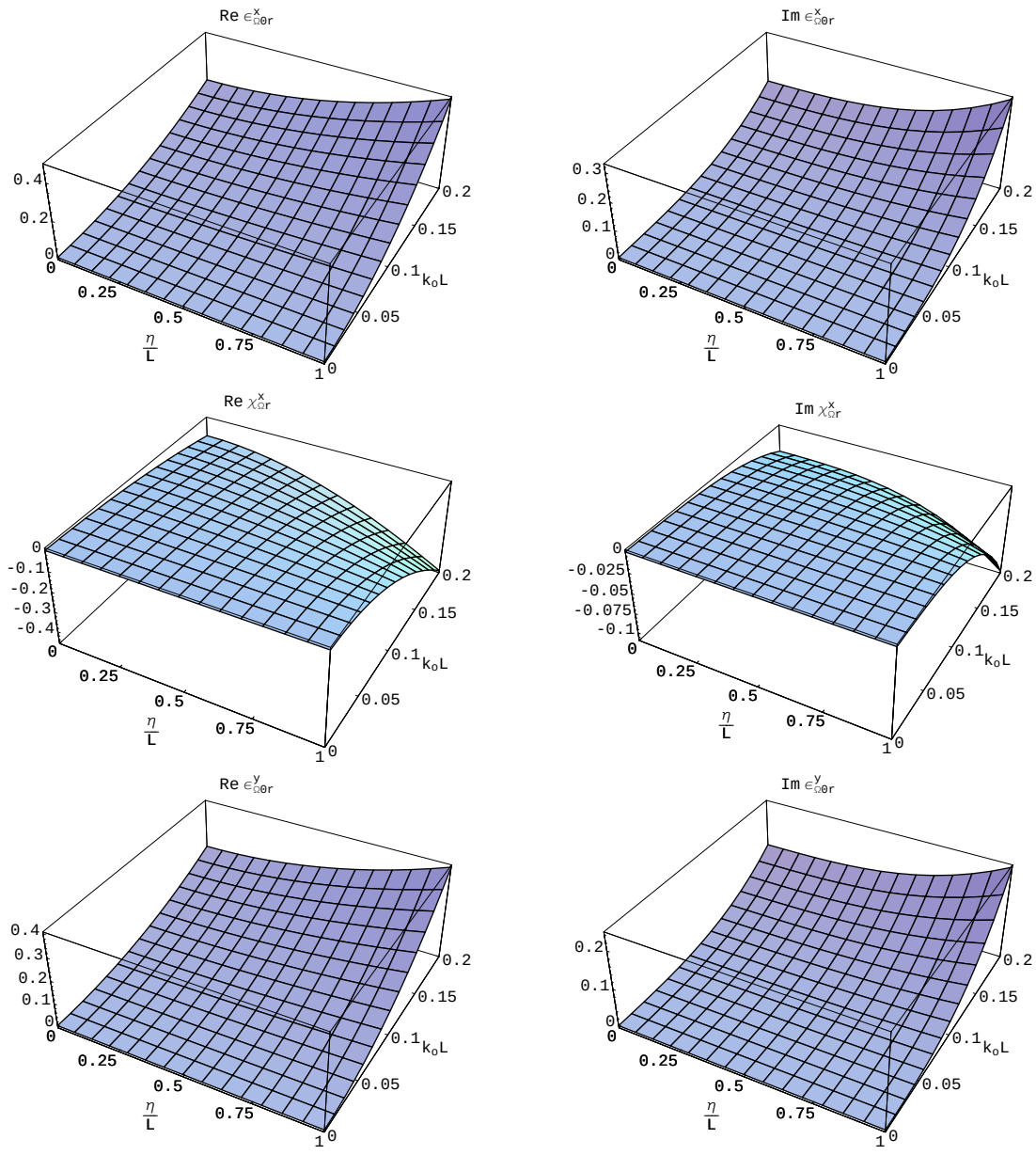

Figure B.3: Real and imaginary parts of the HCM linear permittivity and nonlinear susceptibility parameters $\epsilon^{x,y,z}_{\Omega 0 r}$ and $\chi^{x,y,z}_{\Omega r}$ plotted against L (in nm) and η/L, calculated for $f_a = 0.3$. Component phase parameter values as in Fig. 3.1.

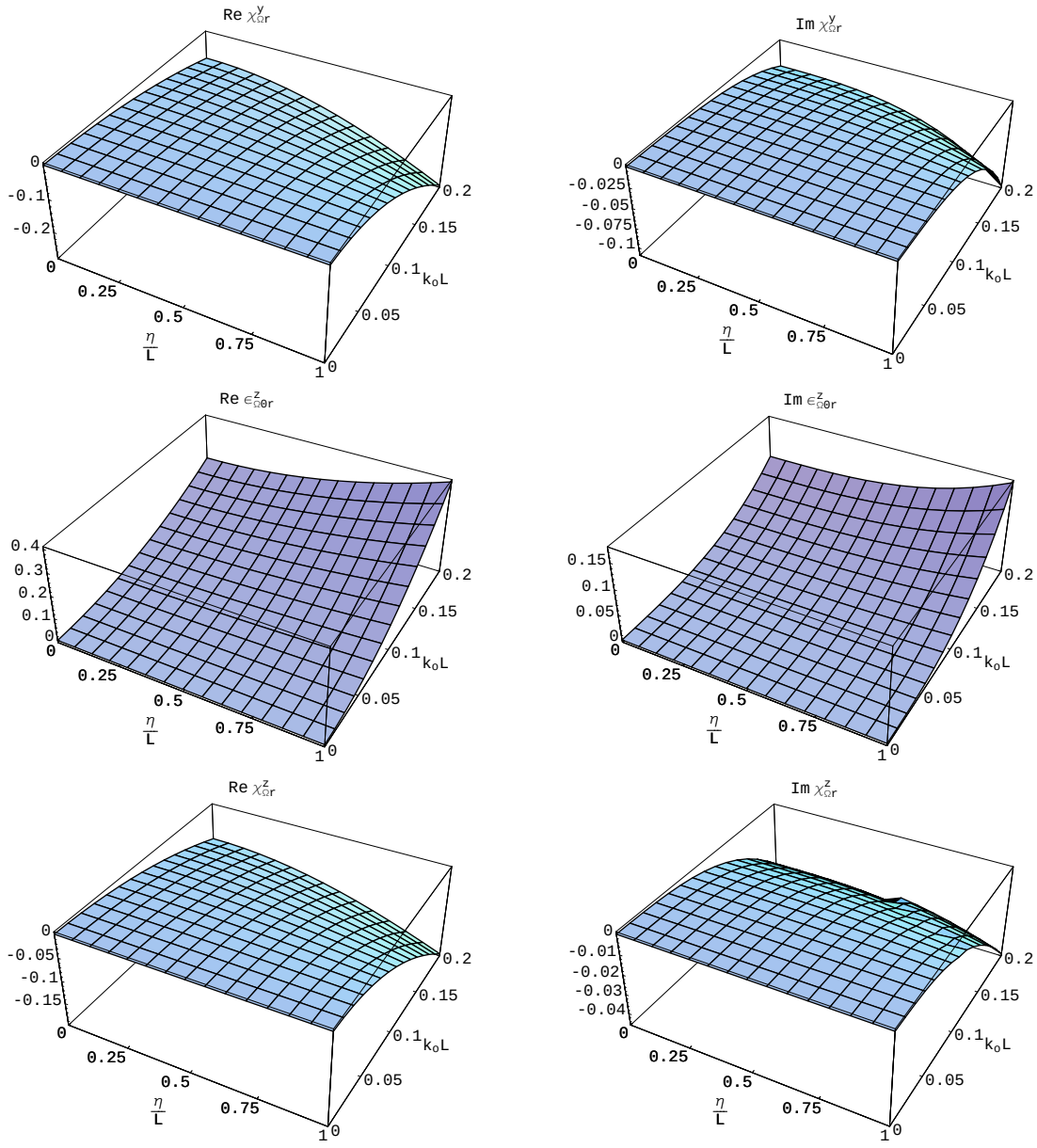

Figure B.3: continued

Appendix C

Third order considerations

In this Appendix we provide additional graphs to supplement those already presented in Chapter 4. See Chapter 4 for a discussion of these.

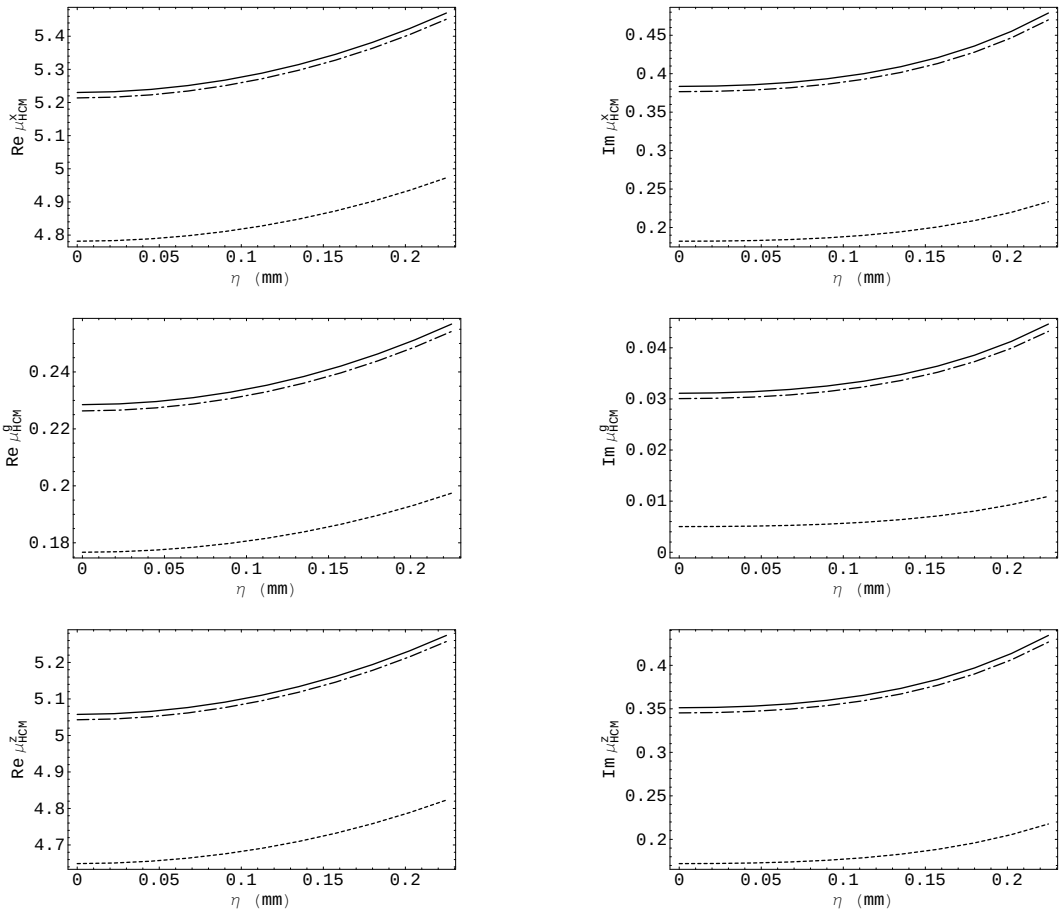

Figure C.1: Real (left) and imaginary (right) parts of the HCM constitutive parameters $\mu^{x,z,g}_{HCM}, \epsilon^{x,z,g}_{HCM}, \xi^{x,z,g}_{HCM}$ plotted against η (mm) for $\delta = 10$. Key: dashed curve is the zeroth–order SPFT estimate; broken dashed curve is the second–order SPFT estimate; and solid curve is the third–order SPFT estimate.

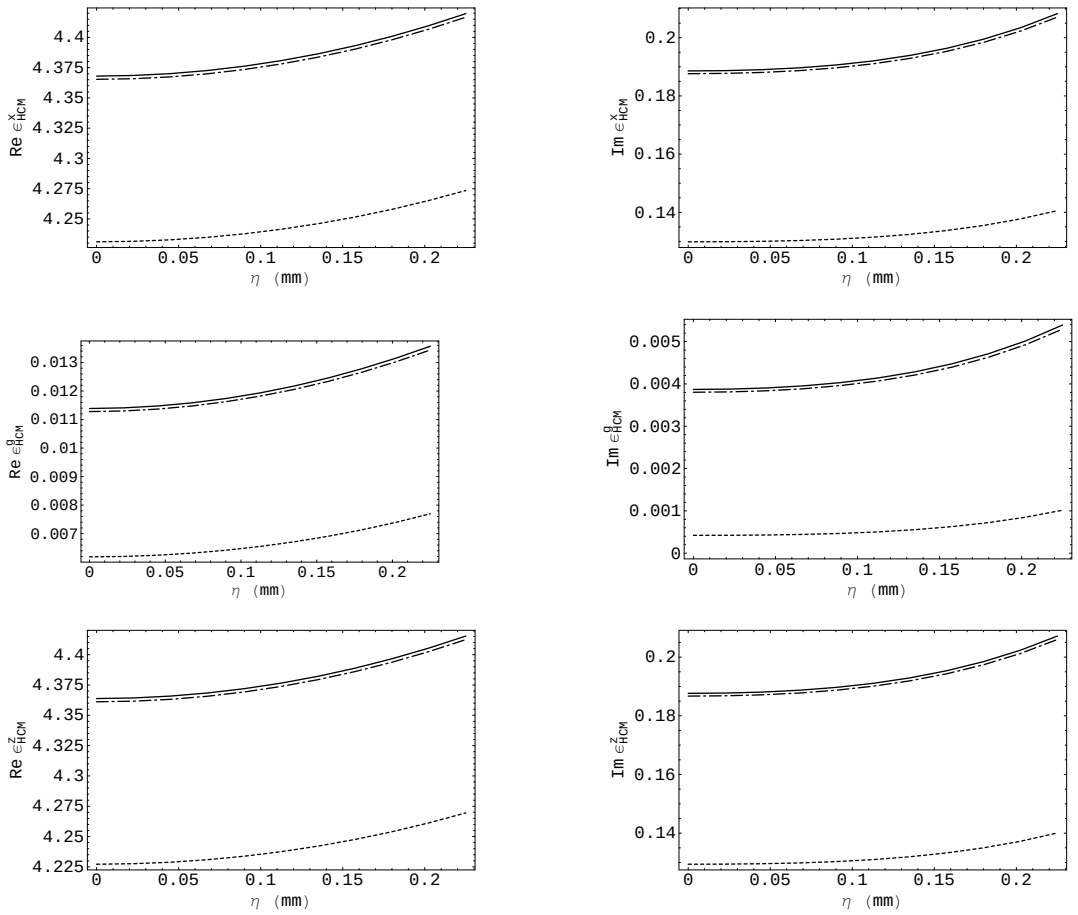

Figure C.1: continued

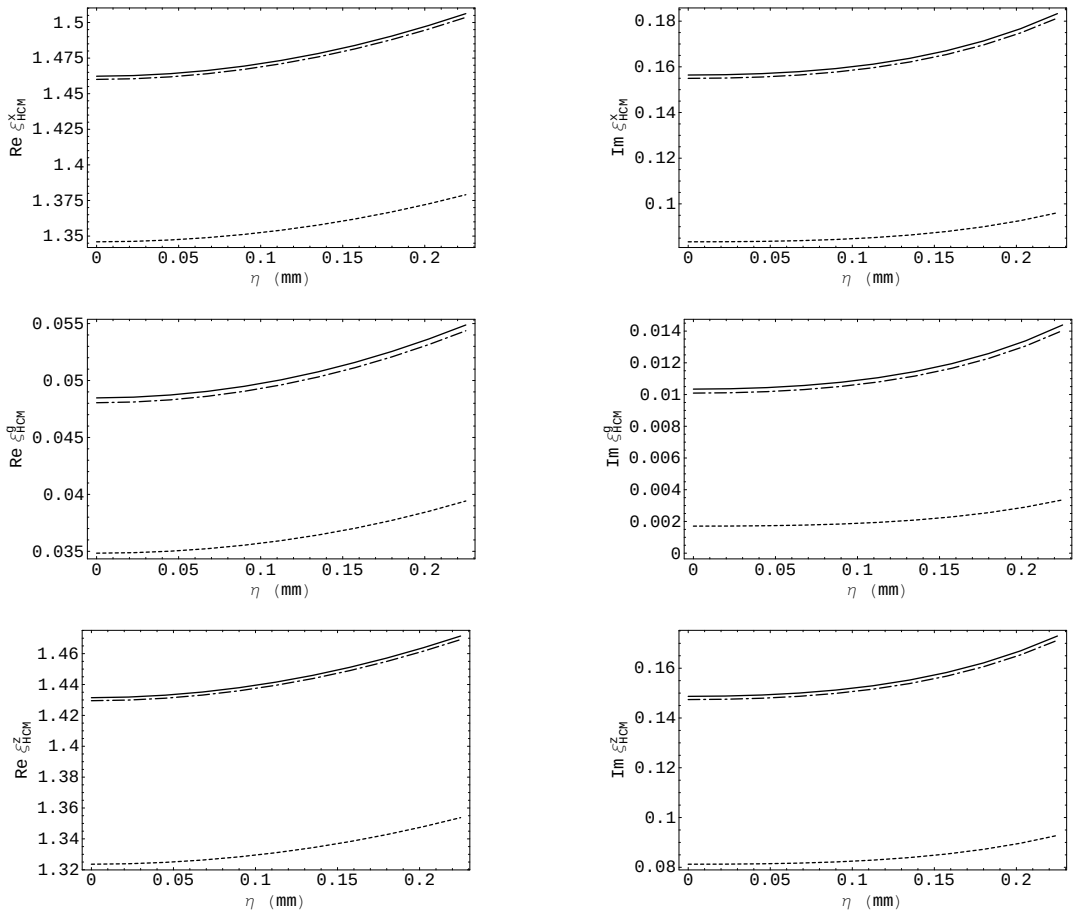

Figure C.1: continued

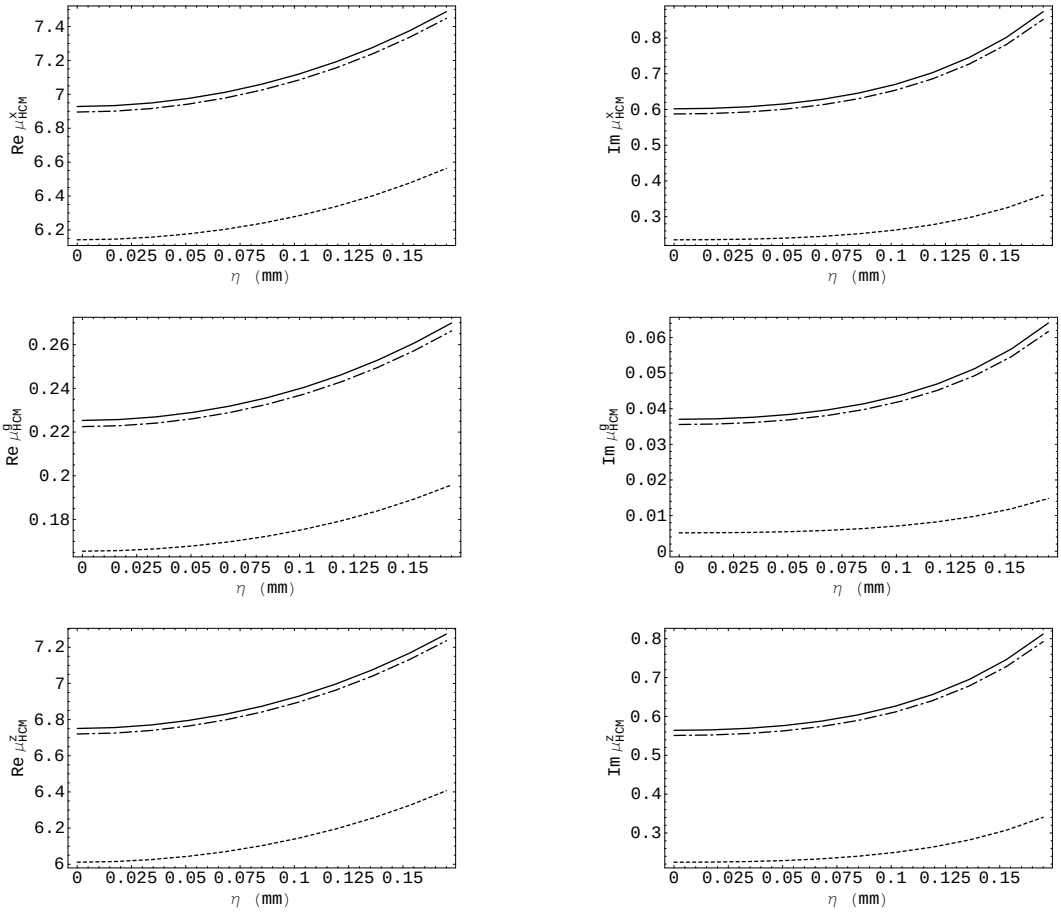

Figure C.2: As Figure C.1 but for $\delta = 20$.

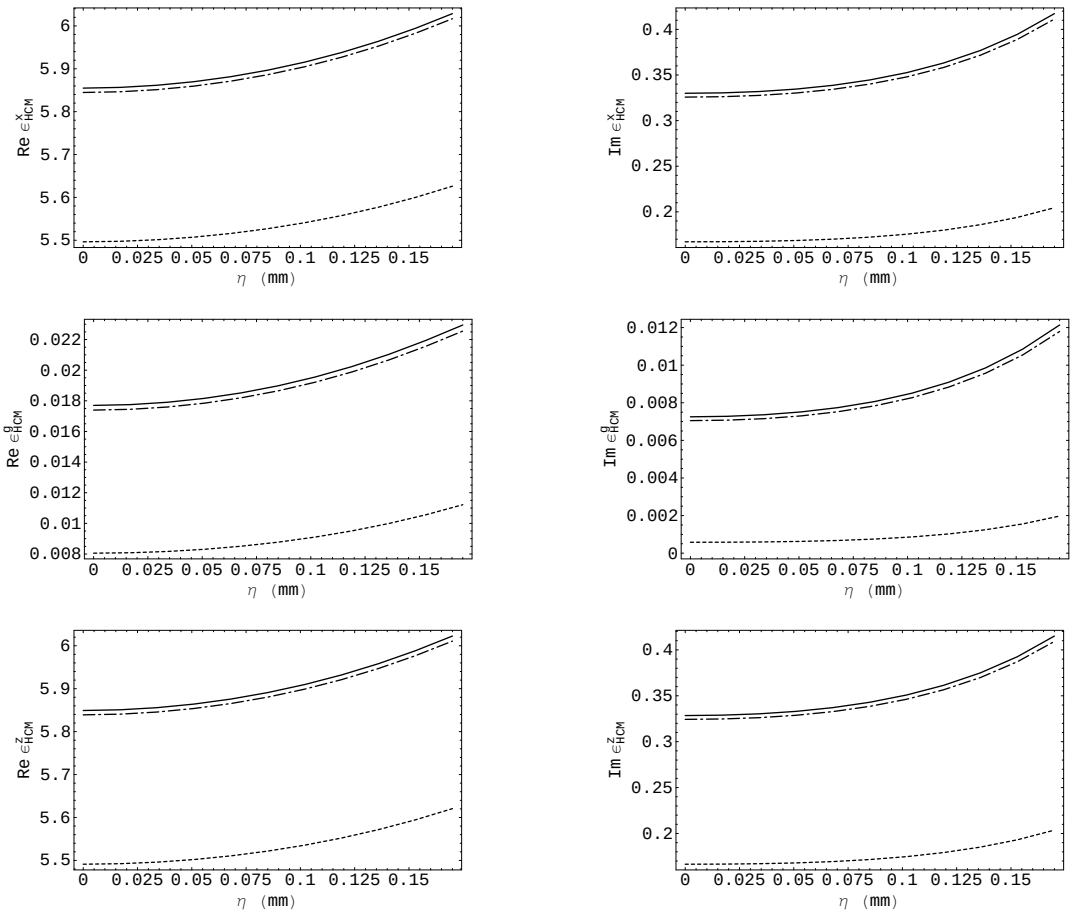

Figure C.2: continued

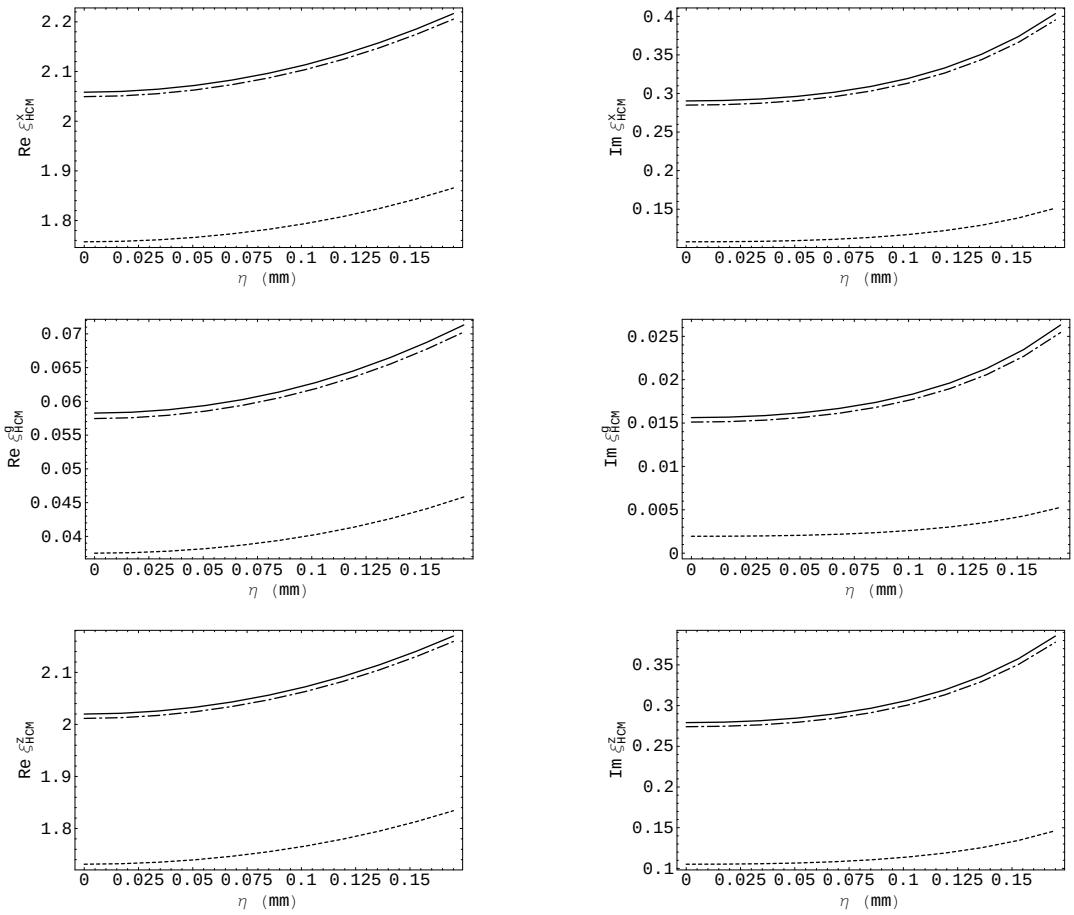

Figure C.2: continued

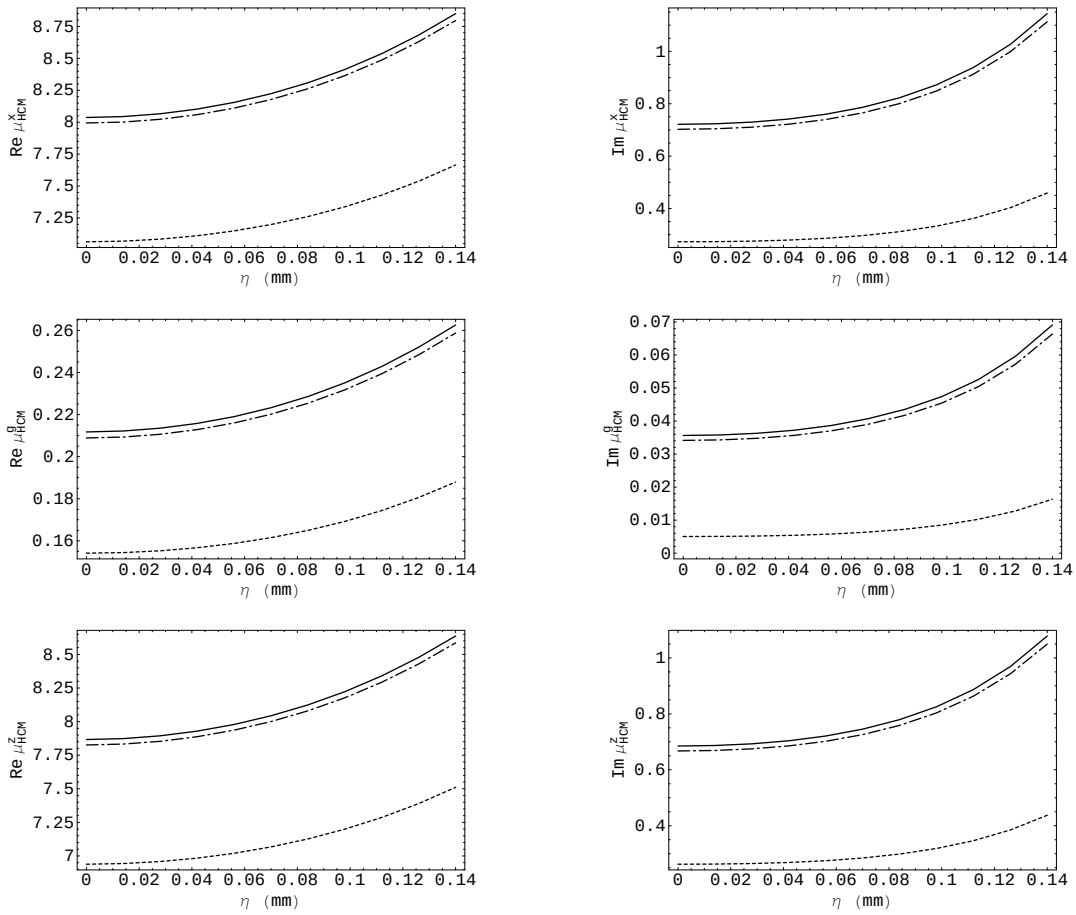

Figure C.3: As Figure C.1 but for $\delta = 30$.

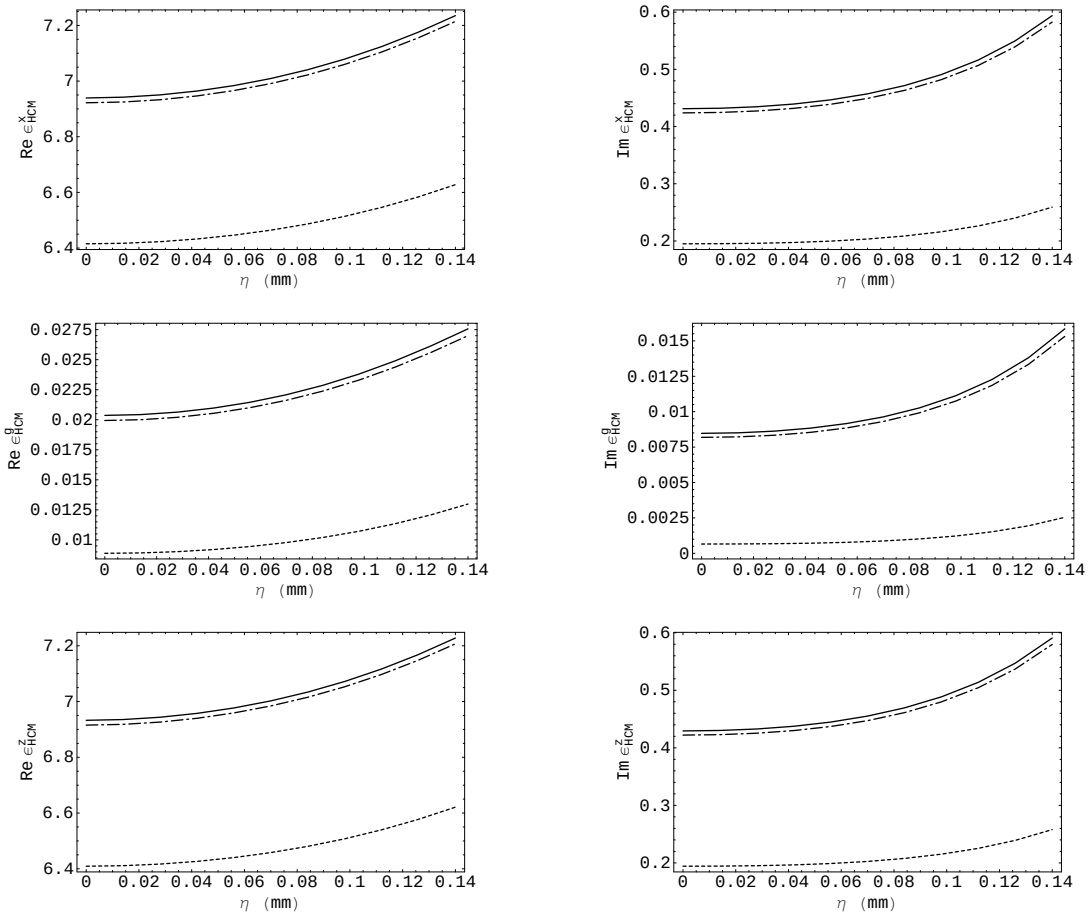

Figure C.3: continued

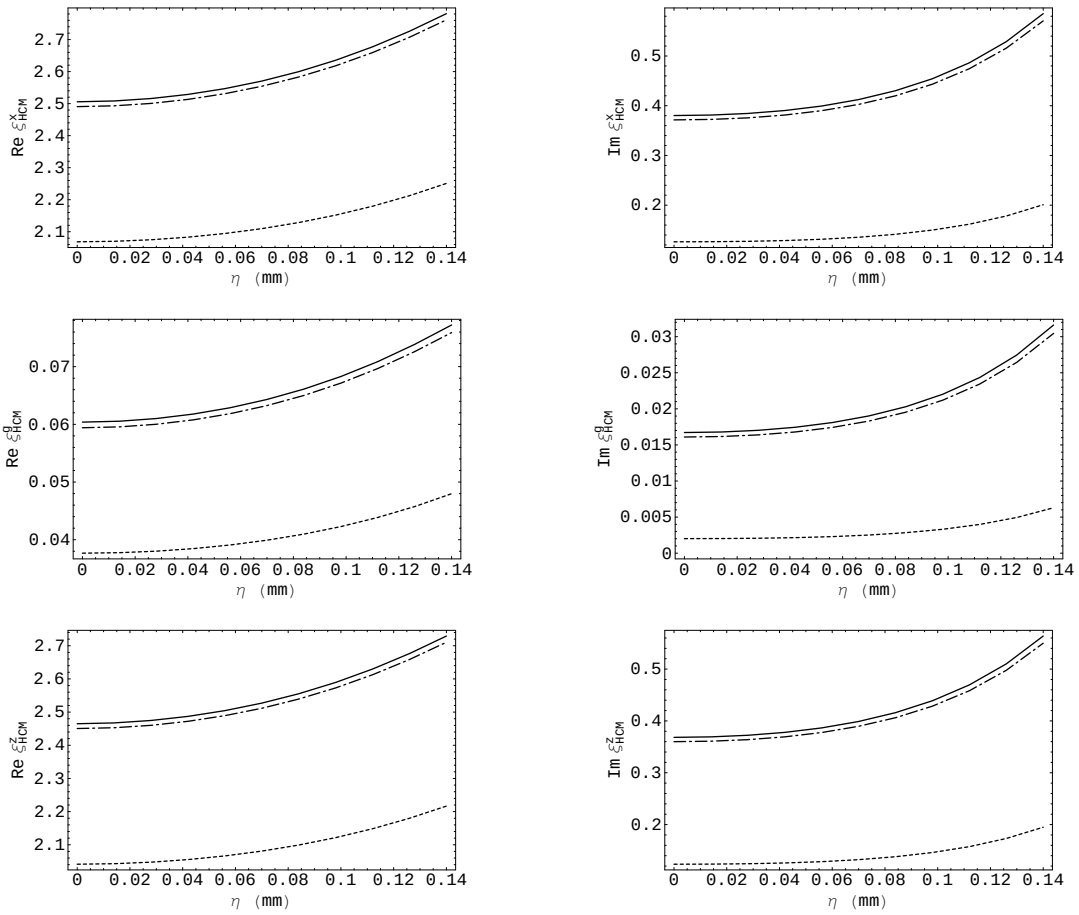

Figure C.3: continued

Bibliography

[1] A. Lakhtakia (ed.), 1996, Selected Papers on Linear Optical Composite Materials, (Bellingham WA, USA: SPIE Optical Engineering Press).

[2] B. Michel, 1997, A Fourier space approach to the pointwise singularity of an anisotropic dielectric material, *Int. J. Appl. Electromagn. Mech.* **8**, 219–227.

[3] B. Michel and W.S. Weiglhofer, 1997, Pointwise singularity of dyadic Green function in a general bianisotropic material, *Arch. Elekron. Übertrag.*, **51**, 219–223; erratum 1998, **52**, 31.

[4] L. Tsang, J.A. Kong, & R.W. Newton, 1982. Application of strong fluctuation random medium theory to scattering of electromagnetic waves from a half–space of dielectric mixture. *IEEE Trans. Antennas Propagat.***30**, 292–302.

[5] Z.D. Genchev, 1992, Anisotropic and gyrotropic version of Polder and van Santen's mixing formula, *Waves Random Media*, **2**, 99–110.

[6] N.P. Zhuck, 1994, Strong–fluctuation theory for a mean electromagnetic field in a statistically homogeneous random material with arbitrary anisotropy of electrical and statistical properties, *Phys. Rev. B*, **50**, 15636–15645.

[7] B. Michel and A. Lakhtakia, 1995, Strong–property–fluctuation theory for homogenizing chiral particulate composites, *Phys. Rev. E*, **51**, 5701–5707.

[8] T.G. Mackay, A. Lakhtakia and W.S. Weiglhofer, 2000, Strong–property–fluctuation theory for homogenization of bianisotropic composites: formulation, *Phys. Rev. E*, **62**, 6052–6064; erratum 2001, **63**, 049901.

[9] J.D. Jackson, 1999, Classical Electrodynamics. 3rd Ed.,*American Association of Physics Teachers*, **67**, 841-842.

[10] A. Lakhtakia, 1993, Frequency-dependent continuum electromagnetic properties of a gas of scattering centers, in: M. Evans and S.Keilich (eds.), *Modern Nonlinear Optics, Part 2. Advances in Chemical Physics Series*,**85** (2) (184 ref.), 311-359.

[11] W.S. Weiglhofer, 1998, A perspective on bianisotropy and Bianisotropics'97, *Int. J. Appl. Electomagn. Mech.* **9**, 93-101.

[12] P. Padley,1956, Some Aspects of Diffraction Theory and their Application to the Ionosphere. *Reports on Progress in Physics.***19** 188-267.

[13] W.S. Weiglhofer, 1995, Frequency-dependent dyadic Green functions for bianisotropic media, in: T.W. Barrett and D.M. Grimes (eds.), *A*dvanced Electromagnetism: Foundations, Theory, Applications. 376-389.

[14] T.G. Mackay, A. Lakhtakia, W.S. Weiglhofer, 2001, Third-order implementation and convergence of the strong-property-fluctuation theory in electromagnetic homogenization, *P*hys.Rev. E, **64** 066616.

[15] W.T. Doyle , 1989, Optical properties of a suspension of metal spheres *Phys. Rev. B* **39** 9852–9858

[16] C.E. Dungey, and C.F. Bohren, 1991, Light scattering by nonspherical particles: a refinement to the coupled–dipole method, *J. Opt. Soc. Am. A*, **8**, 81–87.

[17] M.T. Prinkey , A. Lakhtakia and B. Shanker ., 1994 On the extended Maxwell–Garnett and the extended Bruggeman approaches for dielectric-in-dielectric composites *Optik* **96** 25–30

[18] B. Shanker and A. Lakhtakia , 1993, Extended Maxwell Garnett model for chiral–in–chiral composites *J. Phys. D: Appl. Phys.* **26** 1746–1758

[19] B. Shanker , 1996, The extended Bruggeman approach for chiral–in–chiral mixtures *J. Phys. D: Appl. Phys.* **29** 281–288

[20] W.S. Weiglhofer, A. Lakhtakia and B. Michel, 1997, Maxwell Garnett and Bruggeman formalisms for a particulate composite with bianisotropic host material, *Micro. Opt. Technal. Lett.* **15**, 1263-266 (1997); erratum **22**, 221 (1999)

[21] B. Michel, A. Lakhtadia and W.S. Weiglhofer,1998, Homogenization of linear bianisotropic particulate composite media - Numerical studies, *Int. J. Appl. Electromag. Mech.* **9**, 167-178 (1998); erratum **10**, 537-538 (1999).

[22] U. Frisch, 1970, Wave propagation in random media, *Probabilistic Methods in Applied Mathematics* , A.T. Bharucha–Reid (ed.), (London, UK: Academic Press), **1**, 75–198.

[23] Y.A. Ryzhov, and V.V.Tamoikin, 1970, Radiation and propagation of electromagnetic waves in randomly inhomogeneous media, *Radiophys. Quantum Electron.*, **14**, 228–233.

[24] L. Tsang, and J.A. Kong, 1981, Scattering of electromagnetic waves from random media with strong permittivity fluctuations, *Radio Sci.*, **16**, 303–320.

[25] T.G. Mackay, A. Lakhtakia and W.S. Weiglhofer, 2001, Ellipsoidal topology, orientation diversity and correlation length in bianisotropic composite materials, *Arch. Elekron. Übertrag.*, **55**, 243–251.

[26] T.G. Mackay, A. Lakhtakia and W.S. Weiglhofer, 2001, Homogenisation of similarly oriented, metallic, ellipsoidal inclusions using the bilocally approximated strong–property–fluctuation theory, *Opt. Commun.*, **107**, 89–95.

[27] L. Tsang, J.A. Kong, and R.W. Newton,1982, Application of strong fluctuation random medium theory to scattering of electromagnetic waves from a half–space of dielectric mixture," *IEEE Trans. Antennas Propagat.* **30**, 292–302.

[28] W.S. Weiglhofer, 1993, Analytic methods and free–space dyadic Green's functions, *Radio Sci.*, **28**, 847–857.

[29] W.H. Press, B.P. Flannery, S.A. Teukolsky, & W.T. Vetterling, 1992, *Numerical recipes in fortran*, 2nd. ed. Cambridge, UK: Cambridge University Press.

[30] B. Michel, 2000, Recent developments in the homogenization of linear bianisotropic composite materials, in *Electromagnetic Fields in Unconventional Materials and Structures*, O.N. Singh and A. Lakhtakia (eds.), 39–82.

[31] N. Engheta, D.L. Jaggard, and M.W. Kowarz, 1992, Electromagnetic waves in Faraday chiral media, *IEEE Trans. Antennas Propagat.*, **40**, 367–374.

[32] W.S. Weiglhofer and Lahktakia, A., 1998, The correct constitutive relations of chiroplasmas and chiroferrites, *Microw. Opt. Technol. Lett.*, **17**, 405–408.

[33] C.M. Krowne, 1984, Electromagnetic theorems for complex anisotropic media, *IEEE Trans. Antennas Propagat.* **32**, 1224–1230.

[34] W.S. Weiglhofer, Lahktakia, A. and B. Michel, 1998, On the constitutive parameters of a chiroferrite composite material, *Microw. Opt. Technol. Lett.*, **18**, 342–345.

[35] J.V. Kranendonk, and J.E. Sipe, 1977, Foundations of the macroscopic electromagnetic theory of dielectric media, in *Progress in Optics*, E. Wolf (ed.), (Amsterdam, The Netherlands: North–Holland), Vol. XV, pp245–350.

[36] T.G. Mackay, and A. Lakhtakia, 2008, Electromagnetic fields in linear bianisotropic materials, *Progress in Optics,* (to appear)

[37] B. Shanker, and A. Lakhtakia, 1993, Extended Maxwell Garnett formalism for composite adhesives for microwave-assisted adhesion of polymer surfaces, *J. Composite Mater.*, **27**, 1203–1213.

[38] B. Lax, K.J. Button. 1962, *Microwave ferrites and ferrimagnetics*. New York: McGraw–Hill.

[39] R.M. Walser, 2003, Metamaterials: an introduction, in *Introduction to Complex Mediums for Optics and Electromagnetics*, W.S. Weiglhofer and A. Lakhtakia (eds.), (Bellingham, WA, USA: SPIE Press), 295–316.

[40] T.G. Mackay, 2005, Linear and nonlinear homogenized composite materials as metamaterials, *Electromagnetics*, **25**, 461–481.

[41] L. Ward, 2000, *The Optical Constants of Bulk Materials and Films*, 2nd. edition, (Bristol, UK: Institute of Physics).

[42] T.G. Mackay, 2004, Depolarization volume and correlation length in the homogenization of anisotropic dielectric composites, *Waves Random Media* , **14**, 485–498; erratum 2006.

[43] W.S. Weiglhofer and T.G. Mackay, 2000, Numerical studies of the constitutive parameters of a chiroplasma composite material, *Arch. Elekron. Übertrag.*, **54**, 259–265.

[44] A. Lakhtakia, 2001, Application of strong permittivity fluctuation theory for isotropic, cubically nonlinear, composite materials, *Opt. Commun.* **192**, 145–151 .

[45] T.G. Mackay, A. Lakhtakia, and W.S. Weiglhofer, 2002, Homogenisation of isotropic, cubically nonlinear, composite materials by the strong–permittivity–fluctuation theory: third–order considerations, *Opt. Commun.* **204**, 219–228.

[46] T.G. Mackay, A. Lakhtakia, and W.S. Weiglhofer, 2003, The strong–property–fluctuation theory for cubically nonlinear, isotropic chiral composite materials, *Electromagnetics* **23**, 455–479.

[47] T.G. Mackay, 2003, Geometrically derived anisotropy in cubically nonlinear dielectric composites, *J. Phys. D: Appl. Phys.* **36**, 583–591.

[48] W.S. Weiglhofer, 1999, Electromagnetic field in the source region: A review, *Electromagnetics* **19**, 563–578.

[49] R.W. Boyd, 2003, *Nonlinear Optics*, 2nd. edition, Academic Press, London .

[50] J. Cui, & T.G. Mackay. 2007. Depolarization regions of nonzero volume in bianisotropic homogenized composites. *Waves Random Complex Media* **17** 269–281.

[51] J. Cui, & T.G. Mackay. 2007. Depolarization regions of nonzero volume for anisotropic, cubically nonlinear, homogenized nanocomposites. *J. Nanophotonics* 1:013506.

[52] W.S. Weiglhofer, 1998, Electromagnetic depolarization dyadics and elliptic integrals, *J. Phys. A: Math. Gen.* **31**, 7191–7196.

[53] M.N. Lakhtakia and A. Lakhtakia, 2001, Anisotropic composite materials with intensity–dependent permittivity tensor: the Bruggeman approach, *Electromagnetics* **21**, 129–138.

[54] R.W. Boyd, R.J. Gehr, G.L. Fischer, and J.E. Sipe, 1996, Nonlinear optical properties of nanocomposite materials, *Pure Appl. Opt.* **5**, 505–512.

[55] H.B. Liao, R.F. Xiao, H. Wang, K.S. Wong, and G.K.L. Wong, 1998, Large third–order optical nonlinearity in Au:TiO_2 composite films measured on a femtosecond time scale, *Appl. Phys. Lett.* **72**, 1817–1819.

[56] A. Lakhtakia and T.G. Mackay, Negative phase velocity in isotropic dielectric–magnetic media via homogenization: Part II, *Microw. Opt. Technol. Lett.* **48**, 709–712, 2006.